

*Digital Comprehensive Summaries of Uppsala Dissertations
from the Faculty of Science and Technology 2325*

Energy Transfer Processes and Quenching Pathways in Lanthanide Complexes: The Role of Structural Changes

DANIEL KOCSI



ACTA UNIVERSITATIS
UPSALIENSIS
2023

ISSN 1651-6214
ISBN 978-91-513-1933-9
urn:nbn:se:uu:diva-514326



UPPSALA
UNIVERSITET

Dissertation presented at Uppsala University to be publicly examined in Högssalen, Lägerhyddsvägen 1, Uppsala, Thursday, 7 December 2023 at 09:15 for the degree of Doctor of Philosophy. The examination will be conducted in English. Faculty examiner: Professor Raphaël Tripier (Université de Bretagne Occidentale, Brest).

Abstract

Kocsi, D. 2023. Energy Transfer Processes and Quenching Pathways in Lanthanide Complexes: The Role of Structural Changes. *Digital Comprehensive Summaries of Uppsala Dissertations from the Faculty of Science and Technology* 2325. 112 pp. Uppsala: Acta Universitatis Upsaliensis. ISBN 978-91-513-1933-9.

Due to their unique magnetic and luminescent properties, trivalent lanthanides (Ln(III)) have been widely utilised in cellular imaging. Ln(III) luminescence is usually sensitized by a light-harvesting ‘antenna’, a chromophore that can transfer the excitation energy to the Ln(III). Our research focuses on the understanding and tuning of the luminescent properties of Ln(III) coordination compounds. In order to obtain bright emitters, the optimisation of energy transfer and minimisation of quenching processes are key challenges. In complexes of reducible Ln(III) ions photoinduced electron transfer (PeT) from the excited state antenna to the Ln(III) is possible, often quenching both antenna fluorescence and Ln(III) luminescence.

Chapter 1 is a brief introduction to luminescent Ln(III) coordination compounds. In *Chapter 2* intraligand PeT from the excited state antenna to the pyridines was studied in picolinate-containing TACN (1,4,7-triazacyclononane)-based Ln(III) complexes. Such PeT was found to be thermodynamically favoured and strongly dependent on the electron accepting ability of pyridines.

Chapter 3 addresses the importance on how distant structural changes can lead to improved luminescent properties in Ln complexes. Two sets of complexes with identical coordination environments and antennae were compared. In the first set the antenna was connected to the metal-binding site via a secondary amide linker, while in the second the linker was replaced with a tertiary amide. All tertiary amide linked Ln(III) complexes showed increased quantum yields compared to their secondary amide analogues. Moreover, tertiary complexes showed improved photostability compared to the secondary-amide linked ones.

In *Chapter 4* and *5* we investigated the effects of fluorinated antennae in secondary and tertiary amide-linked DO3A (cyclen-1,4,7-triacetate)-based, and pyridyl-containing TACN-based Ln(III) complexes. Photophysical characterisation revealed that monofluorination yielded no significant improvement in the luminescent quantum yields compared to the non-fluorinated analogues. The fluorination of the carbostyryl antenna in the 3 position drastically effected the excited state behaviour. The presence of several emissive species was observed possibly caused by changes in the coordination environment. 3-CF₃ and the 4-fluoro carbostyryls were excellent sensitisers of Eu(III) and Tb(III) emission. Changes in the antenna T_1 resulted in 5–12-fold increase in Tb(III) luminescent quantum yields in the 3-CF₃ series compared to the 4-CF₃ analogues. Eu(III) luminescent quantum yields and the sensitisation efficiencies were systematically lower in the 3-CF₃ compounds vs the 4-CF₃ emitters, which might be attributed to the differences in the PeT quenching in these complexes.

Keywords: lanthanide, luminescence, sensitisation, quenching, electron transfer, organic chromophores, fluorination

Daniel Kocsi, Department of Chemistry - Ångström, Synthetic Molecular Chemistry, 523, Uppsala University, SE-751 20 Uppsala, Sweden.

© Daniel Kocsi 2023

ISSN 1651-6214

ISBN 978-91-513-1933-9

URN urn:nbn:se:uu:diva-514326 (<http://urn.kb.se/resolve?urn=urn:nbn:se:uu:diva-514326>)

In the loving memory of Dr. Pál Szabolcs Szabados

*Doktori értekezésemet végtelen szeretettel ajánlom
Dr. Szabados Pál Szabolcs emlékére*

List of Papers

This thesis is based on the following papers, which are referred to in the text by their Roman numerals.

- I. Kovacs, D., **Kocsi, D.**, Wells, J. A. L., Kiraev, S. R., Borbas, K. E. (2021) Electron transfer pathways in photoexcited lanthanide(III) complexes of picolinate ligands. *Dalton Transactions*, 50(12):4244–4254.
- II. **Kocsi, D.**, Kovacs, D., Wells, J. A. L., Borbas, K. E. (2021) Reduced quenching effect of pyridine ligands in highly luminescent Ln(III) complexes: the role of tertiary amide linkers. *Dalton Transactions*, 50:16670–16677.
- III. **Kocsi, D.**, Orthaber, A., Borbas, K. E. (2022) Tuning the photophysical properties of luminescent lanthanide complexes through regioselective antenna fluorination. *Chem. Commun.*, 58:6853–6856.
- IV. **Kocsi, D.**, Borbas, K. E. (2023) Synthesis of fluorinated carbostyryl antennae for the sensitization of Eu(III), Tb(III), Dy(III) and Sm(III) luminescence. *manuscript*

Reprints were made with permission from the respective publishers. Papers I–II were previously discussed in the context of a licentiate thesis defence presented on 28 September 2022: *Electron transfer processes in luminescent Ln(III) complexes of picolinate ligands*

Contribution report

- Paper I Contributed to the synthesis and chemical characterisation of ligands and complexes. Performed the synthesis and chemical characterisation of model compounds. Contributed to obtaining single crystals. Performed the ^1H NMR of Eu(III) complexes and cyclic voltammetry measurements of model compounds. Contributed to the photophysical characterisation of lanthanide complexes and data evaluation. Contributed to the writing of the manuscript and supporting information.
- Paper II Contributed to the synthesis and chemical characterisation of ligands and complexes. Performed the synthesis and chemical characterisation of model compounds. Contributed to obtaining single crystals. Performed the ^1H NMR of Eu(III) complexes and cyclic voltammetry measurements. Performed the majority of photophysical characterisation of lanthanide complexes and data evaluation. Contributed to the writing of the manuscript and wrote most of the supporting information.
- Paper III Designed, synthesised and characterised new chromophores, ligands and lanthanide complexes. Performed the ^1H NMR of Eu(III) complexes and cyclic voltammetry measurements of model compounds. Performed the photophysical characterisation of lanthanide complexes and data evaluation. Contributed to the writing of the manuscript and wrote the supporting information.
- Paper IV Designed, synthesised and characterised new chromophores, ligands and lanthanide complexes. Performed cyclic voltammetry measurements of model compounds. Performed the photophysical characterisation of lanthanide complexes and data evaluation. Contributed to the writing of the manuscript and wrote the supporting information.

Papers not included in this thesis

- V. Sollert, C., **Kocsi, D.**, Jane, R. T., Orthaber, A., Borbas, K. E. (2021) C-glycosylated pyrroles and their application in dipyrromethane and porphyrin synthesis. *J. Porphyr. Phthalocyanines*, 25:741-755.
- VI. [‡]Bhimpuria, R., [‡]Tomar, M., **Kocsi, D.**, Thapper, A., Borbas, K. E. (2023) Photocatalytic Generation of Divalent Lanthanide Reducing Agents. *J. Am. Chem. Soc.*, DOI: 10.1021/jacs.3c07508.

[‡] These authors contributed equally.

Contents

Abbreviations.....	11
1. Introduction	13
1.1 General information on lanthanides	13
1.2 Ln(III) luminescence	14
1.3 Ln(III) sensitisation	14
1.4 Ln(III) emission and its characterisation.....	15
1.5 Quenching	17
1.6 Structural features of Ln(III) coordination compounds.....	18
1.7 Suitable chromophores for Ln(III) sensitisation.....	20
1.8 The synthesis of coumarins and carbostyrils.....	21
1.9 Applications of Ln(III) coordination compounds.....	23
1.10 Aims of the thesis	24
2. Lanthanide(III) complexes of picolinate-containing ligands (Paper I) 26	
2.1 Introduction	26
2.2 Synthesis of new ligands and Ln(III) complexes	28
2.2.1 Synthesis of the picolinate pendant arms.....	28
2.2.2 Assembly of ligands and Ln(III) complexes.....	29
2.2.3 Preparation of model compounds for cyclic voltammetry measurements	31
2.3 Electrochemical characterisation of picolinate bearing Ln(III) complexes.....	33
2.4 Structural characterisation of EuLs complexes in solution	35
2.5 Photophysical characterisation of LnLs	37
2.6 Conclusions	42
3. The role of tertiary amide linkers in improving the luminescent properties of TACN-based Ln(III) emitters (Paper II).....	44
3.1 Introduction	44
3.2 Synthesis of new ligands and Ln(III) complexes	46
3.2.1 Preparation of tertiary-linked ligands and Ln(III) complexes	46
3.2.2 Preparation of model compounds for cyclic voltammetry measurements	47
3.3 Electrochemical characterisation of tertiary amide Ln(III) complexes.....	47

3.4 Structural characterisation of Ln(III) complexes	48
3.4.1 X-ray crystallography: comparison of LnLs and LnLt	48
3.5 Photophysical characterisation of LnLt	49
3.6 Photostability of LnL	55
3.7 Conclusions	56
4. Monofluorinated carbostyrils as potential Ln(III) sensitisers (Paper III).....	58
4.1 Introduction	58
4.2 Synthesis of CS^F , L^F and Ln(III) complexes, and model compounds	59
4.2.1 The design of the synthesis.....	59
4.2.2 Preparation of monofluorinated carbostyrils (CS^F)	61
4.2.3 Attempted synthesis of CS^{4F}	64
4.2.4 Assembly of ligands and preparation of Ln(III) complexes	66
4.2.5 Preparation of model compounds for cyclic voltammetry measurements	67
4.3 Structural characterisation of LnL^F compounds	68
4.4 Electrochemical characterisation of model compounds	69
4.5 Photophysical characterisation of CS^F and LnL^F	70
4.6 Conclusions	77
5 Synthesis of fluorinated carbostyryl antennae for the sensitization of Eu(III),Tb(III) luminescence. (Paper IV).....	79
5.1 Introduction	79
5.2 Synthesis of CS^R , ligands L^R , Lt^R and Lpy^R , their Ln(III) complexes and model compounds.....	80
5.2.1 Preparation of CS^{4F}	80
5.2.2 Preparation and functionalisation of CS^{3CF3}	81
5.2.3 Assembly of L^{4F} , L^{3CF3} , Lt^{3CF3} and Lpy^{3CF3} , and preparation of their Ln(III) complexes.....	83
5.2.4 Preparation of model compounds for cyclic voltammetry measurements	86
5.3 Electrochemical characterisation of model compounds	86
5.4 Conclusions	95
Concluding remarks and outlook	97
Popular science summary	99
Populärvetenskaplig Sammanfattning.....	101
Acknowledgments.....	103
References.....	107

Abbreviations

$\text{Ant}^{\bullet+}$	Antenna radical cation
$A_{\text{MD},0}$	The spontaneous emission probability for the ${}^5\text{D}_0 \rightarrow {}^7\text{F}_1$ transition in vacuo
BET	Back energy transfer
A^*/D^*	Excited state acceptor/donor
$D^{\bullet+}$	Donor radical cation
DCM	Dichloromethane
DEE	diethyl ether
DO3A	Cyclen-1,4,7-triacetate
dppf	1,1'-Bis(diphenylphosphino)ferrocene
ED	Electric dipole
EnT	Energy transfer
$E_{\text{ox/red}}$	Oxidation/reduction potential
E_s	Excited state energy
ISC	Intersystem crossing
Ln	Lanthanide
MD	Magnetic dipole
MOM	Methoxymethyl
NIR	Near-infrared
PeT	Photoinduced electron transfer
q	Hydration state of Ln(III)
S_0	Singlet ground state
S_1	First singlet excited state
SAP	monocapped square antiprismatic
T_1	First triplet excited state
TACN	1,4,7-triazacyclononane
<i>t</i> BuDO3A	1,4,7,10-Tetraazacyclododecane-1,4,7-tris(<i>t</i> -butyl acetate)
TSAP	monocapped twisted square antiprismatic
e_0^2/ϵ	Coulombic attraction energy
ϵ	Molar absorption coefficient
η_{sens}	Sensitization efficiency of Ln(III)
λ_{abs}	Local absorption maximum
λ_{em}	Local emission maximum
τ_{D2O}	Observed luminescence lifetime in D ₂ O
τ_{H2O}	Observed luminescence lifetime in H ₂ O

τ_{obs}	Observed luminescence lifetime
τ_{rad}	Radiative lifetime
Φ_{L}	Residual ligand fluorescence quantum yield
Φ_{Ln}	Ln(III) overall quantum yield of luminescence
$\Phi_{\text{Ln}}^{\text{Ln}}$	Ln(III) intrinsic quantum yield

1. Introduction

1.1 General information on lanthanides

Lanthanides (Ln) consist of 15 elements from La to Lu and together with Sc and Y are known as the “rare earths”. Their history stretches all the way back to the early 1800s when the first “earth” oxides were obtained from minerals in Scandinavia. Y, Yb, Er and Tb got their names after Ytterby, a small village close to Stockholm, which had been the source of lanthanide rich ores for decades.¹

Despite the historical name most lanthanides are not rare. For instance, Ce, the most abundant lanthanide, has a comparable abundance to Ni or Cu in Earth’s crust, while the least abundant Tm and Lu are more abundant than Ag, Au or Pt.

The pronounced chemical similarity of the lanthanides to each other made their classification and separation extremely difficult in the beginning. Medeleev could not place the lanthanides in the periodic table, either. Courtesy of the efforts of Moseley and Bohr, lanthanides are known to have atomic numbers 57 to 71, and their valence electrons are in the 4f orbital.

Lns possess increasing numbers of electrons in their 4f orbitals. These partially filled orbitals make them alike but distinguishable at the same time. Due to the shielding of the valence electrons by the 6s and 5d orbitals lanthanides have similar reactivity. The unique 4f electron configurations are responsible for the unique Ln physical properties, such as magnetism and luminescence.²

Every Ln has a stable +3 oxidation state with an electron configuration of $[\text{Xe}]4f^n$ ($n = 0-14$).³ Unoccupied or half-filled 4f orbitals are consistent with unusual oxidation states e.g. Ce(IV) or Eu(II). These oxidation states have found use in organic syntheses. For instance, SmI_2 is a single-electron reductant, while Ce(IV) compounds are excellent oxidants. Apart from the radioactive Pm, all lanthanides have been prepared and characterised at their +2 oxidation state.⁴

Due to the unique magnetic and luminescent properties of trivalent lanthanides, various applications have been developed, such as permanent magnets (Nd), light displays (Tb, Eu), lasers (Yb, Nd), optical fibers (Er), magnetic resonance contrast agents (Gd) and luminescent probes (Tb, Eu).⁵

1.2 Ln(III) luminescence

Ln(III) has long been investigated for their unique luminescent properties. Ln(III) luminescence arises from Laporte forbidden f-f transitions. Excitation of Lns may be possible by direct absorption of light, but due to their very low molar absorption coefficients ($\epsilon < 10 \text{ M}^{-1}\text{cm}^{-1}$) this is inefficient. One way to bypass this limitation, is to use organic chromophores that absorb the excitation energy which can be transferred to the metal ion.⁶ A good chromophore should absorb light efficiently at a suitable wavelength, undergo rapid intersystem crossing (ISC) to populate its first triplet excited state (T_1), which should be well positioned for energy transfer (EnT) to the Ln receiving level. Although EnT from both the first singlet excited state (S_1) and T_1 of the antenna can be efficient,⁷ triplet-mediated sensitisation is considered the primary pathway for most known antennae (Figure 1).

The excited-state Ln(III) ion can relax back to its ground state by emitting a photon. The transitions between the Ln(III) energy levels are invariant, hence the emission consists of sharp, line-like peaks which always appear at the same wavelength(s) for a given Ln(III). The combination of organic chromophores and Lns yields a strongly absorbing species with unique emission properties.

1.3 Ln(III) sensitisation

Antenna excitation can yield the excited state Ln(III) ion via a number of different pathways. The understanding of these is essential for the design of bright Ln(III) emitters.

At this point it is worth recalling the principal energy transfer (EnT) mechanisms between any donor-acceptor pair. The two main types of EnT mechanisms are i) Förster resonance energy transfer, and ii) Dexter energy transfer (electron-exchange mechanism) (**Figure 1, right**).

The donor-acceptor distance is important due to the dependence on the electric field. Förster energy transfer is a through-space mechanism based on Coulombic interaction (i.e. dipole-dipole interaction) between the donor and acceptor. The process can be observed at distances up to 100 Å, and has an r^{-6} distance dependence.⁸ Förster EnT is sometimes called a ‘singlet-to-singlet’ process and provides a reasonable approximation for systems which do not contain heavy atoms.

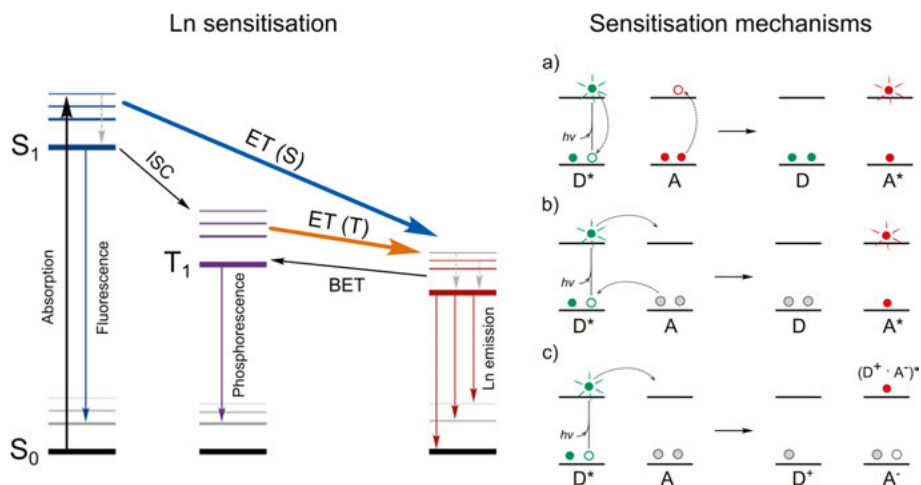


Figure 1 Jablonski diagram of Ln sensitisation mechanism (left). The different sensitisation mechanisms on the right: a) Förster EnT (top), b) Dexter EnT (middle), c) PeT (bottom).

The Dexter EnT is a double electron-exchange mechanism which consists of the simultaneous transfer of one electron in each direction between the donor and the acceptor (**Figure 1b**, right, middle). This process requires through-bond electronic coupling, therefore it is promoted by good orbital overlap in conjugated systems. Consequently, Dexter EnT takes place over much shorter distances ($< 10\text{--}15\text{ \AA}$) and can occur in situations when Förster EnT would be ruled out due to spin selection rules⁹.

In some other cases where the energy acceptor has a readily accessible Ln(II) state, such as Yb or Eu,¹⁰ sensitisation by a redox-based mechanism has been proposed to occur. The process consists of a photoinduced electron transfer (PeT) from the excited state donor D* to the Ln(III) forming a charge separated D^{•+}-Ln(II) species. Back electron transfer can leave the Ln(III) ion in its luminescent excited state⁹.

In terms of triplet mediated sensitization, the generally accepted mechanism is as follows: excitation to the ligand S₁ followed by rapid ISC to T₁, which then transfers its energy to the Ln(III) centre. EnT presumably takes place *via* a Dexter mechanism due to direct contact of the ligand and Ln(III) ion (**Figure 1**, left). On the other hand, several examples exist where direct EnT from S₁ to the Ln(III) was observed¹¹ either exclusively, or as a contributing pathway to the T₁-mediated one.

1.4 Ln(III) emission and its characterisation

All Ln(III) ions are luminescent with the exception of La(III) and Lu(III) which have empty or filled 4f orbitals, respectively.¹² Among other ions,

Eu(III), Tb(III) and Sm(III) are phosphorescent in the visible region, and Yb(III) is fluorescent in the near-infrared (NIR). Gd(III) has high excited state energy level which is not accessible for near UV-absorbing antennae, therefore it usually has no metal-based luminescence in the types of systems discussed in this thesis. Gd(III) complexes may show ligand fluorescence at room temperature. At 77 K the emission spectrum may contain both ligand fluorescence and phosphorescence bands, which can be used to determine S_1 and T_1 states of the ligand. Tb(III) and Eu(III) have excited states at 20 400 cm^{-1} (5D_4) and 17 200 cm^{-1} (5D_0), respectively.¹³ Relaxation happens from these excited states to the final states 7F_J where $J = 0-5$ for Eu and $J = 6-0$ for Tb. The overall colour of Ln complex emission is defined by the most intense transition of the emission spectrum e.g. Eu is red ($\lambda_{\text{em}} = 700 \text{ nm}$, $^5D_0 \rightarrow ^7F_4$) and Tb is green ($\lambda_{\text{em}} = 546 \text{ nm}$, $^5D_4 \rightarrow ^7F_5$).

Luminescent Ln complexes can be characterised by their quantum yield (Φ_{Ln}). According to Eq. 1,¹⁴ Φ_{Ln} is the product of the sensitisation efficiency (η_{sens}) and the intrinsic quantum yield ($\Phi_{\text{Ln}}^{\text{Ln}}$) of the Ln(III)*. The former parameter is dependent on the processes occurring prior to the formation of the excited state Ln(III), including the processes responsible for the population of the antenna feeding level (ISC and EnT), and the quenching processes affecting the antenna excited state. The latter parameter defines the maximum quantum yield of a given ligand environment upon direct Ln(III) excitation. $\Phi_{\text{Ln}}^{\text{Ln}}$ is proportional to the observed lifetime (τ_{obs}) and inversely proportional to the radiative lifetime (τ_{rad}) of the ion.

$$\Phi_{\text{Ln}} = \eta_{\text{sens}} \cdot \Phi_{\text{Ln}}^{\text{Ln}} = \eta_{\text{sens}} \cdot \frac{\tau_{\text{obs}}}{\tau_{\text{rad}}} \quad \text{Eq. 1}$$

For most lanthanides the calculation of η_{sens} and $\Phi_{\text{Ln}}^{\text{Ln}}$ is not trivial, however for Eu(III) these can be calculated from the corrected emission spectrum.^{11a} τ_{rad} can be calculated from the corrected steady-state emission spectrum according to Eq. 2.

$$\frac{1}{\tau_{\text{rad}}} = A_{\text{MD},0} \cdot n^3 \cdot \left(\frac{I_{\text{tot}}}{I_{\text{MD}}} \right) \quad \text{Eq. 2}$$

In Eq. 2, $A_{\text{MD},0}$ (a constant equal to 14.65 s^{-1}) is the spontaneous emission probability for the $^5D_0 \rightarrow ^7F_1$ transition in vacuo, n is the refractive index of the solvent, and $I_{\text{tot}}/I_{\text{MD}}$ is the integrated ratio of the total corrected Eu(III) emission spectrum to the area of $^5D_0 \rightarrow ^7F_1$ transition (i.e. magnetic dipole transition).^{11a}

1.5 Quenching

Unlike organic fluorophores, the excited states of Ln(III) ions are usually not sensitive to quenching by molecular oxygen.¹⁵ Sensitivity to nearby X-H (X = O, N, C) oscillators is well established. Quenching occurs due to vibrational energy transfer of the Ln excited state to the X-H overtones. In aqueous solutions of Eu and Tb, X is O and, depending of the ligand, N.¹⁶ Coupling between X-D oscillators and Ln excited states is usually weaker, therefore the extent of quenching is smaller. Substitution of X-H oscillators (e.g. deuteration or fluorination of the ligand) may improve the luminescent quantum yield. Metal-bound solvent molecules such as water or methanol are responsible for a large part of Ln excited state quenching. Changing the media to a deuterated one (e.g. H₂O to D₂O) leads to the exchange of the bound H₂O with D₂O which provides the basis of hydration state (q) analyses. q values can be calculated according to Eq. 3 and Eq. 4 for Tb and Eu^{16,17}, respectively, where τ_{H_2O} and τ_{D_2O} are the observed lifetimes in H₂O and D₂O, respectively, and m is the number of nearby N-H oscillators in Eu(III) complexes.

$$q(Tb) = 5 \cdot (1/\tau_{H_2O} - 1/\tau_{D_2O} - 0.06) \quad \text{Eq. 3}$$

$$q(Eu) = 1.2 \cdot (1/\tau_{H_2O} - 1/\tau_{D_2O} - 0.25 - m \cdot 0.075) \quad \text{Eq. 4}$$

While there is no actual EnT between Ln(III) and O₂ excited states¹⁵, quenching by molecular O₂ can happen if back energy transfer (BET) to the antenna T_1 from the Ln(III) excited state or slow EnT (i.e. sensitization) from the T_1 results in a long-lived T_1 state.¹⁸ BET is more probable if the antenna T_1 is within 2000 cm⁻¹ of the Ln(III) excited state.

Lastly, PeT may occur from antenna S_1 to Ln(III). This deactivation process was initially suggested in the late 80s, and has been invoked for several Eu(III) complexes.¹⁹ The process involves electron transfer from antenna to Ln(III), yielding oxidised Ant⁺• and reduced Ln(II), respectively. PeT drastically changes the emission properties of both the ligand and the Ln ion. PeT requires the presence of an easily reducible Ln(III) for instance Eu(III) with $E_{red} = -0.35$ V vs NHE,²⁰ or the slightly less reducible Sm, Dy, or Yb. The process was mostly observed in Eu(III) emitters, where the dramatic decrease of ligand fluorescence along with lower than expected Eu(III) emission can be an indication that PeT is taking place.²¹

To determine if PeT is thermodynamically favoured the free energy change of electron transfer (ΔG_{ET}) in such donor-acceptor systems can be estimated according to the Rehm–Weller equation (Eq. 5).^{22,23}

$$\Delta G_{ET} = (E_{ox} - E_{red}) - E_S - \frac{e_0^2}{\epsilon} \quad \text{Eq. 5}$$

E_{ox} is the oxidation potential of the donor (i.e. antenna), E_{red} is the half-wave potential of the acceptor (i.e. Ln(III)), E_s is the excited state energy of the donor and e_0^2/ϵ is the Coulombic attraction energy experienced between the radical ion pair following the electron transfer reaction. The last term is related to the decrease in energy upon the formation of the radical ion pair and dependent on the solvent and the separation of the charges.^{22,23} The more negative ΔG_{ET} is the more thermodynamically favored PeT becomes. According to Eq. 3, a less reducing antenna or a non-reducible Ln (e.g. $E_{\text{red}} < -3.6$ V vs NHE for Gd(III) or Tb(III)) may prevent PeT. On the other hand, moderately reducible Lns such as Yb or Sm ($E_{\text{Ln(III)/Ln(II)}} = -1.15, -1.55$ V vs NHE²⁰, respectively) could be susceptible to PeT in systems where the donor is reducing enough.²¹

1.6 Structural features of Ln(III) coordination compounds

Lanthanide ions can adopt a large variety of coordination geometries. The most stable, trivalent ions have $[\text{Xe}]4f^n$ ($n = 0-14$) configuration, while the 4f orbitals are well shielded by the 5s and 5p sub-shells.¹ Ln(III) ions are hard Lewis acids. A smooth decrease in ionic radii from 1.03 Å for La(III) to 0.861 Å for Lu(III) results in higher charge density, which in turn causes an increased acidity with increasing atomic number, a phenomenon known as the “lanthanide contraction”.²⁴ Ln(III) ions are unlikely to bond covalently, instead, they prefer Coulombic interactions with hard donor atoms (e.g. O, N, F). Due to their large ionic radii they can accommodate large coordination numbers up to 12,²⁵ but a coordination number of 8 or 9 is most frequent.¹

For biomedical applications, designing efficiently chelating ligands is a challenge. The thermodynamic stability and kinetic inertness of Ln complexes play critically important roles in a highly competitive media, such as body fluids. The use of macrocyclic ligands was proved to offer significantly better stability than mono- or polydentate ligands. For instance, the half-life of $[\text{Gd}(\text{DOTA})\text{H}_2\text{O}]^-$ complex (Dotarem[®]) – the most widely used gadolinium-based contrast agent in MRI – was estimated to be 43 years at physiological pH at 37 °C.²⁶ Macrocycles bearing nitrogen atoms provide a flexible platform where the nitrogen atoms in the ring are capable of metal chelation. These backbone nitrogen atoms can be further functionalised with various pendant arms resulting in a highly adaptable coordination environment. Since these ligands can readjust to the size of the metal ion, they serve as universal chelators providing close to identical stability for the series of Lns.

Aza-macrocycles are used for Ln(III) complexation based on their affinity to metal ions. Cyclen (1,4,7,10-tetraazacyclododecane)^{13a} and TACN (1,4,7-cyclononane)²⁷ cores are probably the best known. Through appropriate functionalisation octa- and nonadentate coordination environments are achievable. Cyclen based ligands are usually equipped with monodentate pedants (e.g. carboxylates,²⁸ amides,²⁹ phosphinates,³⁰ phosphonates³⁰), while TACN cores require the use of bidentate pendant arms (e.g. picolines³¹ and its substituted derivatives³²). Representative examples are depicted in **Figure 2**.

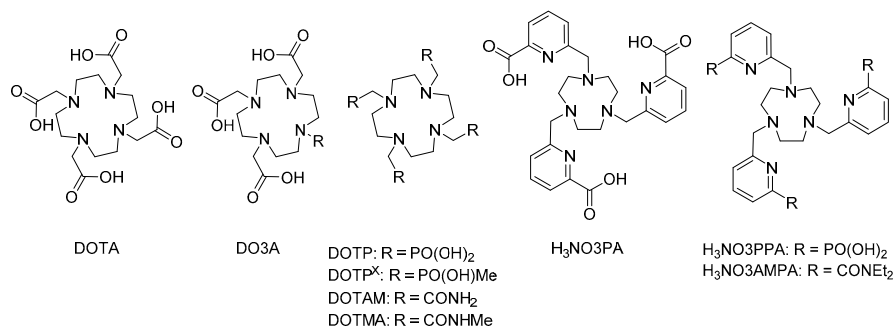


Figure 2 Representative examples of cyclen and TACN based ligands

The characterisation of the geometry of Ln complexes is essential in order to better understand their luminescent, magnetic and relaxation properties. An enormous amount of characterisation data is available in the literature, thus some universal characteristics might be formulated. Cyclen- and TACN-based Ln complexes prefer square antiprismatic (SAP)³³ (**Fel! Hittar inte referenskölla.a**, top) and trigonal tricapped prismatic geometries³¹ (**Fel! Hittar inte referenskölla.a**, bottom), respectively.

Octadentate ligands impose SAP geometry, hence a capping molecule (such as water) is often present in the first coordination sphere fulfilling coordination number 9 for the Lns. The functionalisation of the backbone nitrogens results in several species in solution due to structural dynamics. DOTA type Ln complexes exist in two diastereomeric forms, square antiprismatic (SAP) and twisted-square antiprismatic (TSAP)^{33,30,29} (**Fel! Hittar inte referenskölla.b**). The chirality in SAP and TSAP is addressed to i) the orientation of the ethylene bridges between the macrocyclic nitrogens ($\delta\delta\delta\delta$ and $\lambda\lambda\lambda\lambda$), and ii) the helicity of pendant (carboxylate) arms (Δ and Λ). Interconversion between the isomers ($SAP \leftrightarrow TSAP$) occurs by either ring inversion ($\delta\delta\delta\delta \leftrightarrow \lambda\lambda\lambda\lambda$) or arm rotation ($\Delta \leftrightarrow \Lambda$); successive or concerted occurrence of these processes result in enantiomerisation.³⁴

TACN-based Ln complexes (**Figure 2**), impose trigonal tricapped prismatic geometry with coordination number 9. The three carboxylate oxygen atoms and the macrocycle nitrogens serve as the “capping” planes from the bottom and the top, respectively. The third face consists of the three pyridine nitrogen

donor atoms laying between the “capping” planes. For Ln complexes a slight distortion was observed between the “capping” faces in the solid state.³¹ Conformation of the picolinates can be arranged either clockwise (Δ) or anticlockwise (Λ). Analogously to DOTA complexes, two enantiomeric pairs ($\Delta(\lambda\lambda\lambda)/\Lambda(\delta\delta\delta)$ or $\Delta(\delta\delta\delta)/\Lambda(\lambda\lambda\lambda)$) of diastereomers can be present in solution, and interconversion by ring inversion or arm rotation could arise.³⁵

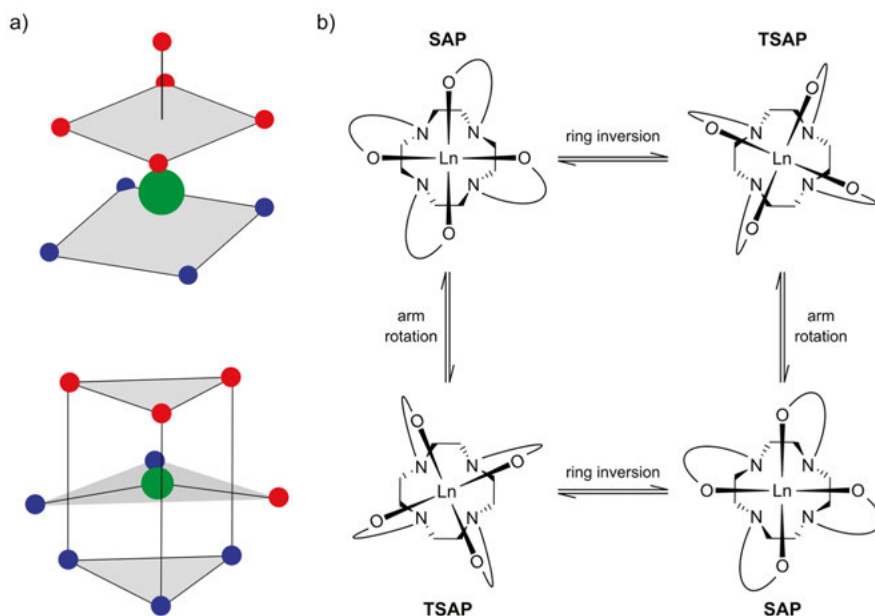


Figure 3 a) Monocapped square antiprismatic geometry (top), trigonal tricapped prismatic geometry (bottom).³¹ Blue spheres, red spheres and green spheres represent N, O and Ln ion, respectively. b) Schematic representation of LnDOTA isomers in solution.^{5b}

1.7 Suitable chromophores for Ln(III) sensitisation

Organic chromophores help overcome the inherently low absorption of Ln(III) ions through efficient absorption of light and transfer of this energy to the metal ions. In 1942, Weissman discovered that the emission of Eu(III) significantly increased in the presence of certain organic molecules, such as salicylaldehyde and benzoylacetate. The increase in emission was attributed to an intramolecular energy transfer from the ligand excited state to the Eu(III). This sensitization process has been extensively studied and is known as the *antenna effect*.³⁶

Many sensitizers have been developed in the past decades, and successfully utilised in Ln-based luminescent emitters and probes for biological and biomedical purposes.³⁷ Despite the infinite variety of organic molecules, only

a small number of truly efficient sensitizers are known. These include both smaller heterocycles such as amido-naphthalene,³⁸ phenanthroline³⁹ and phenanthridine,⁴⁰ and larger moieties, for instance, tetraazatriphenylene,⁴¹ azaxanthone and azathiaxanthone³⁷ (**Figure 4**). Tridentate dipicolinate ligands are well-known to sensitise Eu(III) and Tb(III). Coumarin and carbostyryl derivatives are capable of transferring energy to 2–6 Ln(III) ions, therefore, have attracted attention for multiplex imaging purposes.^{39,21} Coumarins, carbostyryls and picolinates are some of the most widely used chromophores to sensitize Eu(III) and Tb(III).

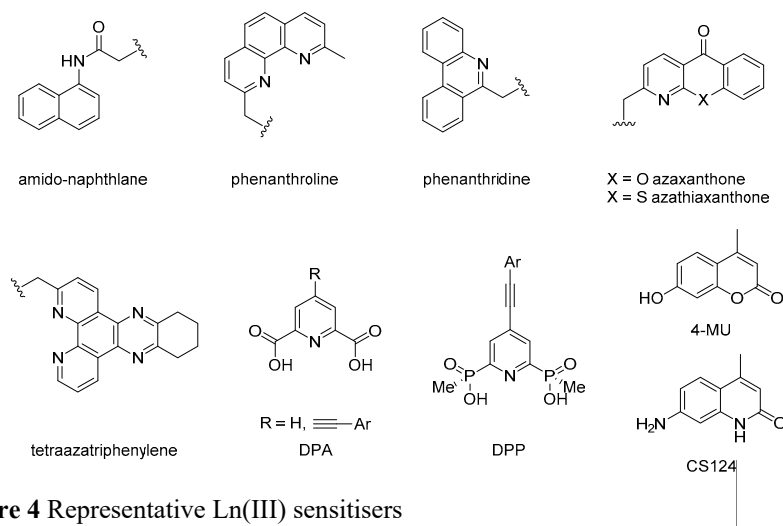


Figure 4 Representative Ln(III) sensitizers

Besides energy transfer between the antenna and Ln(III) ion, further processes *e.g.* back energy transfer, photoinduced electron transfer, vibrational quenching, etc. take place in these systems. The combination of these processes makes the state behaviour of Ln(III) coordination compounds extremely complex; the understanding and therefore the rational design of antenna-sensitized Ln complexes is remarkably challenging.

1.8 The synthesis of coumarins and carbostyryls

Carbostyryls (2(1*H*)-quinolones) are the isomers of 4-quinolones. 4-quinolone antibiotics in use are substituted with a fluorine and belong to the larger fluoroquinolone drug class. The most widely used fluoroquinolone antibiotic is Ciprofloxacin used to treat a number of bacterial infections, *e.g.* bone and joint infections, gastroenteritis and urinary tract infections.⁴² 2-quinolone scaffolds are also a significant topic in medicinal chemistry research. Several carbostyryl-based drugs have been approved for the treatment of respiratory diseases (*e.g.* Indacaterol, Procaterol and Repirinast) or depression (*e.g.* Brexpiprazole).⁴³ On the other hand, carbostyryl-based compounds have been

utilised as metal sensors,⁴⁴ luminescent materials,⁴⁵ fluorescent pH probes⁴⁶ and in dye-sensitised solar cells.⁴⁷

Conventionally, carbostyrils could be synthesised via Friedländer or Knorr-type reactions (**Figure 5**).⁴³ The former consists of a base-assisted double bond formation via Knoevenagel reaction followed by C–N amide bond formation via nucleophilic substitution. In the latter, acid-mediated electrophilic aromatic substitution and successive dehydration forms the double bond. Other two-component methods have been developed on the basis of Heck reaction. Ortho-iodoanilines could be transformed into 2-quinolones through a successive Heck reaction and cyclisation.⁴⁸ Depending on the coupling partners a large variety of carbostyril derivatives become accessible. Complementary to this method, N-protected *o*-aminocinnamates can undergo Heck reaction with aryl iodides yielding substituted carbostyrils.⁴⁹ The scope of olefins has been extended to acryl amides and acrylic acid.⁵⁰ In another variation aryl halides could undergo Buchwald-type amidation with primary amides, followed by a Knoevenagel reaction to form the double bond.⁵¹

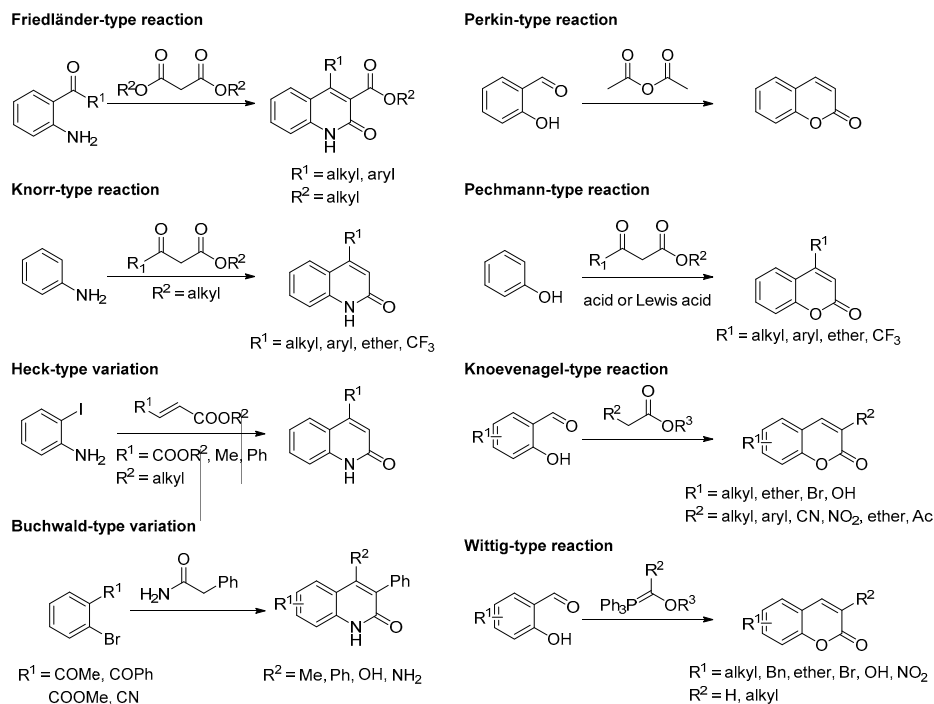


Figure 5 Summary of synthetic approaches of carbostyrils (left) and coumarins (right)

Coumarins are the closest to carbostyrils in structural and chemical properties, as well as fluorescent characteristics. Lončarić *et al.* published a comprehensive summary compiling the most common synthetic approaches to coumarin derivatives.⁵² Coumarins could be synthesised with many different methods, namely, Perkin reaction, Knoevenagel- and Pechmann-

condensation, or Wittig reaction to mention a few of those described in this review. The structural similarities of coumarins and carbostyrils allow synthetic chemists to utilise the methods that were successful in the synthesis of coumarins, in the synthesis of carbostyrils (**Figure 5**).

The most widely used condensation type reaction is a straightforward one-step approach bringing together the Knorr- and Pechmann-type reaction to access functionalised carbostyrils. This advantage comes with a number of considerable problems, though. The reactions often require harsh conditions, high temperatures (often 150–180 °C), long reaction times and the use of solvents such as DMF due to the poor solubility of the product. The potential starting material 1,3-diaminobenzene is not thermally stable, thus further problems appear with degradation side products during the purification, often translating to low isolated yields. The necessity of harsh conditions rules out a large number of functional groups due to their low stability. Another limiting factor might be the lack of (commercial) availability of β -ketoesters as the main source of reactive partners in condensation type reactions. The design of carbostyrils with unique substituents in specific positions through this approach is thus heavily limited.

1.9 Applications of Ln(III) coordination compounds

Trivalent lanthanide ions have attracted attention in biomedical applications for the past several decades. A great amount of research has been conducted in the fields of contrast agents,⁵³ nuclear medicines⁵⁴ and optical imaging.³ The use of azamacrocyclic chelators often leads to stable complexes, offering the opportunity to fine-tune the ligands through specific functionalisation. The large variety of Ln ions with diverse magnetic, optical and nuclear properties along with their similar chemical properties make Lns an exceptionally promising group of elements for the development of biomedical purposes.⁵⁵ Possibly the most widespread Ln used in biomedical application is Gd(III). Gd-based contrast agents for magnetic resonance imaging (MRI) date back to the 1980's when the first contrast agent $[\text{Gd}(\text{DTPA})\text{H}_2\text{O}]^{2-}$ (Magnevist[®]) was published and few years later approved by the FDA. Due to the extremely long half-life of $[\text{Gd}(\text{DOTA})\text{H}_2\text{O}]^-$ under physiological conditions (~43 years), it is probably the most known and widely used contrast agent – known as Dotarem[®].²⁶ This imaging technique originates from the difference in ¹H relaxation rates of water molecules caused by the Gd(III) in its surrounding.⁵³ Several examples of the use of Lns exist in nuclear medicine. For instance, radioisotopes ¹⁷⁷-Lu and ⁹⁰-Y are used to treat prostate cancer⁵⁶ and early stage tumours,⁵⁷ respectively. Furthermore, Tb has several radioisotopes known and used in clinical practice. Certain isotopes (¹⁵²-Tb and ¹⁵⁵-Tb) are used for diagnosis by positron emission topography (PET) and single photon

emission computed tomography (SPECT), respectively; and for radiotherapy.⁵⁸

Tb complexes might be used in photodynamic therapy. In these complexes the chelated Tb(III) is linked to a sensitizer. If the T_1 energy level of the chromophore is too close to the excited state of Tb(III), thermal back energy transfer populates the antenna T_1 . The long-lived T_1 state is sensitive to molecular oxygen, hence through this process singlet oxygen (1O_2) is generated which substantially causes cell death.⁵⁹ Carefully chosen sensitizers or the use of a mixture of Ln complexes might allow development of responsive and reactive candidates for sensing and cell killing, respectively.⁶⁰ Due to the unique luminescent properties Lns are also of interest in optical imaging.^{3,55} Ln emission consists of narrow, line like bands which make them distinguishable even against a strong background. Some of them emit in the visible region (Tb(III), Dy(III), Eu(III) and Sm(III)) turning the colour of the emission green, yellow, red and orange, respectively.³ Others, like Yb(III) or Nd(III) have recognizable emission in the near infrared region. Certainly, the biggest advantage over organic chromophores is the long lived – ms for Tb(III) and Eu(III) – luminescent lifetime. Time-resolved detection of the long lived Ln(III) emission excludes the background fluorescence of the biological medium which is often in the ns range. Time-resolved luminescence microscopy is widely used for imaging Ln luminescence (Tb, Eu) in living cells.⁶¹

1.10 Aims of the thesis

As mentioned before, antenna sensitized Ln(III) emitters are extremely complex systems. A variation of different processes could take place altering the excited state behaviour. With the aim of designing bright emitters, first we need to understand EnT processes and quenching mechanisms. However, to obtain highly luminescent Ln(III) complexes we ought to optimise EnT processes and minimise quenching. Systematic modification of either the coordination sphere or the sensitizer might allow for a better understanding of these systems, therefore rational design of bright emitters may become more conceivable.

In order to better understand how structural changes affect EnT processes and quenching, we planned the following:

- To synthesise new sets of TACN-based octadentate ligands and their Ln(III) complexes equipped with different carbostyryl sensitizers and various picolinate coordinating arms.
- To design and synthesise new chromophores, their DO3A- and TACN-based ligands, and their Ln(III) complexes.

- To study the solution and solid-state structures utilising ^1H NMR and X-ray crystallography, respectively.
- To characterise the appropriate redox-active fragments by cyclic voltammetry.
- To investigate the photophysical properties of Ln(III) complexes using steady-state and time-resolved luminescence spectroscopy.
- To evaluate EnT processes and quenching mechanisms.

2. Lanthanide(III) complexes of picolinate-containing ligands (Paper I)

2.1 Introduction

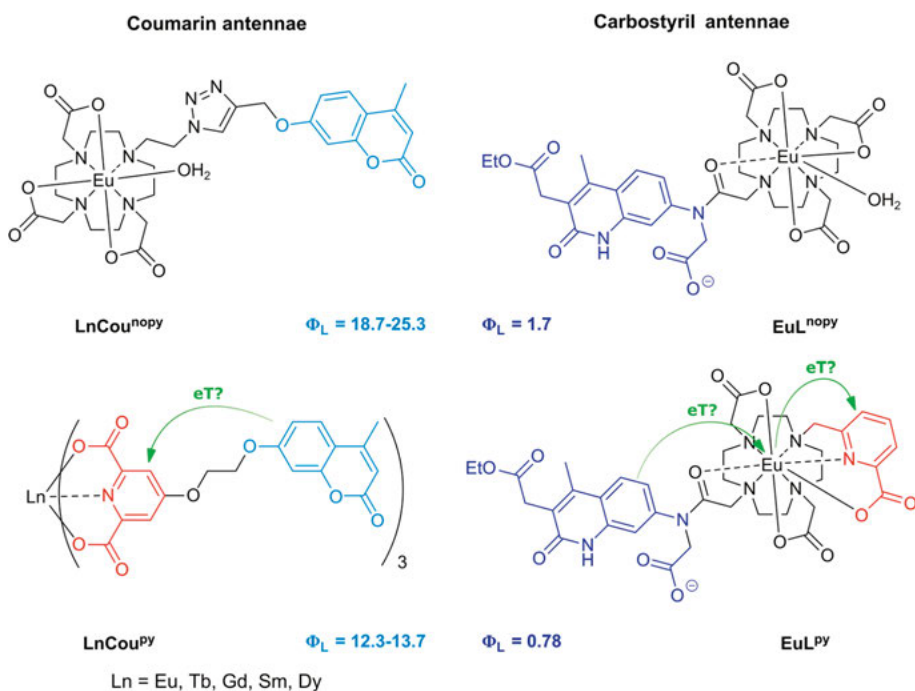


Figure 6 Putative electron transfer steps from carbostyryl (blue)⁶² and coumarin (turquoise)⁶³.

We have recently reported examples where PeT from the antenna to the Ln(III) was a dominant quenching process (**Figure 6**). For instance, the study of coumarin and carbostyryl sensitised Ln(III) complexes (Ln = Gd, Tb, Eu, Yb, Sm, Dy, Nd) established PeT quenching as feasible for several Ln(III) centres, not just the most reducible ones.²¹ In these systems the corresponding Gd(III) complex is the reference for the ligand-centred photophysical properties due to its inaccessible excited state and redox inactivity. The residual antenna fluorescence quantum yield (Φ_L) of luminescent Ln complexes was always lower than for the analogous Gd complexes. The loss

of ligand fluorescence was up to 65–95% in Eu complexes, and may result from a combination of S_1 -mediated energy transfer to the Ln(III) and PeT. The large negative reduction potential of Tb(III) rules out PeT (see Chapter 1.5), hence antenna fluorescence quenching is through S_1 energy transfer. Yb is sensitized by PeT.¹⁰ Assuming the same angle of FRET for the other Lns and a negligible difference in S_1 quenching by intersystem crossing, the reported sequence of quenching followed the reduction potential of Ln ions (Nd < Dy < Sm < Eu) indicating more efficient PeT to the more reducible Lns.

Previously in our group the elimination of a Ln-bound water was investigated with the aim of maximizing Ln(III) luminescence.⁶² DO3A-type complexes equipped with one bidentate picolinate pedant group, which replaced a monodentate methylcarboxylate arm were synthesised to change the ligand from octadentate to nonadentate (**Figure 6**, right). As expected, hydration state analyses confirmed the absence of a metal-bound water molecule. Surprisingly, the nonadentate complex **EuL^{py}** showed the same Eu(III) luminescence quantum yield (Φ_{Eu}) as its octadentate parent **EuL^{nopy}**, while Φ_{L} was halved (1.7 and 0.78 % for **EuL^{nopy}** and **EuL^{py}**, respectively). PeT from the excited state antenna to the pyridine may deplete Φ_{L} . Re-analysis of our previous work on pyridine-linked oxycoumarin antennae further supported the hypothesis.⁶³ The oxycoumarin Φ_{L} significantly decreased when linked to a pyridine (**LnCou^{py}**) compared to the values seen in complexes lacking the pyridine (**LnCou^{nopy}**). This decrease was observed regardless the nature of the lanthanide, including non-photoactive, non-redox active Gd(III), photoactive and redox inactive Tb(III), and luminescent and reducible Eu(III).

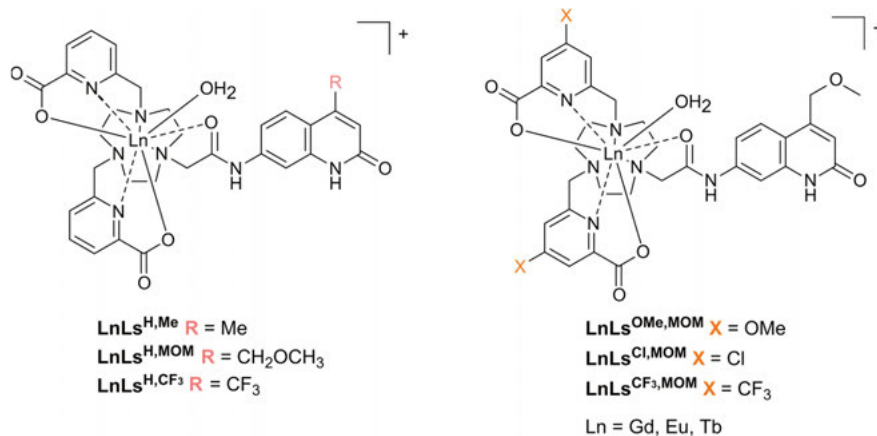


Figure 7 Complexes synthesised for the investigation of antenna-pyridine interactions.

Pyridine-based ligands are well established for Ln coordination, however their role as potential oxidants of the excited state antenna have not been studied yet. Unexpected characteristics of pyridine pedants were found in terms of photoexcited Ln(III) complexes. Pyridines are assumed to be involved in

additional quenching processes. Thus, we designed and synthesised a series of complexes with various carbostyryl light harvesting antennae linked to the 1,4,7-triazacyclononane (TACN) macrocycle *via* a secondary amide linker. The TACN core was equipped with picolinate pendant arms (**Figure 7**). Sensitisation was performed by carbostyryl antennae substituted with either electron-donating Me, or slightly or strongly electron-withdrawing MOM or CF₃ groups in the 4-position (**Figure 8**).

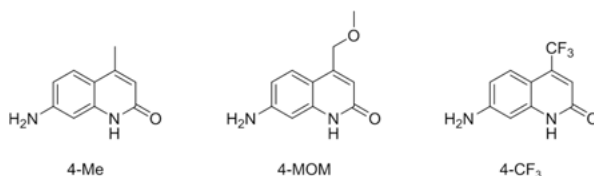


Figure 8 Substituted carbostyryl analogues in the 4-position

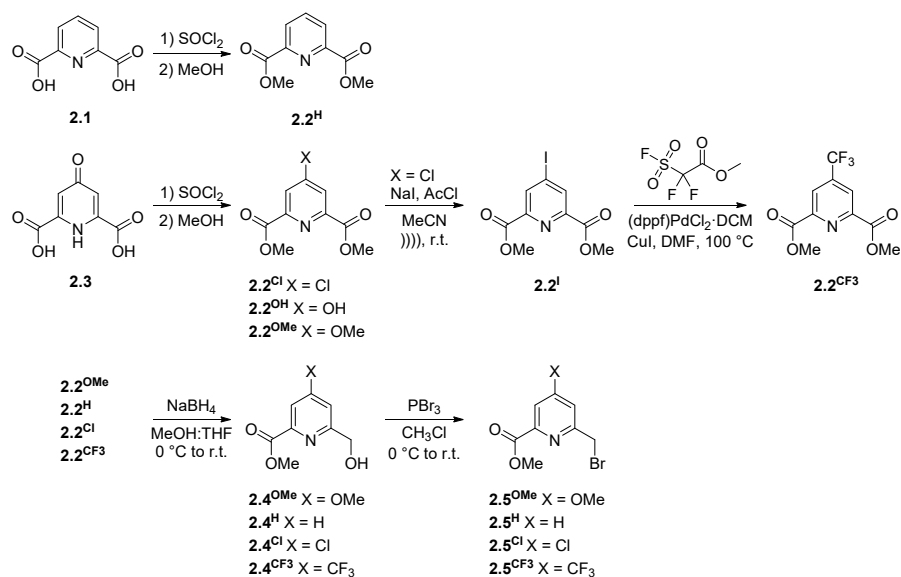
To investigate our hypothesis, two sets of ligands were synthesised. Firstly, unsubstituted picolinates were combined with a series of carbostyryls incorporated into the TACN core (**Ls^{H,Me}**, **Ls^{H,MOM}** and **Lc^{H,CF₃}**, Figure 3, left). In the second set of ligands the coordination sphere was furnished by carboxypyridines with electron-donating (OMe, **Ls^{OMe,MOM}**), electron-neutral (H, **Ls^{H,MOM}**) and electron-withdrawing (Cl, **Ls^{Cl,MOM}** and CF₃, **Ls^{CF₃,MOM}**) *para*-substituents; MOM-substituted carbostyryl was used for this latter series (Figure 3, right). Ligands were octadentate, thus the Ln(III) coordination sphere was completed by a water molecule. Bound water molecules quench Ln(III) emission, hence keeping their number constant is necessary when Ln(III) emission is to be compared.

2.2 Synthesis of new ligands and Ln(III) complexes

2.2.1 Synthesis of the picolinate pendant arms

The design and synthesis of the ligands and the complexes were done in collaboration with Dr. Daniel Kovacs. The 4-substituted picolinates (**2.5^{OMe}**, **2.5^H**, **2.5^{Cl}** and **2.5^{CF₃}**) were synthesised in a sequence of chemical steps where some of the target molecules served as the intermediates for other targets. The synthetic approaches are shown in **Scheme 1**.

2,6-pyridinedicarboxylic acid **2.1** was esterified in the presence of SOCl₂ in MeOH yielding **2.2^H**. Esterification of **2.3** (chelidamic acid) under same conditions afforded a mixture of **2.2^{Cl}**, **2.2^{OH}**, and **2.2^{OMe}**. Addition of methanol directly to the reaction mixture yielded **2.2^{Cl}** and **2.2^{OMe}** in poor yield. However, removal of SOCl₂ followed by the addition of methanol yielded **2.2^{Cl}** and **2.2^{OH}**.



Scheme 1 Synthesis of pyridine moieties **5^X** (X = OMe, H, Cl and CF₃)

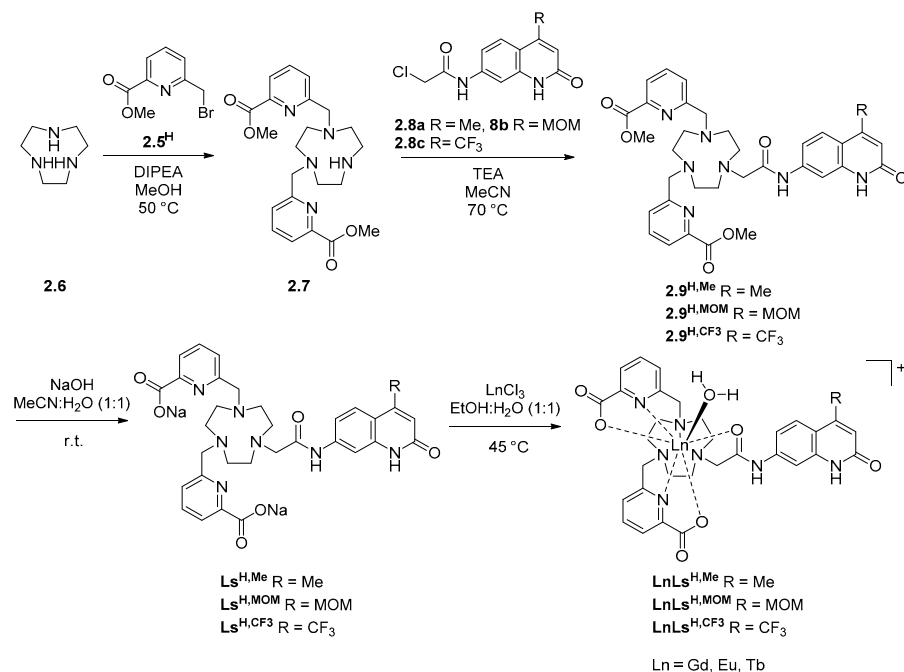
In order to obtain *para*-CF₃ substituted picolinate, **2.2^{Cl}** was converted into the 4-iodo derivative **2.2^I** by sonication with NaI and acetyl chloride in MeCN. Trifluoromethylation was achieved by reacting **2.2^I** with methyl 2,2-difluoro-2-(fluorosulfonyl)acetate using a (dppf)PdCl₂·CH₂Cl₂ catalyst and copper(I) iodide in DMF at 100 °C.⁶⁴ Combination of methyl 2,2-difluoro-2-(fluorosulfonyl)acetate with iodide yields :CF₂ carbene and F[−] which directly forms CF₃[−] with the extrusion of SO₂ and CO₂. In situ-generated [Cu-CF₃] undergoes a Pd-mediated cross-coupling reaction giving **2.2^{CF3}** in excellent yield (81%).

4-substituted diesters **2.2^{OMe}**, **2.2^H**, **2.2^{Cl}** and **2.2^{CF3}** can be reduced to the mono-alcohol using 1.4 eq. NaBH₄ in a MeOH:THF mixture. After addition of NaBH₄ at 0 °C, the mixture was allowed to warm to r.t. and stirred for approximately 2 hours. After aqueous work-up, **2.4^X** was isolated by column chromatography in 58–79% yield. The mono-alcohols **2.4^X**, where X = OMe, H, Cl and CF₃, were treated with PBr₃ yielding **2.5^{OMe}**, **2.5^H**, **2.5^{Cl}** and **2.5^{CF3}**, respectively, as building blocks of the picolinate bearing coordination sphere.

2.2.2 Assembly of ligands and Ln(III) complexes

The synthesis of the ligands could be accomplished following various pathways. Two possible routes are presented below. Following different strategies was necessary in order to be able to present two sets of complexes: differently substituted antennae carrying the same ligand environment vs same antennae carrying differently substituted ligand environment (Figure 3).

The synthesis of intermediates **2.8^X** (X = Me, MOM, and CF₃) was carried out following previously described procedures²¹. The preparation of intermediates and **LnLs^{H,X}** (Ln = Gd, Tb, Eu) is depicted in **Scheme 2**.

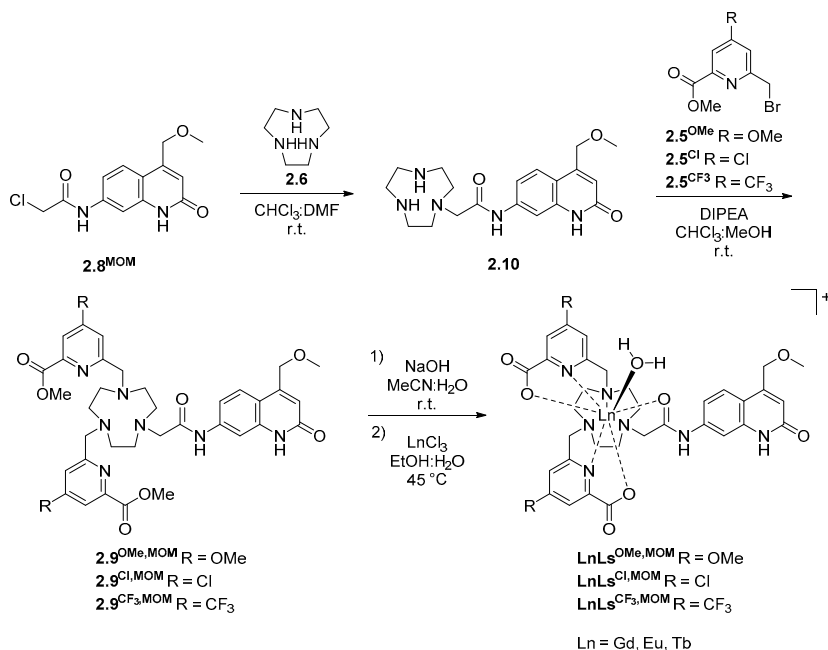


Scheme 2 Preparation of **LnLs^{H,X}** complexes

TACN (**2.6**) was reacted with unsubstituted picolinate methyl ester **2.5^H** in the presence of DIPEA in MeOH. Dialkylated derivative **2.7** was isolated in moderate yield as the major compound of a mixture of mono-, di- and tri-substituted TACN after column chromatography. Further alkylation was performed with chloroacetylated antennae **2.8^X** resulting methyl-ester protected ligands **2.9^{H,Me}**, **2.9^{H,MOM}**, and **2.9^{H,CF3}**. Basic hydrolyses in a mixture of aq. NaOH and MeCN at r.t. yielded the ligands isolated as sodium salts **Ls^{H,X}** after column chromatography. Complexation of **Ls^{H,X}** with **LnCl₃** (Ln = Gd, Eu, Tb) in a mixture of EtOH:H₂O was carried out at 45 °C. Reaction mixtures were directly loaded onto a silica chromatography column and eluted with iPrOH:H₂O to remove excess **LnCl₃** and, in some cases, small amounts of hydrolysed antenna residue. With this strategy we managed to synthesise a series of molecules having variously substituted antennae (Me-, MOM- and CF₃-) and the same ligand environment.

The second series of complexes were prepared following a slightly modified pathway (**Scheme 3**). TACN was monoalkylated with MOM-substituted carbostyryl **2.8^{MOM}** in a mixture of CHCl₃ and DMF. Dialkylation of **2.10** with substituted picolinate **2.5^X** was carried out using DIPEA as a base in a mixture of CHCl₃ and MeOH afforded methyl-ester protected ligands **2.9^{X,MOM}**.

Basic hydrolysis with aq. NaOH of protected esters **2.9^{X,MOM}** followed by chelation with LnCl₃ (Ln = Gd, Eu, Tb) in a mixture of warm EtOH and water yielded complexes **LnLs^{X,MOM}** (X = OMe, Cl and CF₃) according to the previously described procedure.

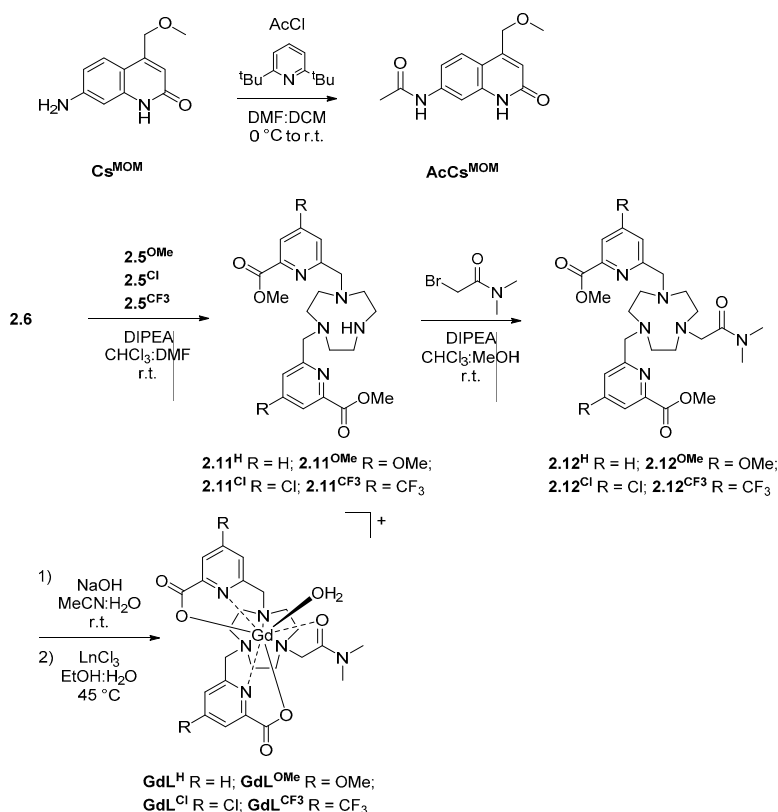


Scheme 3 Synthesis of **LnLs^{X,MOM}** complexes

2.2.3 Preparation of model compounds for cyclic voltammetry measurements

The redox properties of the light harvesting antennae were determined using model compounds lacking the potentially interfering lanthanide core (**Scheme 4**). Acetylation of **CS^{MOM}** was carried out in the presence of the bulky base 2,6-di-*tert*-butylpyridine using AcCl according to a slightly modified procedure that was described previously for acylation reactions.²¹

The model for the lanthanide core (**2.12^R**) contained a dimethyl amide arm instead of the antenna. This model retains the nonadentate coordination sphere, but lacks the redox active antennae which could interfere during the determination of the redox behaviour of the pyridine units. Dimethyl amide-carrying complexes (**GdL^R**) were synthesised in a fashion similar to the one described above and shown in **Scheme 4**. The more convergent route consisting of monoalkylation of **2.6** with *N,N*-dimethyl bromoacetamide followed by diversification with the picolinate moieties was tested.



Scheme 4 Synthesis of AcCS^{MOM} and GdL^{X}

However, monoalkylation yielded a complex mixture of mono-, di- and trialkylated species, the separation of which was difficult and low-yielding. Thus, the picolinate arms were installed first as these intermediates were more readily purified (**Scheme 4**). **2.6** was dialkylated with *para*-substituted bromomethyl derivatives 2.11^{R} ($\text{X} = \text{OMe}, \text{H}, \text{Cl}, \text{CF}_3$) under the previously established conditions (see Chapter 2.2.2). Dialkylated TACN intermediate 2.11^{R} was then further alkylated with *N,N*-dimethyl bromoacetamide. After basic hydrolysis of the methyl ester protected ligands complexation with GdCl_3 was carried out under usual conditions yielding model compounds GdL^{R} after column purification as white solids. Gd(III) was chosen as the model Ln(III) as it is difficult to reduce or oxidise, and was thus not expected to be redox active under the experimental conditions.

2.3 Electrochemical characterisation of picolinate bearing Ln(III) complexes

We hypothesised that excitation of the antenna resulted in PeT to both the reducible Ln(III) as well as to the pyridines, lowering the sensitisation efficiency, and thus decreasing Ln(III) luminescence^{62,63}. To have a better insight whether PeT is thermodynamically feasible the free energy change of electron transfer (ΔG_{ET}) was calculated according to Eq. 5. When charges are closer (i.e. the separation is less efficient), e_0^2/ϵ is greater, which would result more negative ΔG_{ET} values. Using 0.15 eV serves as a decent “worst case” scenario for our systems³⁴.

The calculation requires the determination of the reducing power of the photoexcited antennae and the reducibility of the *para*-substituted pyridines. Both of these could be determined by cyclic voltammetry of the appropriate model compounds **AcCS^{MOM}** and **GdL^X**.

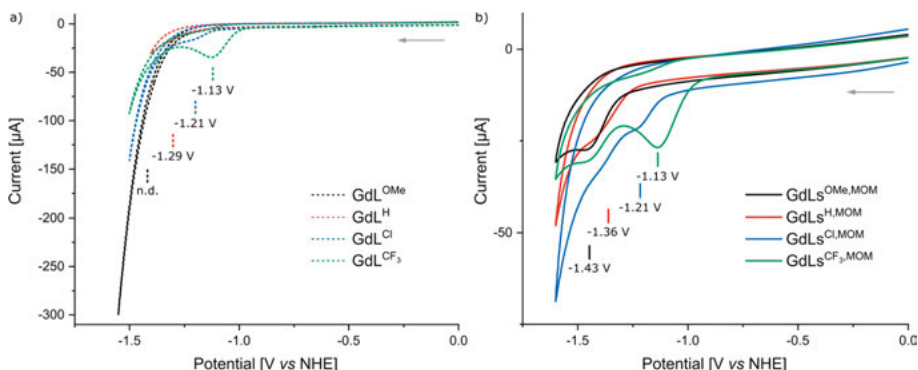


Figure 9 Cyclic voltammograms of 0.2 mM solutions of complexes in 100 mM aqueous NH_4Cl solution under Ar using a glassy carbon working electrode, $\text{Ag}/\text{AgCl}/\text{KCl}_{(\text{sat})}$ reference electrode, and a Pt wire counter electrode at 100 mV s⁻¹ scan rate. a) Overlaid cyclic voltammograms of **GdL^X** complexes. b) Overlaid cyclic voltammograms of **GdLs^{X,MOM}** complexes.

A series of model complexes **GdL^X** was synthesised to determine the reduction potential (E_{red}) of *para*-substituted pyridines by cyclic voltammetry while also avoiding possible interference by the antennae. Measurements were carried out in 100 mM NH_4Cl aqueous solutions under an Ar atmosphere using a glassy carbon working electrode, $\text{Ag}/\text{AgCl}/\text{KCl}_{(\text{sat})}$ reference electrode, and a Pt wire counter electrode at 100 mV/s scan rate. Due to weak responses and irreversibility one cycle was collected and used for further evaluation²⁶. Analyte concentration was 0.2 mM.

The CF_3 -substituted pyridines were expected to be the easiest to reduce providing an irreversible reduction wave at -1.13 V (vs NHE), while the Cl-substituted ones were less reducible and showed diminished response at -1.21 V (vs NHE). Along the series the H-substituted analogues revealed a faint

reduction wave at -1.29 V (vs NHE), while the reduction of the OMe-substituted one was outside of the solvent window (**Figure 9a**). The behaviour of the pyridines is similar to what was observed previously by M. D. C. Teixeira and co-workers addressing irreversible reductions of pyridines at -1.54 V vs Ag/AgCl/KCl_(sat.), -1.34 V vs NHE under acidic conditions.⁶⁵ **GdL**^{X,MOM} showed poorly defined irreversible reduction waves at -1.13 V, -1.21 V, -1.36 V, and -1.43 V (vs NHE) for X = CF₃, Cl, H, and OMe, respectively (**Figure 9b**). For **GdL**^{H,MOM} E_{red} was more negative by ~ 70 mV compared to the model **GdL**^H lacking the antenna. Changing the amide substituent on the antenna side could influence the reduction potential of both the metal and the coordination sphere.⁶⁶ Another reason could be the uncertainty of the determination of E_{red} , which was indeed challenging due to undefined responses.

In order to complete Eq. 1, first the oxidation potential of the donor, which is the ground state of the antenna, was measured in 100 mM TBAPF₆ solutions in MeCN under an Ar atmosphere. A glassy carbon working electrode, Ag/AgCl/KCl_(sat.) reference electrode, and a Pt wire counter electrode were used, and analyte concentration was 0.2 mM.

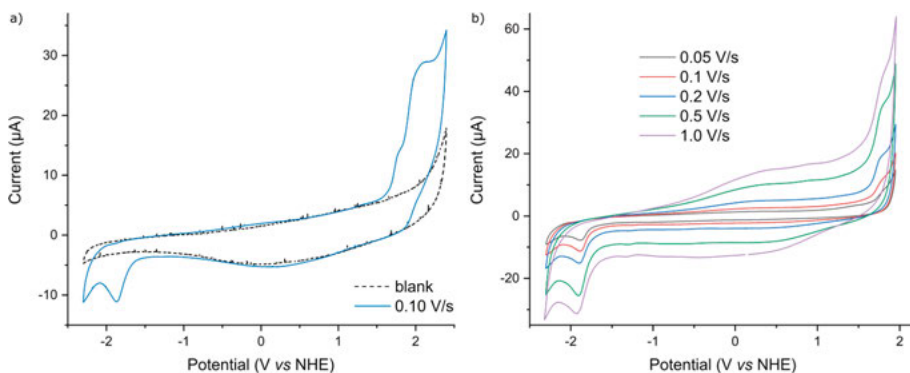


Figure 10 a) Cyclic voltammogram of 0.2 mM **AcCS**^{MOM} in 100 mM TBAPF₆ as a supporting electrolyte in MeCN under Ar using a glassy carbon working electrode, Ag/AgCl/KCl_(sat.) reference electrode, and a Pt wire counter electrode. a) Recorded at 100 mV/s scan rate. b) Variable scan rate measurement of first oxidation event.

According to various scan rate measurements E_{ox} of **AcCS**^{MOM} was 1.76 V vs NHE (**Figure 10**). The excited state energy of the donor was estimated to be 3.53 eV from the first vibronic band of the **GdL**^{X,MOM} emission spectra at 77 K. All values were converted to eV. Using Eq. 1 approximation for ΔG_{ET} in our systems yields:

$$\begin{aligned}\Delta G_{\text{ET}}^{\text{CF}_3} &= (1.76 - (-1.13)) - 3.53 - 0.15 = -0.79 \text{ eV} \\ \Delta G_{\text{ET}}^{\text{Cl}} &= (1.76 - (-1.21)) - 3.53 - 0.15 = -0.71 \text{ eV} \\ \Delta G_{\text{ET}}^{\text{H}} &= (1.76 - (-1.36)) - 3.53 - 0.15 = -0.56 \text{ eV}\end{aligned}$$

$$\Delta G_{ET}^{OMe} = (1.76 - (-1.43)) - 3.53 - 0.15 = -0.49 \text{ eV}$$

Negative ΔG_{ET} was calculated for **GdLs**^{X,MOM}, i.e. -0.79 eV ($X = \text{CF}_3$), -0.71 eV ($X = \text{Cl}$), -0.56 eV ($X = \text{H}$), and -0.49 eV ($X = \text{OMe}$). These large negative values mean that PeT is thermodynamically favored from the excited state antenna to the pyridine acceptors. A strong linear correlation was found between the Hammett σ_p constants and the reduction potential of the pyridine units (**Figure 11**). This observation further supports our hypothesis that as the reducibility of the pyridines increases, PeT quenching of the antenna towards pyridines also increases, which in turn is expected to result lower sensitization efficiency and decreased Ln(III) luminescence.

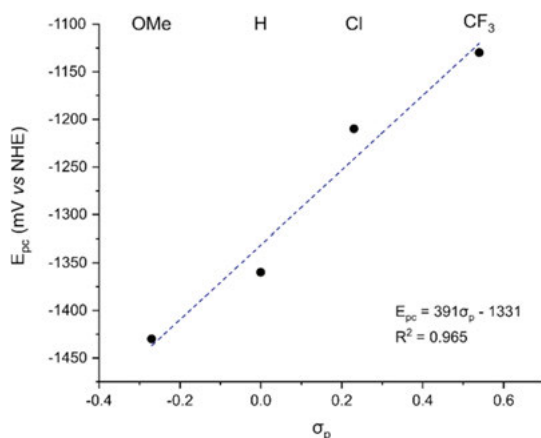


Figure 11 Values for linear fit of Hammett σ_p constants vs pyridine reduction potential

2.4 Structural characterisation of **EuLs** complexes in solution

The solution structures of the complexes were investigated using ^1H and ^{19}F NMR spectroscopic analysis of the paramagnetic Eu(III) species. Numerous studies have investigated the solution behaviour of TACN-based lanthanide complexes, still, full characterisation might be difficult.

The ^1H NMR spectra of the Ln(III) complexes ($\text{Ln} = \text{Nd}, \text{Eu}, \text{Lu}$) of the TACN-based nonadentate ligand equipped with three identical picolinate arms showed the presence of one set of signals with nine resonances. This agrees with the presence of a C_3 symmetric species.³¹ Substitution of one picolinate arm with a carboxymethyl group changes the ligand to octadentate and significantly changes the solution behaviour of the complexes. In theory each magnetically non-equivalent proton gives a separate signal, hence one could observe a set of 24 resonances in the ^1H NMR spectrum representing C_1

symmetry.^{67,35} In solution enantiomeric pairs of diastereomers exist. One set of signals suggests either the presence of a single conformer or rapid exchange between stereoisomers on the NMR timescale.³¹ Consequently, two pairs of diastereomers would result in two sets of proton resonances.

Recent studies have shown that the paramagnetic shift sequence of pyridyl TACN Ln(III) complexes is strongly dependent on the solvent and highly sensitive to the *para*-substituents.⁶⁸ Since minor structural modification of the ligand can cause dramatic changes in the proton NMR chemical shifts, assignment using only literature data is not possible.

On the other hand, full assignment of lanthanide complexes might be achievable. Beyond the standard ^1H and ^{13}C NMR measurements, ^1H - ^1H COSY and ^1H - ^1H NOESY experiments could provide valuable information regarding the position and orientation of protons. Heteronuclear NMR such as ^{19}F or ^{31}P could be essential to identify different species in solution. Variable temperature experiments might reveal the presence or absence of dynamic processes, moreover EXSY could be useful to study the exchange processes.

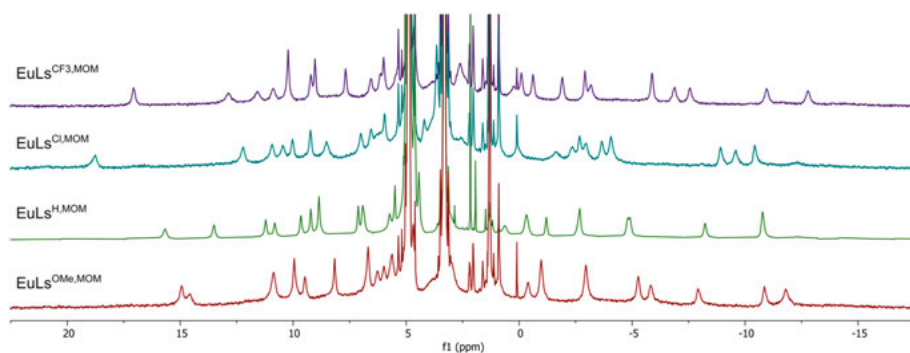


Figure 12 Stacked ^1H NMR spectra of **EuLs** (400 MHz, MeOD, r.t.)

The ^1H NMR spectra of **EuLs**^{CF₃,MOM}, **EuLs**^{Cl,MOM}, **EuLs**^{H,MOM} and **EuLs**^{OMe,MOM} were recorded at r.t. in MeOD (**Figure 12**). ^1H NMR spectra were consistent with the presence of two enantiomers of a single diastereomer. When measuring the samples at 0 or 80 °C signal broadening occurred in the ^1H NMR spectra compared to what was seen at r.t. This observation suggested the presence of a dynamic equilibria in the NMR time scale which was presumably slowed down at 0 and 80 °C. ^{19}F NMR spectrum consist of several resonances for **EuL**^{H,CF₃} at room temperature. Similar solution behaviour was found for **EuL**^{R,MOM}, indeed, differences in the photophysical properties are supposed to be ascribed to the structural changes in the ligand.

2.5 Photophysical characterisation of LnLs

The presence of pyridines in the coordination sphere is expected to change the Ln(III) (Ln = Gd, Tb, Eu) luminescence properties. The different *para*-substituents in the pyridines change their electron accepting ability, hence changes in Φ_L and Φ_{Ln} along with altered quenching and sensitisation processes are expected. Here, we discuss the results of the luminescent characterisation and the main findings on the role of the picolinate-bearing ligand environment.

The LnLs complexes (Ln = Gd, Tb, Eu) were characterised by UV-Vis absorption and steady-state and time-resolved emission spectroscopies. The photophysical properties were determined in PIPES-buffered aqueous solutions (pH 6.5) at complex concentrations in the 10–15 μ M range.

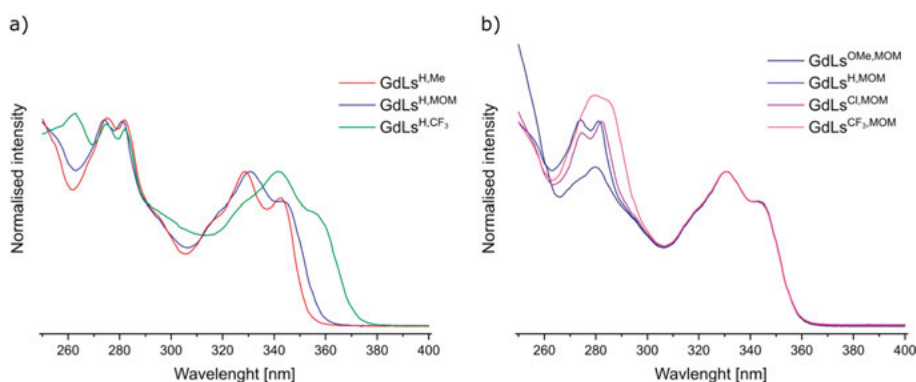


Figure 13 Superimposed normalised absorption spectra a) **GdLs^{H,R}** complexes b) **GdLs^{X,MOM}** complexes. Recorded in PIPES-buffered H₂O solutions at pH = 6.5 at room temperature. [GdL] = 10 μ M.

Changing both the *para*-substituent in the pyridine and the 4-substituent in the carbostyryl resulted different characteristics in the absorption spectra.

Different *para*-substituents yielded changes in the 260–310 nm range which is assigned to pyridine π – π^* transitions, while the absorption bands assigned to the carbostyryl (310–360 nm) remains unchanged (**Figure 13b**).

When the 4-substituent was changed (**Figure 13a**) the carbostyryl absorption maxima were red-shifted in the order **LnL^{H,Me}** ($\lambda_{\text{abs}} = 329$ nm) < **LnL^{H,MOM}** ($\lambda_{\text{abs}} = 331$ nm) < **LnL^{H,CF₃}** ($\lambda_{\text{abs}} = 342$ nm). Emission spectra were collected with $\lambda_{\text{ex}} > 330$ nm due to carbostyryl-based sensitisation. Upon antenna excitation weak antenna fluorescence was observed with a Stokes shift in the 3 600–3100 cm^{-1} range. The order of the emission maxima follows those of the absorption maxima, with the shortest λ_{em} for **LnL^{H,Me}** ($\lambda_{\text{em}} = 366$ nm), followed by **LnL^{H,MOM}** ($\lambda_{\text{em}} = 375$ nm) irrespective to the pyridine *para*-substituent, and finally **LnL^{H,CF₃}** ($\lambda_{\text{abs}} = 391$ nm) having the lowest energy emission (**Table 1**).

Table 1 Antenna photophysical properties of **LnLs**.^a

	λ_{abs} [nm]	λ_{em} [nm] ^b	$E_{00}(\text{S}_1)$ [cm ⁻¹] ^c	$E_{00}(\text{T}_1)$ [cm ⁻¹] ^c
GdLs^{H,Me}	329	366	28900	22900
GdLs^{OMe,MOM}	331	375	28500	22500
GdLs^{H,MOM}	331	375	28500	22500
GdLs^{Cl,MOM}	331	375	28500	22500
GdLs^{CF3,MOM}	331	375	28500	22500
GdLs^{H,CF3}	342	391	27400	21700

^a In aqueous PIPES buffer (10 mM, pH 6.5). ^b λ_{ex} = 329 nm (**GdLs^{H,Me}**), 331 nm (**GdLs^{MOM}**, **GdLs^{H,CF3}**). ^c Calculated from the 0–0 phonon transitions observed in the Gd complex at 77 K.

The T_1 energies of the antennae were determined from the low temperature steady-state emission spectra of the Gd(III) complexes. Samples were measured at 77 K with 10% glycerol added to the nominally 10 μM , PIPES buffered aqueous solutions (**Figure 14**). Gd(III) ion has a similar size and atomic weight as Eu(III), but lacks a low energy metal-centred acceptor level. Excitation at λ_{abs} resulted in ligand-based fluorescence and phosphorescence, the latter is attributed to emission from the ligand T_1 . T_1 energy levels were determined from the 0–0 phonon transitions. The lowest energy T_1 was found for the CF_3 -substituted antenna at 21700 cm⁻¹, followed by the MOM-substituted one at 22500 cm⁻¹, and finally the Me-substituted antenna had the highest energy T_1 at 22900 cm⁻¹ (**Table 1**).

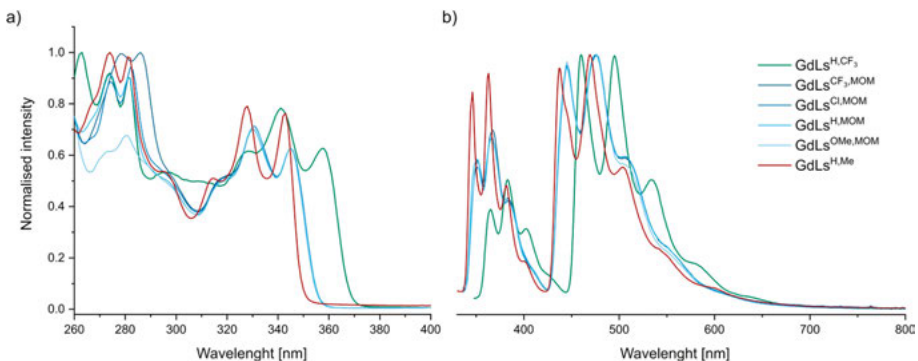


Figure 14 Superimposed a) excitation and b) steady-state emission spectra of **GdLs** at 77 K. λ_{em} = 460, 445, 437 nm and λ_{max} = 341, 335 and 330 nm for **GdL^{H,CF3}**, **GdL^{R,MOM}** and **GdL^{H,Me}**, respectively. Recorded in PIPES-buffered H_2O solutions at pH = 6.5 at room temperature. [**GdL**] = 10 μM .

As expected, no change to the antenna emission spectra was observed upon changing the *para*-substituent in the pyridine unit (**Figure 14**). The excitation spectra of the phosphorescence bands matched the absorption spectra in the whole range. However, the excitation spectra of the fluorescence bands

showed slight differences in the region attributed to the pyridines which could be due to the observable triplet energy levels of picolinates in this region.

Tb and Eu have excited states at 20400 cm^{-1} ($^5\text{D}_4$), and 19000 cm^{-1} ($^5\text{D}_1$) and 17200 cm^{-1} ($^5\text{D}_0$), respectively¹³. The antenna excited state should be above 22000 cm^{-1} in order to avoid thermal BET in Tb complexes^{13a}, and triplet-mediated sensitisation requires an energy gap of $2500\text{--}5000\text{ cm}^{-1}$ between the chromophore and Ln excited state. The antenna T_1 are well-positioned for energy transfer to Eu(III), as they are more than 2000 cm^{-1} but no more than 5000 cm^{-1} above its emissive state ($^5\text{D}_0$). The CF_3 -substituted antenna T_1 (21700 cm^{-1}) was within 2000 cm^{-1} above the Tb(III) excited state ($^5\text{D}_4$) which may facilitate BET.

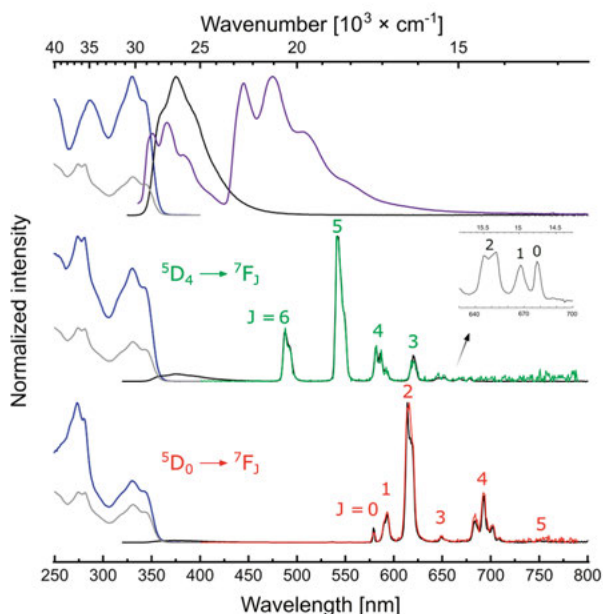


Figure 15 Normalised absorption (grey). Excitation [blue, $\lambda_{\text{em}} = 405\text{ nm}$ (Gd, top), $\lambda_{\text{em}} = 542\text{ nm}$ (Tb, middle), $\lambda_{\text{em}} = 614\text{ nm}$ (Eu, bottom)], steady-state emission [black, $\lambda_{\text{ex}} = 335\text{ nm}$], steady-state emission [purple, $\lambda_{\text{ex}} = 335\text{ nm}$ (Gd) 77 K] and time-resolved emission [green (Tb), red (Eu), $\lambda_{\text{ex}} = 335\text{ nm}$] spectra of $\text{LnLs}^{\text{H,MOM}}$ complexes with transitions indicated. Recorded in PIPES-buffered H_2O solutions at $\text{pH} = 6.5$ at room temperature. $[\text{LnL}] = 10\text{ }\mu\text{M}$.

Tb and Eu complexes had intense Ln-centred emission upon antenna excitation ($\lambda_{\text{ex}} = 330\text{ nm}$) (**Figure 15**). The LnLs excitation and absorption spectra showed great similarity, as expected for chromophore-sensitised Ln emission. Ln emissions were at 488, 543, 582, 620, 652, 668 and 678 nm for Tb and 579, 593, 614, 649, 693 and 751 nm for Eu, corresponding to the $^5\text{D}_4 \rightarrow ^7\text{F}_J$ ($J = 6\text{--}0$) and $^5\text{D}_0 \rightarrow ^7\text{F}_J$ ($J = 0\text{--}5$) transitions, respectively. In the Eu emission spectrum the hypersensitive and higher energy $^5\text{D}_1 \rightarrow ^7\text{F}_J$ ($J = 0, 1$) transitions were located at 537 and 554 nm, respectively. The Tb and Eu

emission profiles were different from the cyclen-based analogues (i.e. same antenna and linker) which represents the different coordination environment.

Table 2 Ligand and metal-based emission quantum yields,^a luminescent lifetimes and calculated inner-sphere water molecules of Gd and Tb complexes.^b

	Φ_L [%] ^a	Φ_{Ln} [%] ^a	τ_{H_2O} [ms] ^c	τ_{D_2O} [ms] ^c	q
GdLs^{H,Me}	4.4	/	/	/	/
GdLs^{OMe,MOM}	6.9	/	/	/	/
GdLs^{H,MOM}	6.4	/	/	/	/
GdLs^{Cl,MOM}	4.6	/	/	/	/
GdLs^{CF3,MOM}	2.1	/	/	/	/
GdLs^{H,CF3}	4.5	/	/	/	/
TbLs^{H,Me}	3.5	27.1	1.12	1.67	1.2
TbLs^{OMe,MOM}	5.2	30.6	0.76	1.01	1.3
TbLs^{H,MOM}	4.9	28.1	0.82	1.08	1.2
TbLs^{Cl,MOM}	3.6	25.4	0.73	0.99	1.5
TbLs^{CF3,MOM}	1.8	13.1	0.60	0.94	-
TbLs^{H,CF3}	4.1	3.3	0.09	0.16	-

^a Relative to quinine sulfate ($\Phi = 0.59$) in H₂SO₄ (0.05 M).⁶⁹ ^b In PIPES buffered (10 mM, pH 6.5), non-deaerated aqueous solutions at nominally 10 μ M complex concentrations. ^c Lifetime values were averaged from three independent measurements and are subject to an error of $\pm 10\%$.¹⁶

The overall luminescence quantum yields (Φ_{Ln}) of the complexes were determined in 10 mM aqueous PIPES buffer (pH = 6.5) using quinine sulfate ($\Phi = 0.59$) in H₂SO₄ (0.05 M)⁶⁹ as the reference. Results are summarised in **Table 2** and **Table 3** for Gd and Tb complexes, and for Eu complexes, respectively. Tb(III) quantum yields were in the 25.4–30.6% range, with exceptions for emitters carrying a CF₃-substituent in either the antenna 4-position ($\Phi_{Tb} = 3.3\%$) or in the pyridine *para*-position ($\Phi_{Tb} = 13.1\%$). As discussed earlier, the CF₃-substituted antenna T_1 was within 2000 cm⁻¹ above Tb(III) excited state (⁵D₄). This gap is sufficient enough to promote thermal repopulation of T_1 from Tb(III) excited state which former is quenched by dissolved ³O₂. Deoxygenation of a sample of **TbLs^{H,CF3}** increased the Tb quantum yield while the ligand fluorescence remained unchanged. Eu(III) quantum yields were 0.8–8.0% which are within the range seen for carbostyryl-sensitised DO3A-based Eu(III) emitters.²¹ Data show a clear connection between the pyridine *para*-substituents and the quantum yields: the more electron withdrawing the substituent the lower the Φ_L . For example, the order of Φ_L in Gd complexes carrying the same antenna decreased in the

order OMe > H > Cl > CF₃ for substituted pyridines. The same trend of Φ_L is observed for Tb and Eu complexes, however the highest Φ_L was found for **EuLs^{H,MOM}** (Table 3). The very small Φ_L values of Eu complexes means that they have a large uncertainty, therefore these data should be handled carefully. The decrease in Φ_L was always together with the decrease in Φ_{Ln} along the series.

Table 3 Ligand and metal-based emission quantum yields,^a luminescent lifetimes, calculated inner-sphere water molecules and Eu(III)-centered photophysical properties of Eu complexes.^b

	EuLs^{H,Me}	EuLs^{OMe,MOM}	EuLs^{H,MOM}	EuLs^{Cl,MOM}	EuLs^{CF3,MOM}	EuLs^{H,CF3}
Φ_L [%] ^a	0.42	0.12	0.16	0.08	0.06	0.61
Φ_{Ln} [%] ^a	0.83	3.61	2.44	1.34	0.75	7.95
τ_{H_2O} [ms] ^c	0.50	0.51	0.50	0.49	0.48	0.51
τ_{D_2O} [ms] ^c	1.27	1.34	1.33	1.20	1.14	1.28
q	1.1	1.1	1.1	1.1	1.1	1.0
τ_{rad} [ms] ^d	2.87	2.67	2.86	2.69	2.85	2.87
Φ_{Eu}^{Eu} [%] ^e	17.4	19.0	17.5	18.2	16.9	17.8
η_{sens} [%] ^e	5	20	14	8	5	46

^a Relative to quinine sulfate ($\Phi = 0.59$) in H₂SO₄ (0.05 M).⁶⁹ ^b In PIPES buffered (10 mM, pH 6.5), non-deaerated aqueous solutions at nominally 10 μ M complex concentrations. ^c Lifetime values were averaged from three independent measurements and are subject to an error of $\pm 10\%$.¹⁶ ^d Calculated using Eq. 2. ^e Calculated using Eq. 1.^{11a}

The luminescent lifetimes of Tb(III) and Eu(III) complexes were determined using time-resolved luminescence spectroscopy (Table 2 and Table 3). Lifetimes measured in H₂O (τ_{H_2O}) were consistently around 0.5 ms for the Eu complexes. In D₂O these (τ_{D_2O}) were lengthened to ~ 1.30 ms. The number of coordinated water molecules (q) can be calculated using the following equations: Eq. 3 for Tb, and Eq. 4 for Eu^{16,17}. As expected, the complexes had one Ln(III)-coordinated water molecule which is consistent with the nine-coordinate environment.

The q -values obtained for **TbLs^{H,CF3}** and **TbLs^{CF3,MOM}** were unrealistic. Considering their structural similarities q is likely to be 1 in all the complexes. These Tb complexes are sensitive to oxygen, which suggests that BET to the antenna T_1 occurs, making the q -value determination impossible using the lifetime method. Furthermore, an alternative energy transfer involving the picolinates was considered. Recent studies have shown that certain substituents on the pyridines drastically lower their T_1 to the 20000–22000 cm⁻¹ range,⁷⁰ which could be well positioned for back energy transfer in our systems. We determined the T_1 energies of the picolinates from the 77 K

luminescent spectra of **GdLs^X** complexes. The luminescent spectra showed a lack of vibrational structure, hence T_1 energies were localised by deconvolution of the emission bands into Gaussian functions. T_1 levels were located at 25600, 25600, 25400 and 25100 cm^{-1} for **GdLs^X** (for X = OMe, H, Cl and CF₃, respectively). Such high T_1 levels are unlikely to be involved in energy transfer from Tb(III) to the pyridines.

The different substituents on the pyridine systematically decrease the overall quantum yield of the Ln complexes. The origin of this effect was analysed by determining η_{sens} and $\Phi_{\text{Ln}}^{\text{Ln}}$ of the Eu(III) complexes using Eq. 1 and 2 (see Chapter 1). The results are summarized in Table 3.

τ_{obs} and τ_{rad} of **EuLs^{X,R}** were in the 0.48–0.51 ms and 2.67–2.87 ms range, respectively. $\Phi_{\text{Ln}}^{\text{Ln}}$ values were all in the 16.9–19.0% range, which suggests similar Eu(III) coordination environment in the emitters. This was further supported by crystallographic data, and the identical luminescent spectral shape. η_{sens} values showed a large variation, between 5 and 46% in **EuLs^{H,Me}** and **EuLs^{H,CF3}**, respectively. The more electron-deficient antennae are less reducing, therefore they are less likely to promote PeT to the Eu(III)^{21,71}. η_{sens} values in this case follow the reducing ability of the antennae: 46% > 14% > 5% for **EuLs^{H,CF3}**, **EuLs^{H,MOM}** and **EuLs^{H,Me}**, respectively. For complexes with identical antennae the diversity in η_{sens} values must be due to the differences in the rest of the ligand. Such effect of η_{sens} might be possible either by shifting the Eu(III) reduction potential or *via* another quenching process which bypasses Eu(III). The former could be explained in a way that Eu(III) is stabilized more in an electron-rich environment, thus the formation of Eu(II) by PeT is disfavored. η_{sens} values decrease in the following order: **EuLs^{OMe,MOM}** > **EuLs^{H,MOM}** > **EuLs^{Cl,MOM}** > **EuLs^{CF3,MOM}**, with η_{sens} = 20, 14, 8 and 5%, respectively. On the other hand, such electron transfer does not explain the decrease in Φ_{L} and Φ_{Ln} for the hard-to-reduce Tb and Gd complexes.²⁰ Φ_{L} and Φ_{Ln} decreases in the same order from 5.3% to 1.8% and 30.6% to 3.1%, respectively for **TbLs^{X,MOM}**. Φ_{L} in Gd(III) complexes goes down from 7.0% to 2.2% with increasingly electron poor picolines (Table 2). These data are consistent with the direct quenching of the excited state antennae by the picolines which was found thermodynamically feasible (see Chapter 2.4).

2.6 Conclusions

A set of structurally related TACN-based Ln(III) complexes equipped with carbostyryl sensitizers was synthesised. The coordination sphere was furnished with differently substituted picolines with the aim of studying their effect on the luminescent properties. Photophysical characterisation confirmed the similarities of Ln complexes carrying OMe-, H-, Cl- and CF₃-substituents in

the pyridine *para*-position. The similarity was indicated by the shape of the Ln(III) emission spectra, and for all Eu(III) emitters similar τ_{obs} and τ_{rad} (average: 0.50 and 2.80 ms, respectively), and intrinsic quantum yield (median: 17.8%) were obtained regardless the pyridine or carbostyryl substituents. Notwithstanding the similarities, noticeable differences in quantum yields occurred in correlation with the picolinate *para*-substituents. Decreasing the electron density on the pyridine unit increases the electron accepting ability from the excited state antenna, thus the overall quantum yield of the complexes decreases in the order of OMe > H > Cl > CF₃. Calculation of ΔG_{ET} further supported this interpretation, as electron transfer to the pyridines was found to be thermodynamically favoured from the antenna S_1 . In Eu(III) complexes this alternative process competes with energy transfer and ligand-to-metal PeT, moreover it effects the emission of non-redox active lanthanides by quenching the residual antenna fluorescence of Gd(III) and Tb(III) emitters. This study demonstrates that pyridines can be involved in unwanted photochemical processes.

3. The role of tertiary amide linkers in improving the luminescent properties of TACN-based Ln(III) emitters (Paper II)

3.1 Introduction

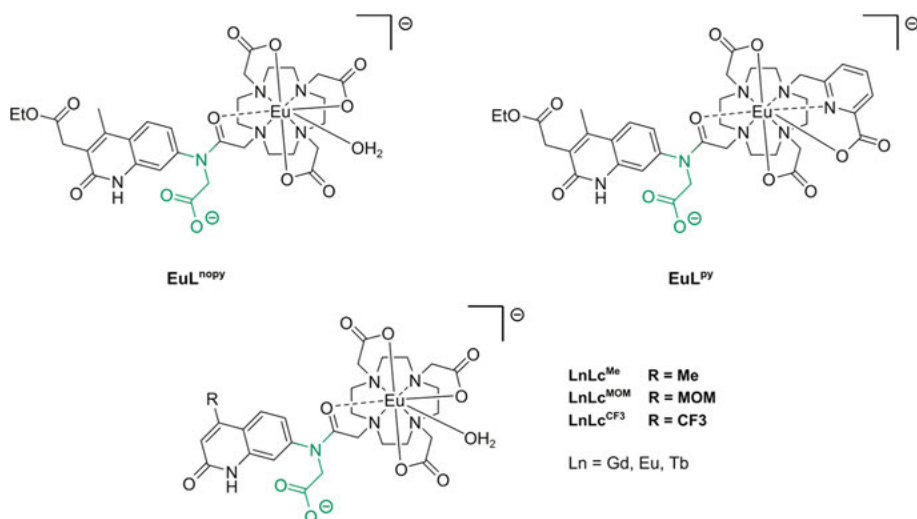


Figure 16 Previously reported tertiary amide-linked complexes with carboxystyryl antennae,⁶² including cyclen-based cores **LnLc^R**.⁷²

In Chapter 2 we concluded that carboxypyridines may be involved in an intra-ligand electron transfer from the excited state antenna. This quenching process was feasible even in the case of non-redox active Lns (e.g. Gd(III) and Tb(III)), and was indicated by a decrease of the residual ligand fluorescence. This alternative process was found thermodynamically favoured in Eu(III) complexes and it presumably competes with EnT and ligand-to-metal PeT. Electron-poor pyridines contribute to quenching and decrease the overall quantum yield.

A series of cyclen-based complexes (**LnLc^R**) was previously prepared equipped with an additional N-carboxymethyl group yielding a tertiary-amide linker (**Figure 16**),⁷² with substantially improved luminescent properties in comparison with the secondary-amide Eu and Tb complexes. The

improvement was much larger than would have been expected from the simple removal of a nearby N-H oscillator. **TbLc^R** had $\Phi_{\text{Ln}} > 40\%$ and showed 2–5-fold higher Φ_{Ln} than their non-alkylated analogues. **EuLc^R** had Φ_{Ln} in the 5.9–11.6% range. Some of these values were twice as high as in the corresponding secondary-amide complexes. The study concluded that a large part of gain in overall quantum yield was due to improved sensitization efficiency, η_{sens} .

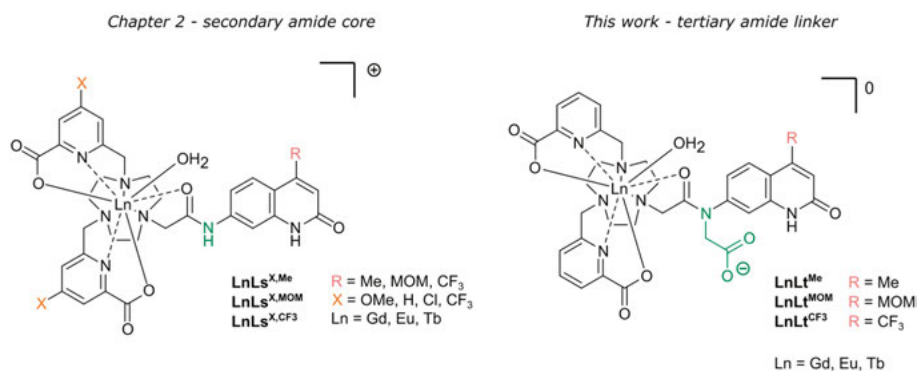
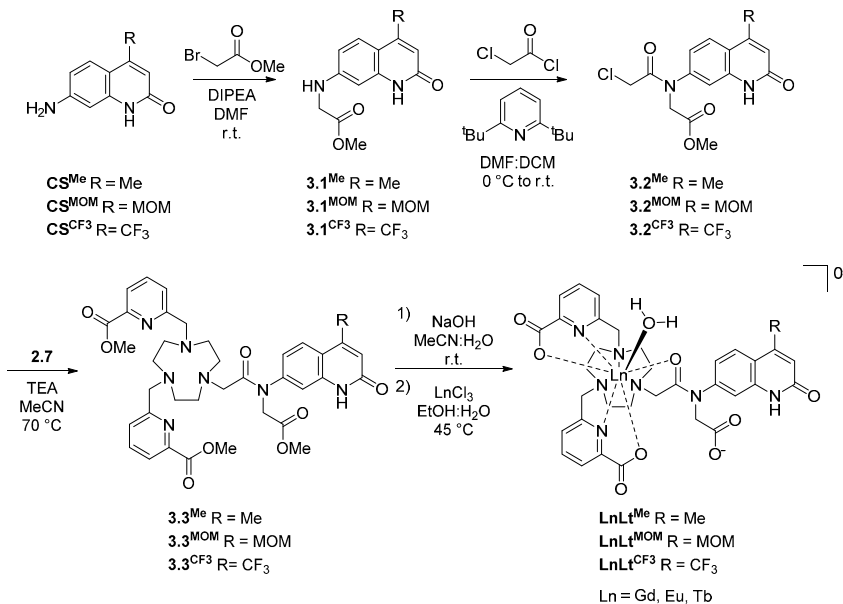


Figure 17 Secondary amide-linked carbostyryl-sensitised **LnLs^{X,R}** consisting of a TACN ligand framework equipped with substituted picolinic acid donors (left)⁷² **LnLt^R** complexes studied in Paper II (right).

In order to better understand sensitization and quenching pathways, we synthesized a new set of complexes **LnLt^R** that were analogous to **LnLs^R** (see Chapter 2.1) but were equipped with a tertiary amide linker (**Figure 17**). X-ray crystallography was used to investigate the Ln(III) coordination environment in the solid state. Photophysical characterization was performed by UV-Vis absorption, and steady-state and time-resolved emission spectroscopies. The luminescent properties of **LnLt^R** were compared to the series of secondary amide linked **LnLs^R**⁷³ and to a series of tertiary linked DO3A complexes **LnLc^R**⁷² (**Figure 16**). As expected, spectroscopic data revealed significant improvements in overall quantum yield and sensitization efficiency. These results show that even subtle structural changes can alter EnT and quenching processes.

3.2 Synthesis of new ligands and Ln(III) complexes

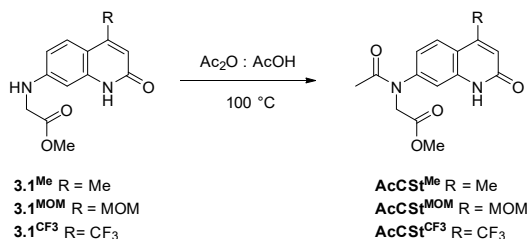
3.2.1 Preparation of tertiary-linked ligands and Ln(III) complexes



Scheme 5 Synthesis of LnLt^{X}

The synthesis of complexes bearing tertiary amide linkers occurred similarly to previously described procedures⁷² and is shown in **Scheme 5**. Firstly, alkylation of primary amine CS^{R} ($\text{R} = \text{Me, MOM, CF}_3$) with methyl bromoacetate was carried out in DMF using DIPEA base to introduce the tertiary amide motif. Acylation of 3.1^{X} using chloroacetyl chloride was performed in the presence of 2,6-di-*tert*-butylpyridine in a mixture of DMF and DCM, yielding key intermediates 3.2^{Me} , 3.2^{MOM} and 3.2^{CF_3} . Disubstituted TACN intermediate **7**, synthesised according to previously reported procedure,⁷³ was then further alkylated with the chloromethyl scaffold 3.2^{X} under the conditions used in section 2.2.2 affording the methyl ester protected ligands 3.3^{X} . Basic hydrolysis followed by chelation with LnCl_3 salts yielded the tertiary-amide complexes as white solids.

3.2.2 Preparation of model compounds for cyclic voltammetry measurements



Scheme 6 Preparation of Cst^{X} for cyclic voltammetry measurements

Model compounds for cyclic voltammetry measurements were prepared via acetylation of secondary amine carbostyrils 3.1^{X} (Scheme 6). The reactions were performed in a mixture of acetic anhydride and acetic acid at high temperature.⁷⁴ Purification by column chromatography on silica gel yielded tertiary amide model antennae AcCSt^{Me} , $\text{AcCSt}^{\text{MOM}}$, and $\text{AcCSt}^{\text{CF}_3}$ as beige solids.

3.3 Electrochemical characterisation of tertiary amide Ln(III) complexes

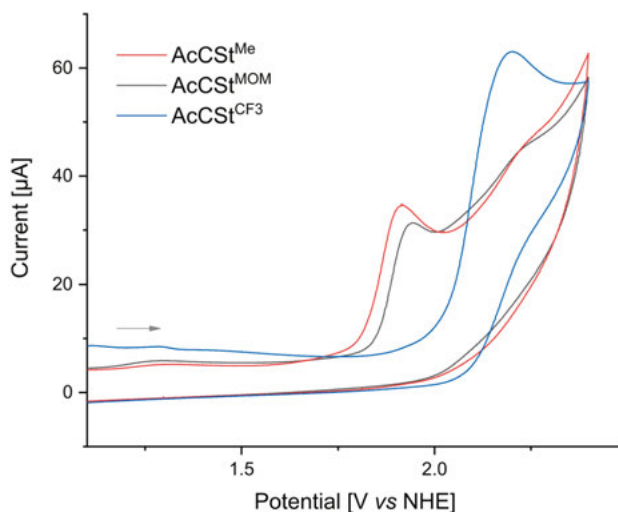


Figure 18 Cyclic voltammograms of 1 mM AcCSt^{Me} (red), $\text{AcCSt}^{\text{MOM}}$ (black), $\text{AcCSt}^{\text{CF}_3}$ (blue) in 200 mM TBAPF₆ as a supporting electrolyte in MeCN under Ar using a glassy carbon working electrode, Ag/AgCl/KCl(sat.) reference electrode, and a Pt wire counter electrode.

The thermodynamic feasibility of PeT from the antennae to the pyridines and to the Eu(III) can be determined using the method described in Chapter 2.3.

The oxidation potentials of the tertiary amide model compounds **AcCSt^{Me}**, **AcCSt^{MOM}** and **AcCSt^{CF₃}** (Scheme 6) were determined by cyclic voltammetry (Figure 18). Measurements were carried out in 200 mM TBAPF₆ solutions in MeCN under an Ar atmosphere using a glassy carbon working electrode, Ag/AgCl/KCl_(sat.) reference electrode, and a Pt wire counter electrode. Analyte concentration was kept at 1 mM. As expected, the carbostyryl carrying the electron donating 4-Me substituent was easiest to oxidise with $E_{ox} = +1.91$ V vs NHE, followed by the slightly electron-withdrawing MOM and strongly electron-withdrawing CF₃ substituted ones, which had $E_{ox} = +1.94$ V and $+2.20$ V vs NHE, respectively (Figure 18).

3.4 Structural characterisation of Ln(III) complexes

3.4.1 X-ray crystallography: comparison of **LnLs** and **LnLt**

The solid-state structures of several complexes were investigated by X-ray crystallography, performed by our collaborator Dr. Jordann Wells. Single crystals suitable for X-ray diffraction analysis were obtained by vapor diffusion of glyme into concentrated aqueous solutions of both secondary and tertiary amide Ln(III) complexes. Single crystals of **GdLs^{H,MOM-F}**, **TbLs^{CF₃,MOM-Cl}**, **GdLs^{Cl,MOM-F}** and **EuLs^{Cl,MOM-Cl}** are carrying secondary-amide linkers, whereas **GdLt^{Me}** and **TbLt^{Me}** are equipped with the extra carboxylic pedant representing the tertiary-linked motifs. The fluoride-containing structures were obtained in experiments where one equiv. KF was added to the complex solutions to facilitate crystal growth.

The Ln centre within the macrocyclic cavity exhibits a nine-coordinate (heavily) distorted tricapped trigonal prismatic geometry for both **LnLs** and **LnLt** complexes (Figure 19a). The trigonal prism is represented by three tacn N-donor atoms (N_{3PL}), and two pyridine N- and the antenna amide O-atoms (NNO_{PL}).

The remaining two pyridine carboxylate ligands and either a fluoride or chloride ion (**LnLs**) cap the trigonal prism. The two planes are not co-planar with N_{3PL}-Ln-NNO_{PL}; angles ranging 114–120° for **LnLs**, 115–117° for **LnLt** owing to the significantly distorted geometry. The distances between the Ln centres and the carboxylate Ln–O (Gd: 2.388(4) Å; Tb: 2.376(6) Å), tacn Ln–N (Gd: 2.646(4) Å; Tb: 2.64(1) Å) and pyridine Ln–N (Gd: 2.548(6) Å; Tb: 2.538(8) Å). Bond distances for **LnLt** compare well to those of related complexes, carboxylate Ln–O (2.403(2)–2.436(3) Å), TACN Ln–N (2.630(6)–2.671(7) Å) and pyridine Ln–N (2.532(6)–2.594(8) Å) for **LnLs**. The complexes are racemic in the solid-state with both Δ and Λ isomers present in the unit cell.

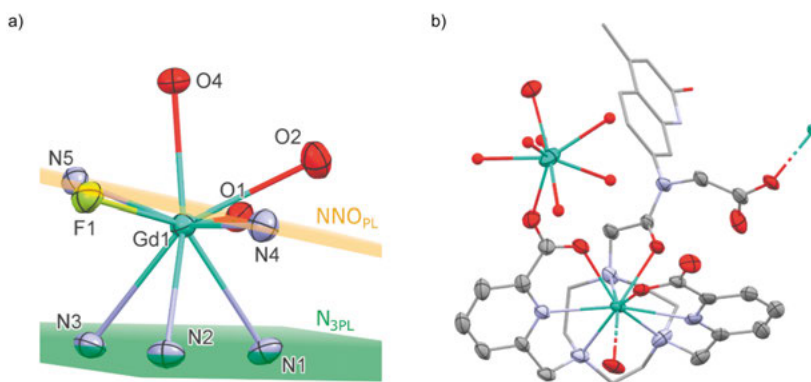


Figure 19 a) Gd coordination environment of $\text{GdL}^{\text{ClMOM-F}}$. b) Solid-state structure of TbLt^{Me} .

The presence of the non-coordinating carboxylate group on the amide functionality of the ligand in GdLt^{Me} and TbLt^{Me} results in a coordination motif not seen for related complexes containing secondary amides (LnLs). The carboxylate group acts as a bridging ligand between LnLt molecules, forming 1D-polymeric chains (**Figure 19b**). In addition, a secondary Ln centre is coordinated to a pyridine carboxylate $\text{C}=\text{O}$ bond, acting as a bridge between 1D-polymeric chains resulting in a 2D-polymeric network.

3.5 Photophysical characterisation of LnLt

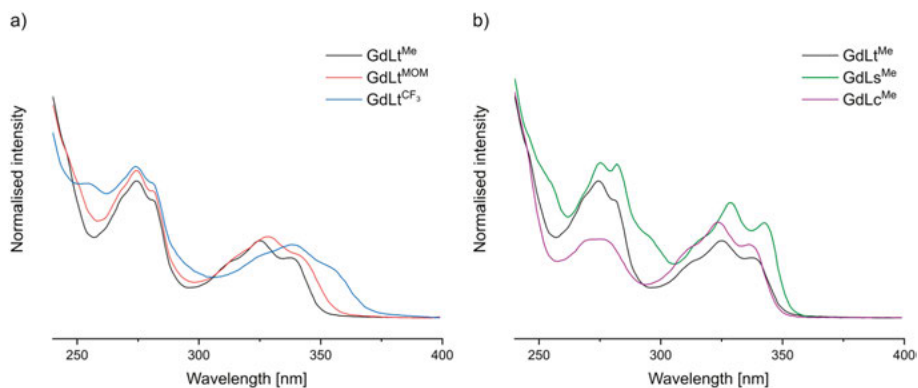


Figure 20 Superimposed normalised absorption spectra of a) GdLt^{R} complexes and b) GdL^{Me} complexes. Recorded in PIPES-buffered H_2O solutions at pH = 6.5 at room temperature. $[\text{GdL}] = 10 \mu\text{M}$.

The LnLt^{R} complexes ($\text{Ln} = \text{Gd}, \text{Tb}, \text{Eu}$) were characterised by UV-Vis absorption and steady-state and time-resolved emission spectroscopies under the same conditions as were used for LnLs^{R} and LnLc^{R} : in PIPES-buffered

aqueous solutions (pH 6.5) at complex concentrations in the 10–15 μM range. The **LnLt^R** absorption spectra contained absorption bands assigned to the pyridine $\pi\text{-}\pi^*$ transition in the 250–300 nm region. Indeed, this band was absent from the spectra of **LnLc^R**, but was present in **LnLs^R** (**Figure 20**). The region 300–370 nm is determined as antenna absorption. As expected, different substituents of the carbostyryl in the 4-position shift λ_{max} in the order **LnLt^{Me}** ($\lambda_{\text{abs}} = 325$ nm) < **LnLt^{MOM}** ($\lambda_{\text{abs}} = 328$ nm) < **LnLt^{CF3}** ($\lambda_{\text{abs}} = 338$ nm). Excitation at λ_{abs} yields weak antenna fluorescence at $\lambda_{\text{em}} = 366\text{--}391$ nm. However, λ_{abs} for **LnLt^R** were 3–4 nm shorter than the corresponding **LnLs^R**, this difference disappears in the emission spectra (**Table 4**).

Table 4 Antenna photophysical properties of **LnLs^R** and **LnLt^R**.^a

	λ_{abs} [nm]	λ_{em} [nm] ^b	$E_{00}(\text{S}_1)$ [cm^{-1}] ^c	$E_{00}(\text{T}_1)$ [cm^{-1}] ^c
GdLs^{Me}	329	366	28900	22900
GdLt^{Me}	325	365	29200	23000
GdLs^{MOM}	331	376	28500	22500
GdLt^{MOM}	328	375	28900	22800
GdLs^{CF3}	342	391	27400	21700
GdLt^{CF3}	338	391	27500	22000

^a In aqueous PIPES buffer (10 mM), pH 6.5, at 10 μM complex concentrations. ^b $\lambda_{\text{ex}} = 329$ nm (**GdLs^{Me}**), 325 nm (**GdLt^{Me}**), 335 nm (**GdLs^{MOM}**), 328 nm (**GdLt^{MOM}**), 331 nm (**GdLs^{CF3}**), 330 nm (**GdLt^{CF3}**).

^c Calculated from the 0–0 transitions of the Gd-complexes recorded at 77 K.

The antenna first triplet excited states (T_1) were determined from the 77 K steady-state emission spectra of the Gd-complexes. T_1 energy levels were calculated from the 0–0 phonon transitions observed in the low temperature spectra (see Chapter 2.5). Only a 100–300 cm^{-1} shift was observed in the antenna T_1 levels of **LnLt^R** compared to **LnLs^R** (**Table 4**). CF_3 -substituent in the 4-position lowered T_1 enough (21700 cm^{-1} for **LnLs^{CF3}**) to allow BET and make the complex sensitive to oxygen.⁷³ Generally, the antenna T_1 should be above 22000 cm^{-1} in order to avoid BET in Tb complexes.^{13a} The 300 cm^{-1} increase in triplet energy to 22000 cm^{-1} for **LnLt^{CF3}** is probably not enough to prevent BET.

Emission spectra were obtained upon antenna excitation $\lambda_{\text{exc}} > 325$ nm to avoid any interference from the pyridine units. Strong Ln(III) emission was observed for both Tb(III) and Eu(III) complexes (**Figure 21**). The spectral shape and ratio of peak intensities correlate with the Ln(III) coordination environment. Great similarity in emission spectral shapes was found for the secondary and tertiary complexes having picolates as the coordination sphere. In comparison, DO3A-based complexes **LnLc^R** impose different coordination geometry, hence spectral features differ from what was seen in

LnLs^R and **LnLt^R**. Ln emissions were at 488, 543, 582, 620, 652, 668 and 678 nm for Tb and 579, 593, 614, 649, 693 and 751 nm for Eu, corresponding to the $^5D_4 \rightarrow ^7F_J$ ($J = 6-0$) and $^5D_0 \rightarrow ^7F_J$ ($J = 0-5$) transitions, respectively. In the Eu emission spectrum, the hypersensitive and higher energy $^5D_1 \rightarrow ^7F_J$ ($J = 0, 1$) transitions were located at 537 and 554 nm, respectively.

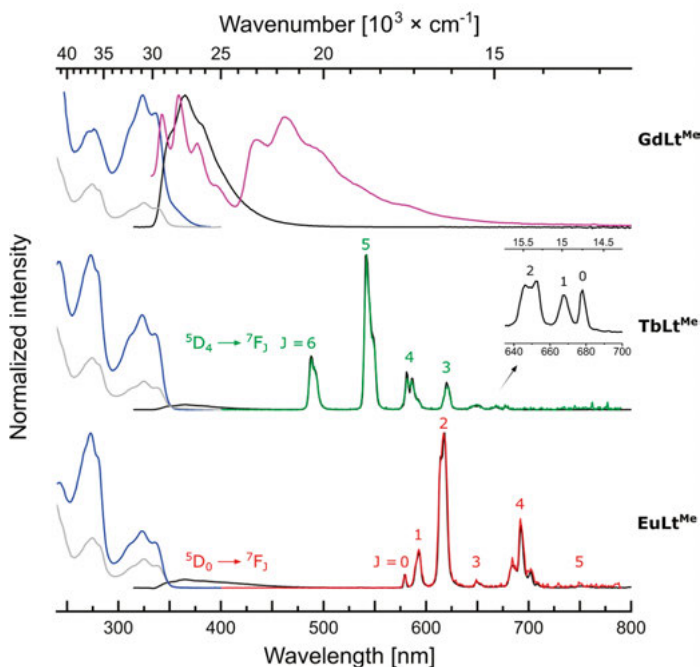


Figure 21 Normalised absorption (left, grey). Excitation [left, blue, $\lambda_{em} = 405$ nm (Gd), $\lambda_{em} = 542$ nm (Tb), $\lambda_{em} = 618$ nm (Eu), 298K], steady-state emission (middle, black, $\lambda_{ex} = 325$ nm, 298 K), steady-state emission [middle, purple, $\lambda_{ex} = 325$ nm (Gd), 77 K] and time-resolved emission (right, green (Tb), red (Eu), $\lambda_{ex} = 325$ nm) spectra of **LnLt^{Me}** complexes. Recorded in PIPES-buffered H₂O solutions at pH = 6.5 at room temperature. [**LnL**] = 10 μ M.

The luminescence quantum yields were measured according to the same procedure described in Chapter 2.5.⁶⁹ Data are summarized in **Table 5**. Clearly, Φ_{Ln} values obtained for the new series of Tb(III) and Eu(III) complexes were within the range of tertiary-amide linked DO3A-based Ln emitters (**LnLc^R**). The structural modification yielded significant increase in Φ_{Ln} in every case compared to the secondary amide-linked analogues (**LnLs^R**). The highest Φ_{Ln} value was obtained for **TbLt^{MOM}** (42%) and **EuLt^{CF3}** (13%). Ligand fluorescence Φ_L did not strictly follow the enhancement seen for the Ln emissions. Furthermore, no readily identifiable pattern in Φ_L was found for the different ligand frameworks.

Table 5 Ligand and metal-centred emission quantum yields.^a

	Φ_L [%]	Φ_{Ln} [%]	Complex	Φ_L [%]	Φ_{Ln} [%]	Complex	Φ_L [%]	Φ_{Ln} [%]
GdLs^{Me}	4.4	/	GdLs^{MOM}	6.4	/	GdLs^{CF3}	4.5	/
GdLt^{Me}	5.5	/	GdLt^{MOM}	4.9	/	GdLt^{CF3}	3.6	/
GdLc^{Me}	6.8	/	GdLc^{MOM}	5.1	/	GdLc^{CF3}	3.2	/
TbLs^{Me}	3.5	27.1	TbLs^{MOM}	4.9	28.1	TbLs^{CF3}	4.2	3.24
TbLt^{Me}	4.6	40.4	TbLt^{MOM}	4.3	41.5	TbLt^{CF3}	3.3	19.0
TbLc^{Me}	5.9	43.4	TbLc^{MOM}	4.5	45.1	TbLc^{CF3}	3.1	15.9
EuLs^{Me}	0.42	0.83	EuLs^{MOM}	0.16	2.44	EuLs^{CF3}	0.61	7.95
EuLt^{Me}	0.96	3.45	EuLt^{MOM}	1.32	5.22	EuLt^{CF3}	1.32	13.0
EuLc^{Me}	1.50	6.00	EuLc^{MOM}	2.5	8.9	EuLc^{CF3}	2.5	11.6

^a Relative to quinine sulfate ($\Phi = 0.59$) in H₂SO₄ (0.05 M).⁶⁹

The ligand environment was designed to be octadentate, hence one metal-bound water molecule was expected, similarly to the secondary-amide linked complexes. The number of coordinated water molecules (q) were calculated from the luminescent lifetimes of the Tb(III) and Eu(III). Lifetimes measured in H₂O (τ_{H_2O}) were consistently 0.51–0.52 ms for the Eu complexes. In D₂O these (τ_{D_2O}) were lengthened to 1.43 ms. As expected, the complexes had one Ln(III)-coordinated water molecule ($q = 1$) which is consistent with the nine-coordinate metal in an octadentate ligand environment (**Table 6**). The q -values obtained for Tb(III) complexes confirmed the presence of one water molecule bound to the metal.

Table 6 Ln(III) τ_{obs} and q -values in EuLt^R and TbLt^R.^a

	τ_{H_2O} [ms]	τ_{D_2O} [ms]	q^b
TbLt^{t,Me}	1.37	2.13	1.0
EuLt^{t,Me}	0.51	1.43	1.2
TbLt^{t,MOM}	1.30	2.01	1.1
EuLt^{t,MOM}	0.52	1.43	1.2
TbLt^{t,CF3}	0.62	1.01	2.7*
EuLt^{t,CF3}	0.52	1.43	1.2

^a Recorded in PIPES-buffered H₂O or D₂O solutions at pH = 6.5 at room temperature. ^b Calculated using $q = (5 \text{ ms}) \cdot (1/\tau_{H_2O} - 1/\tau_{D_2O} - 0.06 \text{ ms}^{-1})$ for Tb, and $q = (1.2 \text{ ms}) \cdot (1/\tau_{H_2O} - 1/\tau_{D_2O} - 0.25 \text{ ms}^{-1} - m \cdot 0.075 \text{ ms}^{-1})$ for Eu; m = number of nearby amide N-H oscillators.^{16,17} * Real q value could not be determined.

Nevertheless, the q -value was not possible to obtain for **TbLt**^{CF₃}. BET in **TbLt**^{CF₃} was already presumed due to the low lying T_1 excited state of the antenna which makes the q -value determination unreliable. Considering the structural similarities with the other complexes, q is likely 1.

Φ_L and Φ_{Ln} values in **LnLt**^R appeared within the same range than in **LnLc**^R. Plausible explanations could be that i) PeT to the pyridines was less efficient in **LnLt**^R than in **LnLs**^R or ii) energy transfer to the Ln(III) was more efficient than the competing PeT.

The free energy change of electron transfer was calculated using Eq. 5. E_{ox} is the oxidation potential of the donor, here the tertiary amide-modified antennae. $E_{ox} = +1.91, +1.94$ V and $+2.20$ V vs NHE was determined in **AcCSt**^{Me}, **AcCSt**^{MOM} and **AcCSt**^{CF₃}, respectively. E_{red} is the reduction potential of the acceptor (unsubstituted pyridine or Eu(III)), E_s is the (singlet) excited state energy of the antenna. As in section 2.4, the last term was taken to be ~ 0.15 eV. E_{red} of the non-substituted pyridines was approximated with the value obtained in Chapter I, -1.29 V vs NHE.⁷³ The excited state energies of the antennae were determined from the first vibronic band of the **GdLt**^x emission spectra at 77 K, and were located at 3.60, 3.57, and 3.39 eV for **GdLt**^{Me}, **GdLt**^{MOM}, and **GdLt**^{CF₃}, respectively. Using these values in Eq. 1 to calculate ΔG_{ET} yields:

$$\Delta G_{ETMe} = (1.91 - (-1.29)) - 3.60 - 0.15 = -0.55 \text{ eV}$$

$$\Delta G_{ETMOM} = (1.94 - (-1.29)) - 3.57 - 0.15 = -0.49 \text{ eV}$$

$$\Delta G_{ETCF3} = (2.20 - (-1.29)) - 3.39 - 0.15 = -0.05 \text{ eV}$$

PeT was found to be thermodynamically feasible in all cases, with the possible exception of the CF₃-substituted antenna. ΔG_{ET} for PeT from this antenna to the pyridine was -0.05 eV, which is not sufficiently negative to compensate for the margin of error in the calculation. The Coulombic attraction energy (e_0^2/ϵ) (see Chapter 2.4) has been taken as ~ 0.15 eV, which was used for exciplexes in acetonitrile.³⁴ Additionally, both reduction and oxidation potentials were derived from cyclic voltammograms showing irreversible processes, which adds further uncertainty to the calculations. ΔG_{ET} for PeT from the more electron-rich antennae were more negative, -0.49 eV and -0.55 eV for the MOM- and Me-substituted ones, respectively. If the separation of charges is greater, e_0^2/ϵ becomes smaller, hence PeT from the CF₃-substituted antennae may not be thermodynamically feasible.

PeT from the antennae to Eu(III) was calculated to be favourable, too. E_{red} of Eu(III) was approximated using the +1 charged cyclen-based complex and found to be -0.80 V vs NHE for a MOM-substituted antenna.⁷¹ This approximation was necessary due to the similar reduction potentials of Eu(III) and the pyridines, which could make E_{red} determination unreliable. As Eu(III) is easier to reduce than the pyridines, Eu(III) reduction was found to be even

more favorable thermodynamically, with ΔG_{ET} values of -1.04 , -0.98 , and -0.54 eV, for Me-, MOM- and CF_3 -substituted complexes, respectively.

Since the ΔG_{ET} values for electron transfer are negative, PeT is thermodynamically possible. The largest negative value is expected to result in the fastest PeT. Other factors can however have an impact on the rate of PeT, such as competition between EnT and PeT which is expected. Their rates would be dependent on the complex geometry as well as the thermodynamics. Furthermore, results suggest that other Lns for example Yb or Sm ($E_{\text{LnIII/LnII}} = -1.15$, -1.55 V vs NHE,²⁰ respectively) could be susceptible to PeT in our systems. On the other hand, Gd and Tb can be excluded due to their redox potentials below -3.6 V vs NHE.

The overall quantum yield can be determined by the efficiency of the sensitization η_{sens} and the intrinsic quantum yield $\Phi_{\text{Ln}}^{\text{Ln}}$. These values are well-determined for Eu(III) and can be calculated from the corrected Eu(III) luminescent spectra. While η_{sens} is affected by quenching processes of the antenna excited state e.g X-H oscillators, or PeT to or from the antenna, $\Phi_{\text{Ln}}^{\text{Ln}}$ is indicative of the coordination environment of the Ln(III) ion. The intrinsic quantum yield is proportional to the observed $\tau_{\text{H}_2\text{O}}$, and radiative lifetime τ_{rad} , which can be calculated according to Eq. 3. (see Chapter 1.4 and 2.5).

Table 7 τ_{rad} , $\Phi_{\text{Ln}}^{\text{Ln}}$, and η_{sens} of **EuL**.

	τ_{rad} [ms] ^a	$\Phi_{\text{Eu}}^{\text{Eu}}$ [%] ^b	η_{sens} [%] ^b
EuLt^s,Me	2.87	17.4	5
EuLt^t,Me	2.94	17.7	28
EuLc^t,Me	5.41	12.0	50
EuLt^s,MOM	2.86	17.5	14
EuLt^t,MOM	2.96	17.9	30
EuLc^t,MOM	5.40	12.2	73
EuLt^s,CF₃	2.87	17.8	46
EuLt^t,CF₃	2.99	17.4	75
EuLc^t,CF₃	5.40	12.2	95

^a Calculated using Eq. 2. ^b Calculated using Eq. 1.^{11a}

Similar τ_{rad} (~ 2.9 ms) was determined for **EuLs^R** and **EuLt^R** (Table 7). The slightly longer τ_{rad} yielded barely noticeable improvements in $\Phi_{\text{Ln}}^{\text{Ln}}$ of the tertiary-linked Eu(III) complexes ($\sim 17.5\%$ vs 12%). This observation was expected knowing that the additional arm attached to the tertiary amide is unlikely to impose dramatic changes in the coordination environment and is not coordinating to the metal. On the other hand, $\Phi_{\text{Ln}}^{\text{Ln}} \sim 17.5\%$ obtained for

EuLt^R is a considerable improvement compared with $\Phi_{Ln}^{Ln} \sim 12\%$ in DO3A-based **EuLc^R**. Consequentially, if complexes with identical antennae and similar coordination geometries have different η_{sens} , this difference might be due to differences in PeT. η_{sens} is remarkably higher in **EuLt^R** than in **EuLs^R** (e.g. 28% and 5% in **EuLt^{Me}** and **EuLs^{Me}**, respectively), but still not as high as in **EuLc^R** (50% in **EuLc^{Me}**). Despite the improvement in Φ_{Ln}^{Ln} in **EuLt^R** compared to **EuLc^R**, Φ_{Ln} remains similar or lower due to the lower η_{sens} . Another reason for the observed results may be a different antenna orientation or more efficient population of the Ln(III) feeding level (i.e. antenna T_1) courtesy to a more efficient intersystem crossing. Both **LnLc^R** and **LnLt^R** have tertiary-linked antennae, therefore the similar values of Φ_L correspond to a very similar level of antenna S_1 quenching. Furthermore, diminished η_{sens} in **LnLt^R** compared to **LnLc^R** is consistent with a more efficient energy transfer in DO3A-based complexes.

3.6 Photostability of LnL

The photostability of Ln(III) emitters is a crucial parameter from the practical point of view. Ln(III) excited states are not sensitive to oxygen¹⁴, therefore degenerative processes often occur to the organic chromophore yielding photodegradation of the complex. The antenna triplet is sensitive to quenching by molecular oxygen, thus the longer the lifetime of T_1 is, the greater the degradation. Long-lived antenna T_1 may arise due to BET from the Ln(III) excited state or because of slow energy transfer from T_1 to Ln(III) caused by too small or too large energy gap between antenna T_1 and Ln(III), respectively. The photostability of **LnLt^R** was compared to the secondary-linked **LnLs^R** and tertiary-linked DO3A based **LnLc^R** complexes. Samples were dissolved at $\sim 10 \mu\text{M}$ in PIPES-buffered distilled water at pH 6.5. The samples were continuously irradiated at the maximum excitation wavelength of the sample (see Figure 17 footnotes) for 4 h. The steady-state Ln(III) emission was recorded every 30 mins over a 4 h-period upon continuous irradiation. Integrated emission intensities for the entire spectral range (450–750 nm for Eu, 550–800 nm for Tb) were normalised to the value at t_0 (**Figure 22**).

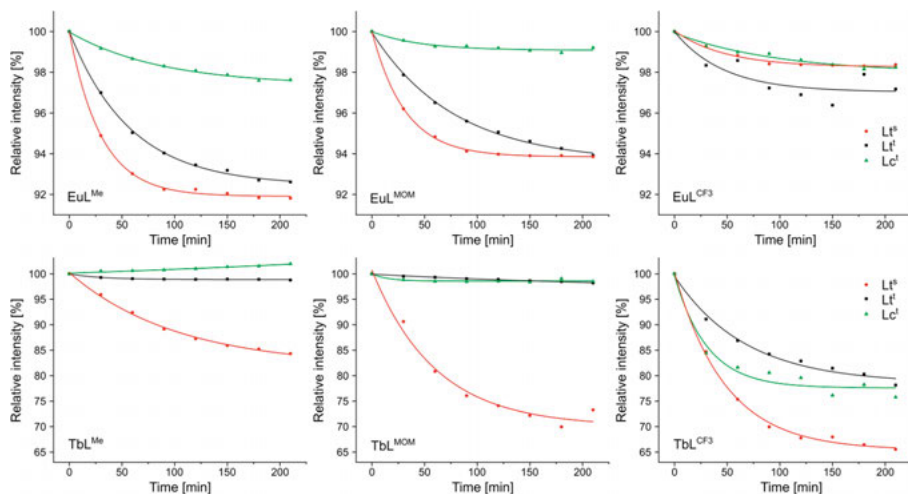


Figure 22 Photostability of Tb and Eu complexes (10 μ M) in aqueous PIPES buffer (10 mM), pH = 6.5, using 395 nm filter for Tb and 500 nm filter for Eu complexes, respectively. $\lambda_{\text{ex}}(\text{LnLc}^{\text{t,Me}}) = 324$ nm, $\lambda_{\text{ex}}(\text{LnLt}^{\text{t,Me}}) = 325$ nm, $\lambda_{\text{ex}}(\text{LnLc}^{\text{t,MOM/CF}_3}) = 327$ nm, $\lambda_{\text{ex}}(\text{LnLt}^{\text{s,Me/LnLt}^{\text{t,MOM}}}) = 328$ nm, $\lambda_{\text{ex}}(\text{LnLt}^{\text{s,MOM}}/(\text{LnLt}^{\text{s,CF}_3}/\text{LnLt}^{\text{t,CF}_3})) = 330$ nm. Values normalised to integrated emission intensity at t_0 .

The Eu(III) complexes preserved at least 90% of their luminescent intensities over the 4 h period of irradiation. **EuLc^R** seemed to be more stable than the tacn-based **EuLt^R** and **EuLs^R**, while the former was somewhat more stable than the latter. Retaining the luminescence intensities followed the order CF₃ > MOM > Me substituted carbostyrils. These observations suggest that PeT enhances a degradation pathway of these complexes. For the picolinate-containing complexes **EuLs^R** and **EuLt^R**, this pathway is amplified due to the presence of the pyridines and Eu(III) as a potential electron acceptor. For the Tb(III) complexes the stability order was the opposite than in Eu(III) complexes (Me > MOM > CF₃). As a result of the low antenna T_1 in **TbL^{CF3}** rapid degradation was observed. **TbLc^R** and **TbLt^R** had similar resistance against photodegradation, however secondary-linked **TbLs^R** suffered ~25–35% loss of luminescent intensity in the 4 h period. Tertiary-linkers in **TbLt^R** and **TbLc^R** caused sufficient increase in antenna T_1 to diminish BET.

3.7 Conclusions

We demonstrated the effect of methylcarboxylate-substituted tertiary-amide linkers in structurally related TACN based emitters on the photophysical properties. A set of Ln (III) complexes were synthesised carrying substituted carbostyrils in the 4-position and non-substituted picolines. Structural similarities enabled us to compare the luminescent properties with complexes possessing secondary-amide linkers and cyclen-based systems lacking the

reducible pyridines. Single crystal X-ray analysis showed that the extra carboxylate arm did not coordinate to the metal in the solid state, hence it did not alter the coordination geometry of the Ln(III) compared to the secondary linked complexes. This was further supported by the shape of the Ln(III) emission spectra and, τ_{obs} and τ_{rad} in Eu(III) emitters. Within the series of tertiary-linked Tb(III) and Eu(III) emitters increased quantum yields were obtained compared to the secondary-linked analogues. Such high quantum yields were comparable and, in some cases even higher than, those obtained for cyclen-based systems lacking the quenching pyridine. The residual antenna fluorescence was not rigorously following the enhancement and no correlation was found for the different carbostyrils. The tertiary-linker resulted higher T_1 energy level of the antenna which was found to be beneficial preventing BET for Tb(III) complexes. Photostability studies showed the significance how minor structural changes can effect the excited state behaviour of Ln(III) emitters. Suppressing PeT and BET quenching pathways yielded highly photostable and robust emitters.

4. Monofluorinated carbostyrils as potential Ln(III) sensitisers (Paper III)

4.1 Introduction

Luminescent Ln(III) compounds have been widely used for optical purposes.^{3,55} Molecular Ln(III) complexes have been utilised as responsive and reactive probes in cellular imaging.⁶¹ Ln(III) ions are often sensitised by an organic chromophore which helps overcome the inherently low absorption of Ln(III).

In order to develop brighter emitters, the optimisation of EnT and minimisation of quenching processes are essential. To achieve the former, one needs to find the optimal excited state energies of the antenna which are well-placed for efficient EnT.⁶ EnT could take place from the antenna S_1 or T_1 energy level. Any subtle change in the chromophore might have unexpected consequences in S_1 and T_1 energy levels, subsequently altering the EnT processes and the metal centred luminescence. The most frequently used strategy for minimising quenching is the removal of X–H oscillators nearby the Ln(III). Deuteration^{16a} and fluorination² of the ligand have proved beneficial for decreasing the quenching of the excited state Ln(III) by X–H oscillators.

The antenna S_1 and T_1 are involved in EnT to the Ln(III) receiving levels. Thus, quenching of the antenna S_1 and T_1 states could result in diminished metal luminescence. Reducible Lns (e.g. Eu, Yb, Sm and Dy) can be susceptible to PeT from the antenna S_1 which might be detrimental to Ln(III) emission.²¹ PeT can be suppressed by modifying the ligand environment to stabilise the +3 oxidation state of the Ln,⁷¹ or through antenna modifications that raise the oxidation potential of the antenna. For instance, the protonation of phenanthridine antenna increased Eu(III) luminescence by reducing PeT, however incremental changes in the antenna T_1 decreased Tb(III) emission.⁷⁶ Antenna substitution by an EWG group (e.g. CF_3) reduced the extent of PeT in DO3A-based Eu(III) complexes resulting in higher Eu(III) emission.²¹

Tuning the chromophore through functionalisation might be beneficial or detrimental to Ln(III) emission, and the outcome of such an undertaking is difficult to predict. There is a lack of in-depth structure-activity studies targeting carbostyryl sensitisers, and, broadly, most types of sensitisers, possibly due to the synthetic challenges. Here, we designed a series of

monofluorinated carbostyryl antennae. The incorporation of the electronegative fluorine in the carbostyryl was expected to reduce PeT by raising the oxidation potential of the antenna. Furthermore, the C–F bond replaces a more efficient quencher i.e. a C–H oscillator, although this effect was expected to be undetectable for visible-emitting complexes.² The hydrogen isostere fluorine improves the metabolic stability, the H-bond acceptor ability and alters the lipophilicity of fluorinated substances. Therefore, fluorination is a strategy often used in pharmaceuticals.⁷⁷ The presence of a fluorine in the molecule would make it appealing for diagnostic applications. ¹⁹F-MRI has been a developing sensitive imaging technique,⁷⁸ while ¹⁸F is a well-known isotope used for radiolabelling of drugs or in imaging e.g. positron emission tomography.⁷⁹

Here, we report the preparation of monofluorinated carbostyryls which were incorporated into DO3A-based octadentate ligands and the Gd(III), Tb(III) and Eu(III) chelates that were synthesised. The complexes were characterised by ¹H NMR spectroscopy, cyclic voltammetry, UV-vis absorption, and steady-state and time-resolved emission spectroscopy. This study is intended to represent a structure-activity study. The results suggest that subtle changes in the antennae influence the excited state properties of Ln(III).

4.2 Synthesis of CS^F, L^F and Ln(III) complexes, and model compounds

4.2.1 The design of the synthesis

Despite the popularity of carbostyryl sensitizers, they have received less attention synthetically than coumarin derivatives. This could be due to a combination of their lower extinction coefficient and hypsochromic absorption maxima. The lack of synthetic access has led to limited knowledge about the tunability of photophysical properties through structural modification. However, carbostyryls possess some attractive features, such as resistance to pH change and bleaching (e.g. chemical or thermal), which make these small molecules attractive.⁸⁰

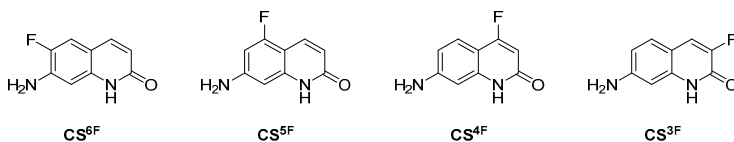
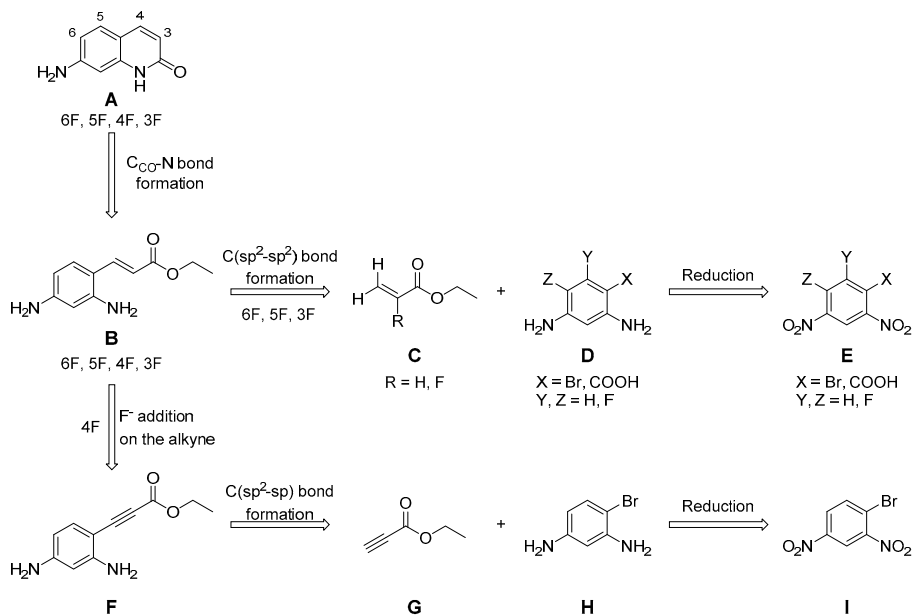


Figure 23 Monofluorinated carbostyryls CS^{6F}, CS^{5F}, CS^{4F} and CS^{3F}

We aimed to synthesise a series of monofluorinated carbostyryls (**Figure 23**). The fluorine was expected to make the carbostyryl harder to oxidise compared

to unsubstituted analogues, thus quenching pathways, such as PeT, might be diminished in the corresponding Eu(III) complexes.

We envisaged a convergent synthetic approach which meets the following criteria: i) the use of commercially available starting materials and readily synthesisable intermediates, ii) robust and scalable chemistry, iii) exclusion of harsh reaction conditions and minimal use of toxic substances, and iv) regiocontrolled fluorine incorporation.



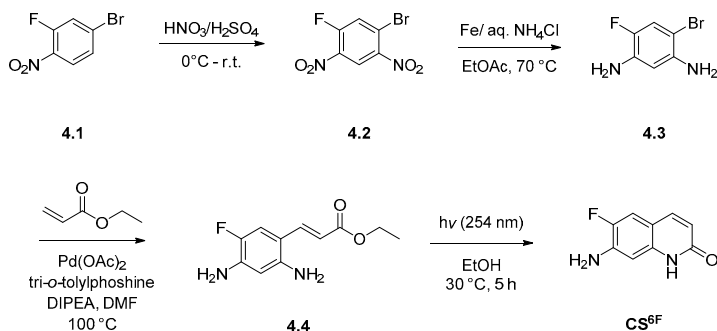
Scheme 7 Retrosynthetic analysis of monofluorinated carbostyrils

Through retrosynthetic analysis (**Scheme 7**) one can see that a late-stage C_{CO}-N bond formation is desirable. This kind of cyclisation is well-known in the literature and offers some advantages: it is simple to carry out and does not require any harsh reaction conditions. The overall problem with carbostyrils arises from their low solubility in most of the common solvents, therefore the isolation and purification could be challenging. The formation of the double bond might be possible in different ways starting from the appropriate aryl halide, e.g. palladium-catalysed Heck-type reaction. Ethyl acrylate and methyl 2-fluoroacrylate **C** are commercially available and this type of reaction has been reported.⁸¹ The synthesis of the dinitro intermediates (**E** and **I**) is known⁸² and nitro group reduction is well established,⁸³ thus this reaction route seemed to be feasible for three of the regioisomers (**Figure 23**, CS^{6F}, CS^{5F}, CS^{3F}). The formation of β -fluoro acrylates is challenging, further complicated in this case by the need to have amino or nitro groups in fixed positions in order to obtain the desired CS^{4F} (**Figure 23**). Out of the few reported strategies, the addition of fluoride to an alkyne **F** becomes appealing in terms of synthetic

accessibility and versatility.⁸⁴ Accessing the key intermediate alkyne **F** could be desired *via* a C-C bond formation; Pd-catalyzed Sonogashira coupling – a well-established method for the formation of C(sp²-sp) bonds – could be envisioned in this case. Starting materials for such a coupling are readily available.

4.2.2 Preparation of monofluorinated carbostyrils (CS^F)

As discussed above the syntheses of the monofluorinated carbostyrils were designed to be robust and scalable. In the synthesis of CS^{5F} and CS^{6F} the Heck coupling was carried out starting from the benze-1,3-diamine intermediate. The synthesis of CS^{3F} started with the decarboxylative Heck reaction of 2,4-dinitrobenzoic acid⁸⁵ followed by the reduction of the nitro groups. Overall, all synthetic steps provided good to excellent isolated yields. Chemical steps were optimised to an acceptable level, and then applied without further modification. A brief description of considerations and optimisation is given in the next paragraph along with the detailed synthesis of CS^{6F} (**Scheme 8**). Intermediate **4.3** was synthesised according to a literature method.^{82a} Commercially available 4-bromo-2-fluoro-1-nitrobenzene **4.1** was reacted with 5.0 equiv. of 65% nitric acid in sulfuric acid. The temperature was maintained in the 0 °C to r.t. range. After a few hours at r.t. the reaction mixture was poured onto ice and the solids were collected by filtration. The procedure provided intermediate **4.2** in 78% yield in good purity without further purification.



Scheme 8 Synthesis of CS^{6F}

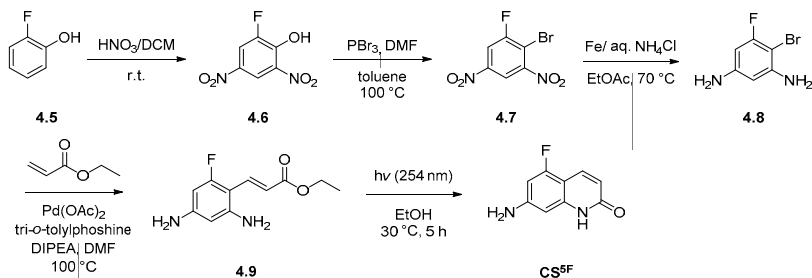
Following a literature precedent,⁸³ the reduction was carried out with Fe in EtOH. Sn and Zn were tried as well. In the former case the aqueous work-up became complicated after the quenching of the reaction, while in the latter case the reaction was sluggish compared to iron (16 h for Zn vs 1 h for Fe). After further optimisation the solvent was changed to a biphasic mixture of water and EtOAc, and the reaction was carried out at an elevated temperature in the presence of 6.0 equiv. of Fe and 8.0 equiv. of NH₄Cl for 1 h. Aqueous

work-up followed by column chromatography on silica yielded the intermediate **4.3** in 75% yield.

The Heck reaction has been widely used to synthesise substituted olefins and a large variety of modifications have been developed in the past three decades. Despite this, only a few Pd catalysts are widely useful in combination with trialkyl- or triarylphosphine ligands and organic or inorganic bases. A classic combination of reagents consists of Pd(OAc)₂, tri-*o*-tolylphosphine, and TEA or DIPEA.⁸¹ The coupling reactions are usually carried out in polar aprotic solvents such as DMF or acetonitrile. Originally, the dinitro analogue **4.2** was going to be introduced in the Heck-coupling. Initial test reactions showed no product formation according to HPLC-MS analysis, instead, dehalogenation and homocoupling occurred. Performing the Heck coupling on the benzene-1,3-diamine intermediate **4.3** yielded the desired intermediate **4.4**, as shown by HPLC-MS. It seemed that unprotected amine groups are tolerated by the reaction, even though there are very few examples in the literature. The Heck reaction was performed on a gram scale in the presence of Pd(OAc)₂, tri-*o*-tolylphosphine and DIPEA in DMF at 100 °C. Complete conversion of the starting material was achieved in 1 h, as shown by HPLC-MS analysis of the reaction mixture. Aqueous work-up followed by column chromatography on silica gel provided the cinnamic ester derivative **4.4** in 80% yield. Olefin **4.4** was isolated as the *Z* isomer. The stereochemical assignment was based on the ³*J*_{HH} = 15.4 Hz.

The cyclisation step was envisaged to be performed under acidic conditions at elevated temperature. Several acids, such as, HCl, H₂SO₄ and AcOH were tested under either under neat conditions or in solutions of MeOH, EtOH, *n*-BuOH, THF or 1,4-dioxane, while also varying the temperature between 60 °C and 100 °C. Due to the poor carbostyryl solubility in most common organic solvents (e.g. DCM, EtOAc, or MeOH) work-up and purification were difficult. Unfortunately, neither full conversion of the starting material, nor reproducible isolated yield and affordable purity were realised during the optimisation trials. However, performing the reaction under irradiation⁸⁶ allowed us to take advantage of the low solubility of the desired product as a tool of isolation and purification. After a short optimisation the ring closing reaction was carried out in a relatively dilute solution in EtOH (0.1 M). A stock solution of starting material **4.4** was split into 10 mL fractions, which were transferred to quartz vessels. The reaction mixtures were irradiated (λ = 254 nm) typically for 5 h in a photoreactor, at which point HPLC-MS analysis showed full consumption of the starting material. The slurries were combined, the volatile components were evaporated, and the obtained solid was washed

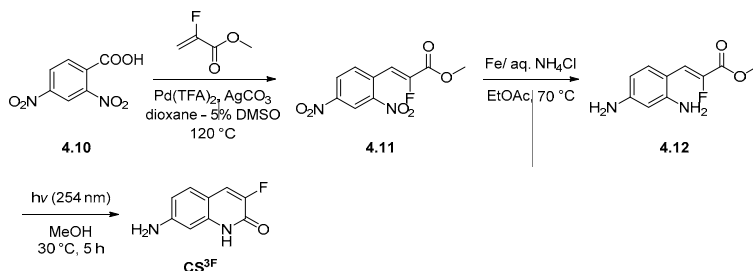
with DCM yielding **CS**^{6F} in 86% yield and excellent purity as shown by ¹H NMR spectroscopy.



Scheme 9 Multistep preparation of **CS**^{5F}

The synthesis of **CS**^{5F} is shown in **Scheme 9**. Intermediate **4.7** was synthesised according to literature methods.⁸² 2-fluorophenol **4.5** was reacted with 2.5 equiv. of fuming nitric acid in DCM at room temperature. The dinitro intermediate **4.6** was isolated in 83% yield after aqueous work-up. The next step was carried out in the presence of 1.2 equiv. of PBr_3 in a mixture of DMF and toluene (1:9). The reaction mixture was stirred for 1 h at $100\text{ }^\circ\text{C}$, after which an aqueous work-up provided intermediate **4.7** in 94% isolated yield. The reduction of the nitro groups was carried out according to previously optimised conditions in the presence of Fe and NH_4Cl , and afforded the appropriate benzene-1,3-diamine **4.8** in 77% yield. Compound **4.8** was reacted with ethyl acrylate using the general Heck coupling conditions – $\text{Pd}(\text{OAc})_2$, tri-*o*-tolylphosphine, DIEPA , in DMF at $100\text{ }^\circ\text{C}$ – and the olefin **4.9** was isolated in 43% yield after column chromatography. Intermediate **4.9** was isolated as the *Z* isomer and the stereochemical assignment was based on the $^3J_{\text{HH}} = 15.9\text{ Hz}$. Cyclisation was performed under irradiation in EtOH yielding the desired **CS**^{5F} in 48% yield. The low yield of both the Heck reaction and cyclisation is attributed to undesired side reactions. HPLC analysis revealed debromination under Pd catalysis conditions. The presence of the debrominated side-product made the purification of **4.9** to an acceptable level unsuccessful. Due to incomplete separation, some residual impurity ($\sim 40\text{ mol\%}$ according to ^{19}F NMR) was carried into the cyclisation step lowering

the yield to 48%. The impurity was unreactive under irradiation and was readily removable during the isolation of **CS**^{5F}.

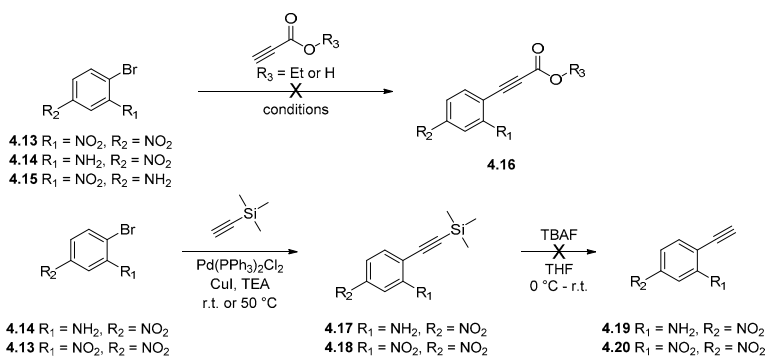


Scheme 10 Synthesis of **CS**^{3F}

The successful implementation of the Heck reaction encouraged us to follow up this pathway. Due to the increasing interest in fluorinated small molecules for various applications, their synthetic accessibility is vital. Regarding 2-fluoro acrylates Pd-catalysed decarboxylative approaches have been developed and showed to be applicable in our synthesis (**Scheme 10**). 2,4-dinitrobenzoic acid **4.10** was reacted with methyl-2-fluoroacrylate. The reaction was carried out in the presence of Pd(TFA)₂ as the catalyst, Ag₂CO₂ base in 1,4-dioxane with 5% DMSO. A relatively long reaction time (3–5 days) resulted in 37% percent isolated yield. This yield is slightly higher than the reported value (24%), and can be attributed to the larger scale (4 g starting material) and the elongated reaction time in our experiment. Possibly a significant amount of starting material undergoes decarboxylation, limiting the yield. Dinitro olefin **4.11** formed as the *Z* isomer due to a steric clash between the acrylic ester and the aromatic ring, and the stereochemical assignment was based on the ³J_{HF} = 33.0 Hz.^{85c} The rest of the synthesis was performed according to the established route consisting of an Fe-mediated reduction and an isomerization-cyclisation reaction upon irradiation (λ_{em} = 254 nm). The combined yield of **CS**^{3F} over these two steps reached 70%.

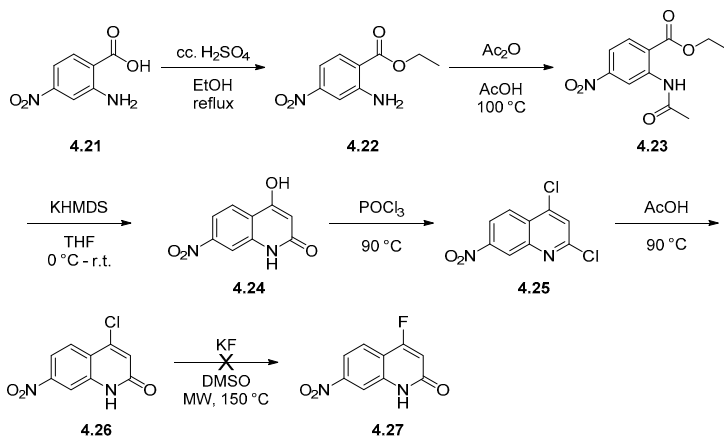
4.2.3 Attempted synthesis of **CS**^{4F}

The formation of β-fluoro acrylate was proposed through a regioselective addition of fluoride to an alkyne. The desired acetylene could potentially be formed via Sonogashira coupling (**Scheme 11**). During the optimisation process a few catalysts, such as Pd(PPh₃)₃Cl₂, Pd(PPh₃)₄ and Pd(dppf)Cl₂ in combination with CuI, different bases like TEA, DIPEA, DBU, Na₂CO₃ and K₂CO₃ were tested in different solvents e.g. DMF, DMSO, NMP, THF.



Scheme 11 Synthetic approaches for acetylene derivatives

Three different starting materials (**4.13**, **4.14** and **4.15**) were chosen for the validation process, and the reaction was performed with ethyl propiolate and propiolic acid. Despite extensive experimentation the desired alkyne **4.16** could not be obtained. This failure could be due to the decreased reactivity and diminished stability of alkyl propiolates, as they often undergo degradation or self-condensation.⁸⁷ In order to overcome the abovementioned issues of alkyl propiolates, an alternative pathway was designed. **4.14** and **4.15** were successfully reacted with TMS-acetylene in the presence of $\text{Pd}(\text{PPh}_3)_2\text{Cl}_2$, CuI in TEA affording the acetylene **4.17** and **4.18**, respectively. To expose the terminal acetylene for further derivatization, cleavage of the TMS protecting group was carried out under mild conditions using TBAF at 0 °C. The deprotection resulted in immediate degradation of the product, therefore this route had to be ruled out.⁸⁸



Scheme 12 Convergent synthesis of compound **4.26**

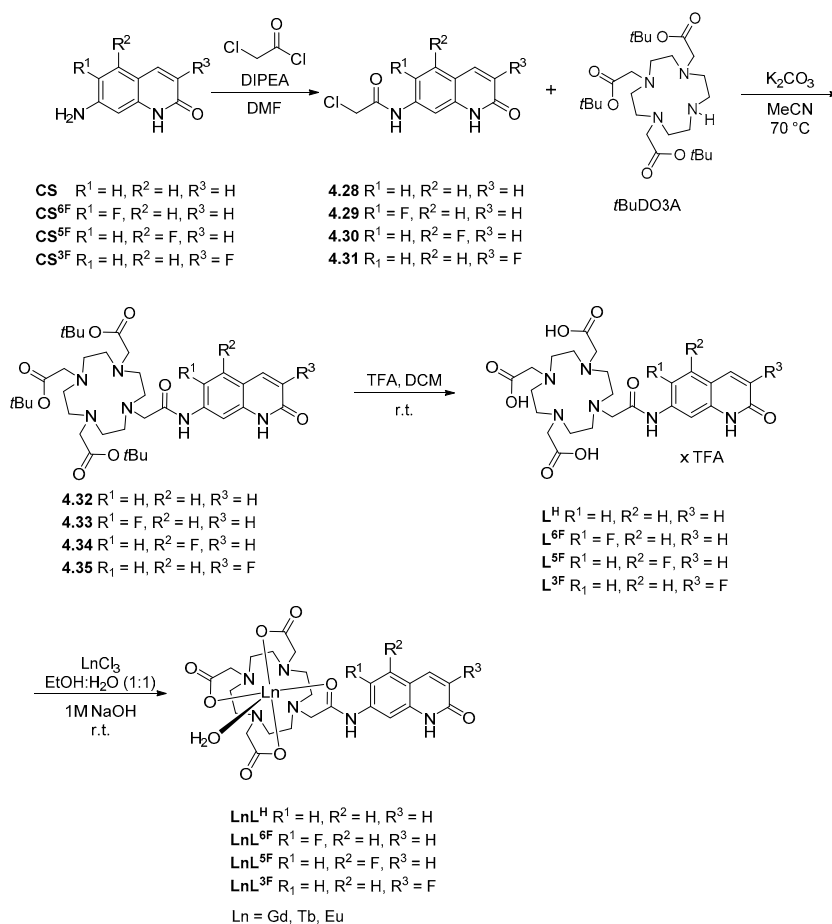
Another option for the regioselective introduction of fluorine is a nucleophilic fluorination⁸⁹ i.e. **4.26** \rightarrow **4.27**. Several successful examples of this transformation have been reported for coumarin derivatives. We considered

the synthetic utilisation of such a reaction on the appropriate carbostyryl derivative **4.26** (**Scheme 12**). Intermediate **4.26** was prepared in 5 chemical steps according to modified literature procedures.⁹⁰ Several different conditions were tested for chloride to fluoride exchange. Two main sources of fluoride were investigated, KF and CsF. These inorganic salts are hygroscopic, thus specific pre-treatment (drying) is crucial. Solvents, such as DMF, DMA, DMSO and NMP are usually used for this chemistry provided no solubility issues arise for the starting material. The temperature and the reaction times were changed, including in combination with microwave irradiation. HPLC-MS and ¹⁹F NMR analysis of the reaction mixture suggested the formation of multiple side products. Continuous monitoring of the reaction revealed the degradation of the desired product. Therefore, we concluded that this transformation is not reproducible and lacks robustness. Several different strategies have been explored for the synthesis of **CS**^{4F}. Sadly, in most cases reactants or the product were unstable under the reaction conditions making the reactions unreproducible. Consequently, the synthesis of **CS**^{4F} remained unsolved at the time. Nevertheless, in Chapter 5.2.1 we will demonstrate a successful attempt for the preparation of **CS**^{4F}.

4.2.4 Assembly of ligands and preparation of Ln(III) complexes

The preparation of the ligands and Ln(III) complexes was carried out according to established methods (**Scheme 13**).²¹ In some cases the conditions or the work-up and isolation were modified in order to improve the procedure and avoid lengthy column chromatography. **CS**, **CS**^{6F}, **CS**^{5F} and **CS**^{3F} were readily acylated with α -chloroacetyl chloride in the presence of DIPEA in DMF at r.t. The product was precipitated by pouring the reaction mixture on ice, separating by centrifugation and washing with water in order to get rid of residual solvent and base. The crude product was dried and washed twice with DEE to afford the chloroacetylated intermediates **4.28–4.31**. *t*BuDO3A was alkylated with **4.28–4.31** in the presence of K₂CO₃ in MeCN at 70 °C. After full conversion of the starting material the solids were removed by filtration and the crude product was purified by column chromatography on neutral alumina yielding the *t*Bu-ester protected ligands **4.32–4.35**. Hydrolysis was performed under acidic conditions using a 1:1 mixture of TFA and DCM. Normally after 24 h HPLC-MS analysis indicated full conversion of the starting material. The mixture was concentrated *in vacuo* and the remaining oil was triturated with MeOH and DEE to afford the ligand **L**^H, **L**^{6F}, **L**^{5F} or **L**^{3F} as its TFA salt. The procedure yielded **L**^{6F} and **L**^{3F} analytically pure as shown by HPLC-MS and ¹H NMR. **L**^{5F} and **L**^H was further purified by column chromatography on silica and by reverse phase chromatography, respectively. Complexation with Ln(III) was carried out in a mixture of EtOH:H₂O at r.t. using LnCl₃. The pH was adjusted to 8 by the addition of 1M NaOH solution

after which the reaction mixtures were directly purified by column chromatography LnL^{H} , $\text{LnL}^{6\text{F}}$, $\text{LnL}^{5\text{F}}$ and $\text{LnL}^{3\text{F}}$ lanthanide complexes where Ln = Gd, Eu and Tb.

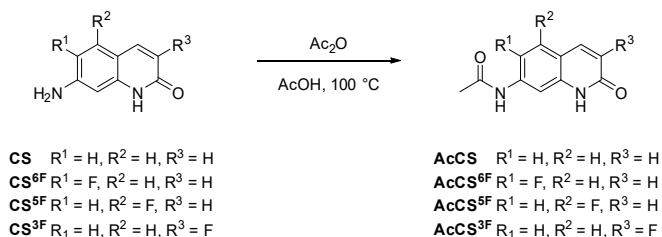


Scheme 13 Synthesis of DO3A complexes

4.2.5 Preparation of model compounds for cyclic voltammetry measurements

Model compounds for cyclic voltammetry measurements were prepared via acetylation of the appropriate **CS** (**Scheme 14**). The reactions were performed in a mixture of acetic anhydride and acetic acid at high temperature.⁷⁴ The product was precipitated by the addition of water, and the solid was separated

by centrifugation, washed with water and DEE to afford **AcCS**, **AcCS^{6F}**, **AcCS^{5F}** and **AcCS^{3F}**.



Scheme 14 Preparation of acetylated carbostyrils

4.3 Structural characterisation of **LnL^F** compounds

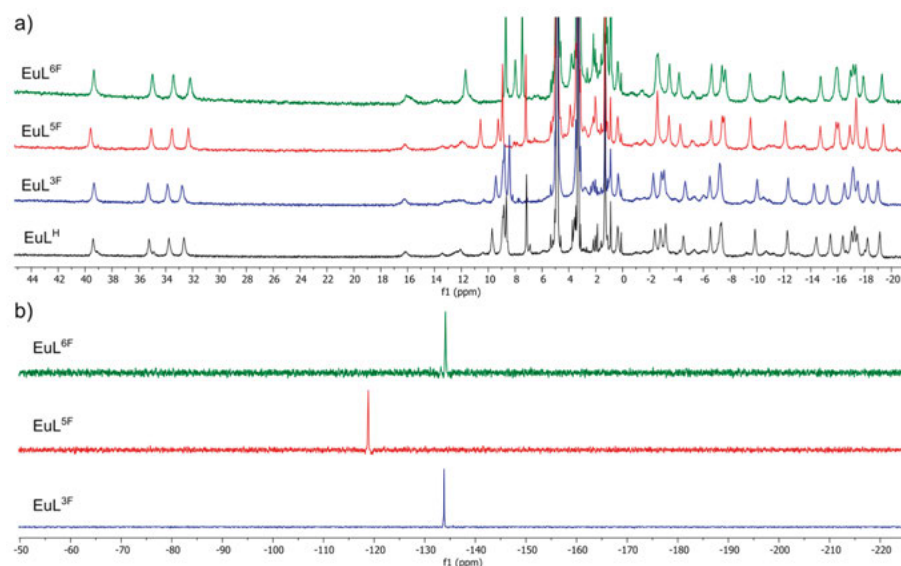


Figure 24 a) Stacked ^1H NMR spectra of **EuL** (400 MHz, MeOD, r.t.) b) Stacked ^{19}F NMR spectra of **EuL^F** (376 MHz, MeOD, r.t.)

DO3A-based Ln(III) complexes can exist in two diastereomeric forms, SAP or TSAP. Since the axial CH_2 protons of the cyclen core are more shielded in the SAP geometry, these protons resonate at a higher frequency, therefore distinguishing the diastereomers by ^1H NMR is possible. The ^1H NMR spectra of **EuL^H** and **EuL^F**, and the ^{19}F NMR spectra of **EuL^F** were recorded at r.t. in MeOD (**Figure 24a**). Four signals were found in the 32–40 ppm range in each case indicative of similar geometries in solution. These signals were attributed to the major isomer, SAP.^{33,29} TSAP signals resonated at 12–16 ppm range, and indicated the presence of trace amounts of this isomer. ^{19}F NMR analysis

mirrored this observation for **EuL^{6F}**, **EuL^{5F}** and **EuL^{3F}** providing a single resonance at -134.1 , -118.8 and -133.8 ppm, respectively (**Figure 24b**). Each magnetically non-equivalent proton would give a separate signal (29 and 28 resonances for **EuL^H** and **EuL^F**, respectively). Accordingly, the number of signals observed in the ^1H NMR spectra suggests the presence of a single diastereomer or a mixture of diastereomers undergoing rapid exchange on the NMR timescale in solution. Similar isomeric distribution was found for **EuL^H** and **EuL^F** in solution, indeed, differences in the photophysical properties are supposed to be ascribed to the various antennae.

4.4 Electrochemical characterisation of model compounds

Electrochemical characterisation of redox-active fragments of Ln(III) complexes is important in order to understand their photochemical behaviour. Acetylated model compounds can be studied without the possible interference of the ligand and the metal. Determination of the oxidation potential allows for the estimation of the likelihood of electron transfer processes in Ln(III) complexes. Electronegative fluorine was expected to make the carbostyrils harder to oxidise, therefore diminishing the extent of PeT in Ln(III) complexes. A series of model compounds **AcCS**, **AcCS^{6F}**, **AcCS^{5F}** and **AcCS^{3F}** were synthesised for electrochemical characterisation.

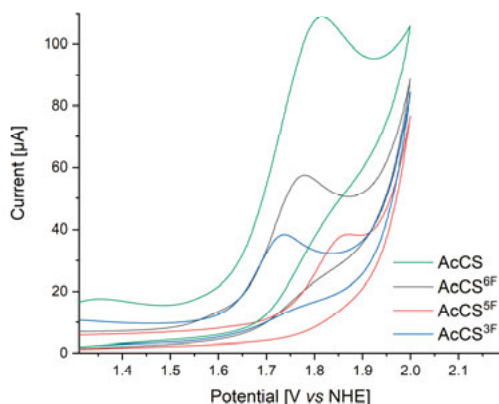


Figure 25 Cyclic voltammogram of 2 mM **AcCS** and **AcCS^F** in 100 mM TBAPF₆ as a supporting electrolyte in DMF under Ar using a glassy carbon working electrode, Ag/AgCl/KCl(sat.) reference electrode, and a Pt wire counter electrode.

The oxidation potentials of the model compounds **AcCS**, **AcCS^{6F}**, **AcCS^{5F}** and **AcCS^{3F}** (**Scheme 14**) were determined by cyclic voltammetry (**Figure**

25). Measurements were carried out in 100 mM TBAPF₆ solutions in DMF under an Ar atmosphere using a glassy carbon working electrode, Ag/AgCl/KCl_(sat.) reference electrode, and a Pt wire counter electrode. Analyte concentration was kept at 2 mM. At 100 mV/s scan rate irreversible oxidation processes were seen at +1.81, +1.77, +1.86, and +1.73 V (vs NHE) for model compounds **AcCS**, **AcCS**^{6F}, **AcCS**^{5F} and **AcCS**^{3F}, respectively. Monofluorination made the antenna oxidation more difficult in only one case, that of **AcCS**^{5F} (+1.86 V vs NHE). Fluorination in the 6- and 3-positions, however, had the opposite effect. Fluorine has the highest electronegativity in the periodic table, thus it is expected to decrease the electron density in the substituted molecule via inductive effect. However, fluorine can also act as an EDG by donation of a lone pair. Fluorine in the 6- and 3- position makes the 1 e⁻ oxidation easier compared to **AcCS**^{5F} and non-substituted **AcCS**.

4.5 Photophysical characterisation of **CS**^F and **LnL**^F

This work was proposed to serve as a structure-activity study which might help us better understand the relation between structural modifications of carbostyrils and the photophysical properties of Ln(III) complexes. In this section we will discuss the photophysical properties of the new chromophores **CS**^F and that of their Ln(III) complexes (**LnL**^F) and compare them to the non-substituted species **CS** and **LnL**^H.

CS and **CS**^F were characterised by UV-Vis absorption and steady-state emission spectroscopies. Due to their low solubility in aqueous media the characterisation was carried out in MeCN at a concentration of 10 μM.

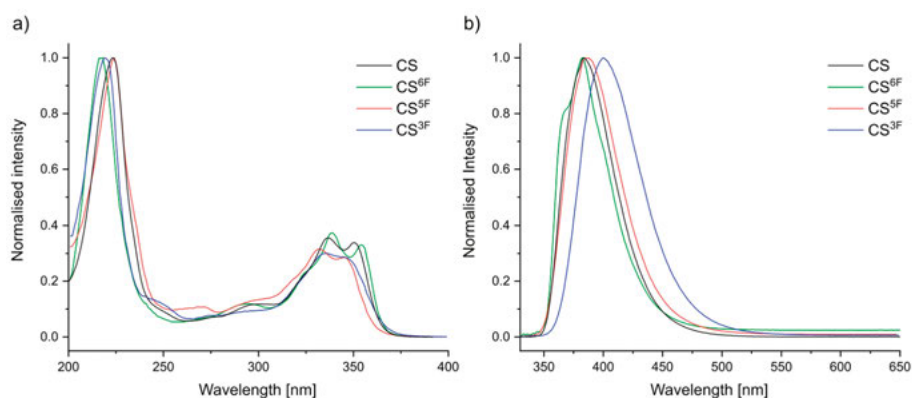


Figure 26 a) Superimposed normalised absorption spectra b) superimposed normalised emission spectra of **CS** and **CS**^F. λ_{ex} = 335, 338, 331 and 332 nm for **CS**, **CS**^{6F}, **CS**^{5F} and **CS**^{3F}, respectively.

The characteristic absorption bands of carbostyrils were located in the 320–370 nm region; these bands were attributed to π - π^* transitions (**Figure**

26). The absorption maxima were at $\lambda_{\text{max}} = 339, 332$ and 335 nm for **CS**^{6F}, **CS**^{5F} and **CS**^{3F}, respectively (**Table 8**). **CS** fell within the range of **CS**^F (339–332 nm) with $\lambda_{\text{max}} = 337$ nm. Excitation at λ_{max} resulted in fluorescent emission maxima at $\lambda_{\text{em}} = 384, 382, 387$ and 400 nm for **CS**, **CS**^{6F}, **CS**^{5F} and **CS**^{3F}, respectively. The largest Stokes shift was found for **CS**^{3F} (4900 cm^{-1}) followed by **CS**^{5F}, **CS** and **CS**^{6F} ($4300, 3700$ and 3300 cm^{-1} , respectively). The fluorescent quantum yield (Φ_{L}) was largest for **CS**^{3F}, $\Phi_{\text{L}} = 56\%$. Fluorination in the 6-position dramatically lowered Φ_{L} to 10%, however **CS**^{5F} retained its Φ_{L} compared to the non-substituted **CS** (25 and 27%, respectively). **CS**^F fluorescent lifetimes (τ_{fl}) showed good correlation with Φ_{L} , rendering τ_{fl} the longest for **CS**^{3F} and the shortest for **CS**^{6F} (2.84 and 0.41 ns, respectively). **CS** and **CS**^{5F} had almost identical τ_{fl} , 1.15 and 1.09 ns, respectively.

Table 8 Photophysical properties of **CS**^a, **CS**^{F a}, **GdL**^{H b} and **GdL**^{F b}

	λ_{max} [nm]	λ_{em} [nm] ^c	S_1 [cm ⁻¹] ^d	T_1 [cm ⁻¹] ^d	Φ_{L} [%] ^e	τ_{fl} [ns]
CS	337	384	-	-	27	1.15(5)
CS ^{3F}	335	400	-	-	56	2.84(6)
CS ^{5F}	332	387	-	-	25	1.09(2)
CS ^{6F}	339	382	-	-	10	0.41(6)
GdL ^H	330	369	28700	22500	7.6	0.34(3)
GdL ^{3F}	325	364	29200	22100	12.8	0.60(5)
GdL ^{5F}	327	367	28900	22400	6.1	0.44(8)
GdL ^{6F}	337	380	28100	22300	5.9	0.36(4)

^a In acetonitrile at 10 μM concentration. ^b In aqueous PIPES buffer (10 mM), pH 6.5, at 10 μM complex concentrations. ^c $\lambda_{\text{ex}} = 332$ nm (**CS**^{3F}), 331 nm (**CS**^{5F}), 338 nm (**CS**^{6F}), 335 nm (**GdL**^{6F}), 327 nm (**GdL**^{5F}), 325 nm (**GdL**^{3F}). ^d Calculated from the 0–0 transitions of the Gd-complexes recorded at 77 K. ^e Relative to quinine sulfate ($\Phi = 0.59$) in H_2SO_4 (0.05 M).⁶⁹

LnL^H and **LnL**^F were characterised by UV-Vis absorption and steady-state and time-resolved emission spectroscopies. Measurements were carried out in PIPES-buffered aqueous solutions at pH 6.5 at a complex concentration of 10–15 μM . Absorption maxima of Gd(III) complexes followed the order of **CS**^{6F}, **CS**, **CS**^{5F} and **CS**^{3F} with $\lambda_{\text{max}} = 337, 330, 327$ and 325 nm, respectively (**Figure 27**).

λ_{max} in the Gd(III) complexes was slightly blue-shifted (2–10 nm) compared to the carbostyrils and followed the order observed in **CS**^F; **GdL**^{6F} (337 nm) > **GdL**^H (330 nm) > **GdL**^{5F} (327 nm) > **GdL**^{3F} (325 nm). Fluorination in the 3-position resulted in the largest blue shift compared to **GdL**^H parent (**Table 8**).

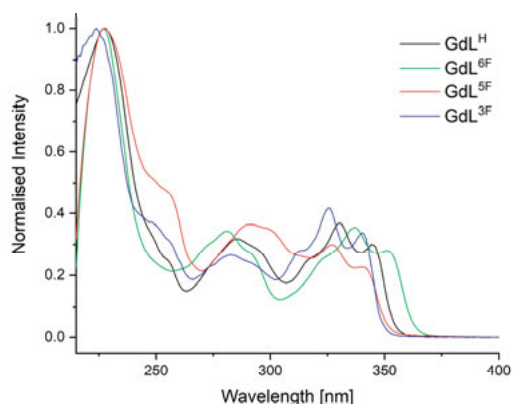


Figure 27 Superimposed normalised absorption spectra of **GdL**

The S_1 and T_1 energies of the antennae were determined from the low temperature emission spectra of the Gd(III) complexes. Samples of **GdL^H** and **GdL^F** were measured at 77 K with 10% glycerol added to the nominally 10 μ M, PIPES buffered aqueous solutions. Excitation at λ_{max} resulted in ligand-based fluorescence and phosphorescence (**Figure 28b**). The latter is attributed to emission from the ligand T_1 energy levels which were determined from the 0–0 phonon transitions (**Table 8**).

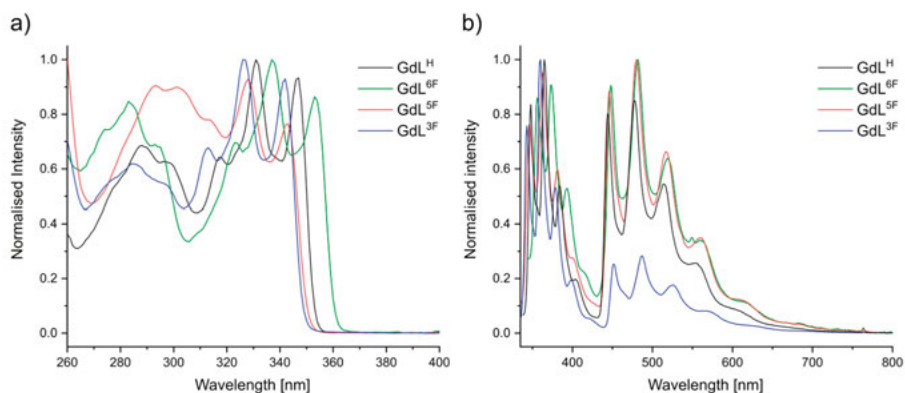


Figure 28 Superimposed a) excitation and b) steady-state emission spectra of **GdL** at 77 K. $\lambda_{\text{em}} = 444, 448, 446, 452$ nm and $\lambda_{\text{ex}} = 330, 335, 327$ and 325 nm for **GdL^H**, **GdL^{6F}**, **GdL^{5F}** and **GdL^{3F}**, respectively.

The lowest energy T_1 within **GdL^F** was found for **GdL^{3F}** at 22100 cm^{-1} , followed by **GdL^{6F}** and **GdL^{5F}** at 22300 and 22400 cm^{-1} , respectively. T_1 energy level of **GdL^H** was the highest at 22500 cm^{-1} . These incremental differences could have dramatic changes in Ln(III) emission. The excitation spectra of the phosphorescence bands (**Figure 28a**) matched the absorption

spectra in the whole range. Antenna based photophysical characterisation allows us to make careful considerations regarding EnT and BET. Tb and Eu have excited states at 20400 cm^{-1} ($^5\text{D}_4$), and 19000 cm^{-1} ($^5\text{D}_1$) and 17200 cm^{-1} ($^5\text{D}_0$), respectively¹³. T_1 energy levels of **GdL**^F are $\sim 5000\text{ cm}^{-1}$ higher than the Eu excited state $^5\text{D}_0$ (at 17200 cm^{-1}), and are therefore well-positioned for energy transfer to sensitise Eu(III) emission. Considering the low lying T_1 state in **GdL**^{3F} (and **GdL**^{6F}), **TbL**^{3F} and possibly **TbL**^{6F} may suffer from BET resulting in diminished Tb(III) luminescence.

Excitation at λ_{max} resulted in strong red and green luminescence for Eu and Tb complexes, respectively. The spectral shape and the ratio of peaks were in good correlation with other DO3A-based Eu and Tb complexes. Ln(III) emissions were located at 579, 593, 615, 653 and 700 nm for Eu and 487, 546, 587, 620, 650, 667 and 681 nm for Tb, corresponding to the $^5\text{D}_0 \rightarrow ^7\text{F}_J$ ($J = 0-4$) and $^5\text{D}_4 \rightarrow ^7\text{F}_J$ ($J = 6-0$) transitions, respectively (**Figure 29**).

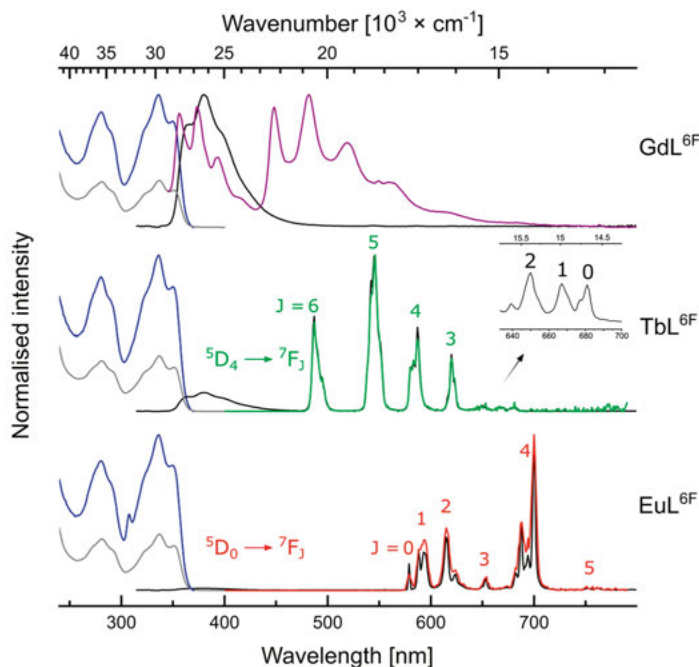


Figure 29 Normalised absorption (grey, 298 K), excitation [blue, $\lambda_{\text{em}} = 380\text{ nm}$ (Gd), $\lambda_{\text{em}} = 546\text{ nm}$ (Tb), $\lambda_{\text{em}} = 615\text{ nm}$ (Eu), 298 K], steady-state emission at 298 K [black, $\lambda_{\text{ex}} = 335\text{ nm}$], steady-state emission at 77 K [purple, $\lambda_{\text{ex}} = 335\text{ nm}$] and time-resolved emission [green (Tb), red (Eu), $\lambda_{\text{ex}} = 335\text{ nm}$ at 298 K] spectra of **LnL**^{6F}. [**LnL**^{6F}] = $10\text{ }\mu\text{M}$.

DO3A-based ligands are octadentate, therefore a metal-bound water molecule was expected to complete the first coordination sphere. The luminescent lifetimes of Tb(III) and Eu(III) complexes were determined using time-resolved luminescent spectroscopy. Lifetimes measured in water ($\tau_{\text{H}_2\text{O}}$) were

consistently ~ 0.6 ms in **EuL**, which is in correlation with other DO3A-based Eu(III) complexes. These values in D₂O (τ_{D2O}) lengthened to ~ 2.2 ms. However, lifetime values determined in **TbL** were quite inconsistent, within the 0.34–0.98 ms and 0.38–1.39 ms range in H₂O and D₂O, respectively (**Table 9**).

Table 9 Photophysical properties of **LnL^H** and **LnL^F**^a

	Φ_L (%) ^b	Φ_{Ln} (%) ^b	τ_{H2O} (ms)	τ_{D2O} (ms)	q ^c	τ_f [ns]
TbL^H	5.1	22.5	0.96	1.39	1.3	0.21(4)
TbL^{3F}	8.1	5.6	0.34	0.38	1.4	0.39(2)
TbL^{5F}	4.6	21.7	0.98	1.24	0.8	0.36(3)
TbL^{6F}	4.6	16.7	0.64	0.77	1.1	0.25(4) ^d
EuL^H	0.26	4.34	0.62	2.27	1.0	–
EuL^{3F}	0.68	1.09	0.62	2.26	1.0	0.93(6) ^d
EuL^{5F}	0.81	5.05	0.60	2.13	1.0	0.47(6) ^d
EuL^{6F}	0.21	5.10	0.61	2.18	1.0	0.20(1) ^d

^a [LnL] = 10 μ M in 10 mM PIPES buffered H₂O at pH 6.5. ^b Relative to quinine sulfate ($\Phi = 0.59$) in H₂SO₄ (0.05 M).⁶⁹ ^c Calculated using $q = (5 \text{ ms}) \cdot (1/\tau_{H2O} - 1/\tau_{D2O} - 0.06 \text{ ms}^{-1})$ for Tb, and $q = (1.2 \text{ ms}) \cdot (1/\tau_{H2O} - 1/\tau_{D2O} - 0.25 \text{ ms}^{-1} - m \cdot 0.075 \text{ ms}^{-1})$ for Eu; m = number of nearby amide N-H oscillators.^{16,17} ^d Biexponential fit better based on χ^2 .

The number of coordinating water molecules can be calculated using Eq. 3 for Tb and Eq. 4 for Eu (see Chapter 1.5). q -values obtained for **EuL** ($q \sim 1$) are consistent with nine-coordinate environments (**Table 10**). Divergence of **TbL** from $q = 1$ is likely due to thermal BET, which makes the lifetime method inapplicable. Tb(III) and Eu(III) have similar ionic radii, and we would expect these ions to adopt similar coordination geometries with the same types of ligands. Isostructural Ln(III) complexes impose similar geometry, thus nine-coordinate environment ($q = 1$) could be expected along the series. Furthermore, the Tb(III) emission spectra in the different ligands had shapes similar to each other. While Tb(III) emission is not as sensitive to the coordination environment as Eu(III) luminescence, the highly similar Tb(III) spectra are consistent with **TbL** having similar coordination geometries, and thus the same q -values.

The antenna- and metal-based luminescence quantum yields of the complexes were determined in 10 mM aqueous PIPES buffer (pH = 6.5) using quinine sulfate ($\Phi = 0.59$) in H₂SO₄ (0.05 M)²⁸ as the reference. Results are summarised in **Table 8** and **Table 9** for Gd, and Tb and Eu complexes, respectively. Residual antenna fluorescence in **TbL** was 25–37% lower compared to those of the analogous **GdL**. This is possibly due to some S₁-mediated EnT to the Tb(III). Φ_{Tb} were in the 17–23% range with the exception

of **TbL**^{3F}, $\Phi_{\text{Tb}} = 5.6\%$ (Table 9). The significantly lower Φ_{Tb} in **TbL**^{3F} could be ascribed to thermal BET.

Antennae were significantly quenched in **EuL**. **TbL** had slightly lower Φ_{L} than **GdL**, however Φ_{L} loss in **EuL** reached as high as 87–96% compared to the corresponding **GdL**. The former is likely due to some S_1 -mediated EnT, while the latter can be attributed to a combination of S_1 -mediated EnT and depopulation of S_1 , by PeT. The free energy change of electron transfer can be calculated using Eq. 5 (see Chapter 2.3). E_{ox} is the oxidation potential of the donor, i.e. model compounds **AcCS**, **AcCS**^{6F}, **AcCS**^{5F} and **AcCS**^{3F}. E_{red} is the reduction potential of the acceptor (Eu(III)), E_{s} is the (singlet) excited state energy of the antenna and the last term was approximated to be ~ 0.15 eV. E_{red} of Eu(III) was approximated with the cathodic potential of the overall uncharged 4-CF₃-substituted DO3A-based complex with a value of -0.89 V (vs NHE).⁷¹ E_{s} is the excited state energy of the antenna, determined from the first vibronic band of the **GdL**^F spectra at 77 K as 3.56, 3.48, 3.58, and 3.61 eV for **GdL**, **GdL**^{6F}, **GdL**^{5F} and **GdL**^{3F}, respectively. Having everything in hand, the driving force of PeT can be approximated using Eq. 5. ΔG_{PeT} values were found to be -1.01 , -0.97 , -0.98 , and -1.14 eV for **EuL**^H, **EuL**^{6F}, **EuL**^{5F} and **EuL**^{3F} complexes, respectively. These results suggest that PeT might be thermodynamically feasible in DO3A-based Eu(III) complexes bearing mono-fluorinated antennae. In reality, these systems are extremely complicated. Mono-fluorination of the antenna alters S_1 , T_1 and E_{ox} at the same time, therefore the overall effect on the extent of PeT is hardly predictable. Further analysis of the Eu(III) luminescence was carried out to obtain crucial insight into the differences between the analogous systems. η_{sens} and $\Phi_{\text{Ln}}^{\text{Ln}}$ were determined according to Eq. 1 (Table 10). Results are summarized in Table 10. Very similar τ_{rad} was obtained for **EuL**^{6F} (5.28 ms) and **EuL**^{5F} (5.25 ms) which were in a good agreement with the value 5.18 obtained for **EuL**^H for a similar coordination environment. These small differences in τ_{rad} resulted in minor differences in $\Phi_{\text{Ln}}^{\text{Ln}}$; 11.6% for **EuL**^{6F}, 11.5% for **EuL**^{5F} and 11.9% for **EuL**^H. Since the intrinsic quantum yield is mostly influenced by the coordination environment, similar values obtained for **EuL**^{6F}, **EuL**^{5F} and **EuL**^H suggested very similar geometry. This was further supported by the identical spectral shapes of these complexes with the exception in **EuL**^{3F}.

Table 10 Eu(III)-centred photophysical properties of **EuL^H** and **EuL^F**

	τ_{rad} (ms) ^a	Φ_{Ln}^{Ln} (%) ^b	η_{sens} (%) ^b
EuL^H	5.18 ^c 4.73 ^d	11.9 ^c 13.1 ^d	36.2 ^c
EuL^{3F}	9.25 ^c 5.10 ^d	6.7 ^c 12.3 ^d	16.1 ^c
EuL^{5F}	5.25 ^c 5.11 ^d	11.5 ^c 11.8 ^d	43.4 ^c
EuL^{6F}	5.28 ^c 5.19 ^d	11.6 ^c 11.8 ^d	43.8 ^c

^a Calculated using Eq. 2. ^b Calculated using Eq. 1. ^c Calculated using the steady-state emission spectra. ^d Calculated using the time-resolved emission spectra.

Interestingly, an almost 2-fold larger τ_{rad} was obtained in **EuL^{3F}** (τ_{rad} = 9.25 ms) resulting in a diminished Φ_{Ln}^{Ln} (6.7%) compared to the other Eu(III) emitters. The largest η_{sens} values were found in **EuL^{6F}** and **EuL^{5F}** (43.8 and 43.4%, respectively), whereas this was somewhat lower in **EuL^H** (36.2%). This could be attributed to a slightly better EnT i.e. spectral overlap, or a decrease in PeT quenching in **EuL^{6F}** and **EuL^{5F}**. However, η_{sens} was markedly lower in **EuL^{3F}** (16.1%) compared to **EuL^{6F}** and **EuL^{5F}** (~43%).

The highest Φ_{Ln} values were determined for **EuL^{6F}** and **EuL^{5F}** to be within experimental error, $\Phi_{\text{Eu}} = 5.10$ and 5.05%, respectively. Φ_{Ln} in **EuL^H** was somewhat lower (4.3%), however **EuL^{3F}** had only ~20% of Φ_{Eu} (1.09%) compared to **EuL^{6F}** or **EuL^{5F}**. Φ_{Ln} in these emitters were comparable to other uncharged DO3A-based Eu(III) complexes with the exception on **EuL^{3F}**. The largest negative ΔG_{PeT} value was estimated for **EuL^{3F}** (−1.14 eV, see Chapter 4.3) which suggest the greatest probability of PeT quenching. Hence, the low Φ_{Eu} (1.09%) in **EuL^{3F}** could be attributed to depopulation of S_1 by PeT. Due to the complexity of these systems these values still require careful consideration.

The steady-state and time-resolved emission spectra of **EuL^{3F}** were different, (**Figure 30**) which is an indication of the presence of several emissive species. The slow-decaying species would dominate in the time-resolved spectrum, while emission from the fast-decaying species would contribute to and alter the shape of the steady-state spectrum. The luminescence spectrum of **TbL^{3F}** was similarly time-dependant but the differences in the time-resolved and steady-state spectra were smaller. The ligand fluorescence lifetimes τ_{fl} were measured in **LnL^F**, however τ_{fl} of **EuL^F** and **GdL^F** were not directly comparable. Based on χ^2 values the biexponential decay was a better fit and suggested the presence of additional emitters in **EuL^F** compared to those of **GdL^F**. The spectral shape of the slow-decaying species in **EuL^{3F}** resembles those of **EuL^{6F}** and **EuL^{5F}**. The fast-decaying species which dominates in the steady-state spectrum alters the ratios of $\Delta J = 0, 1$ and 2 compared to what was seen in the time-resolved spectrum.

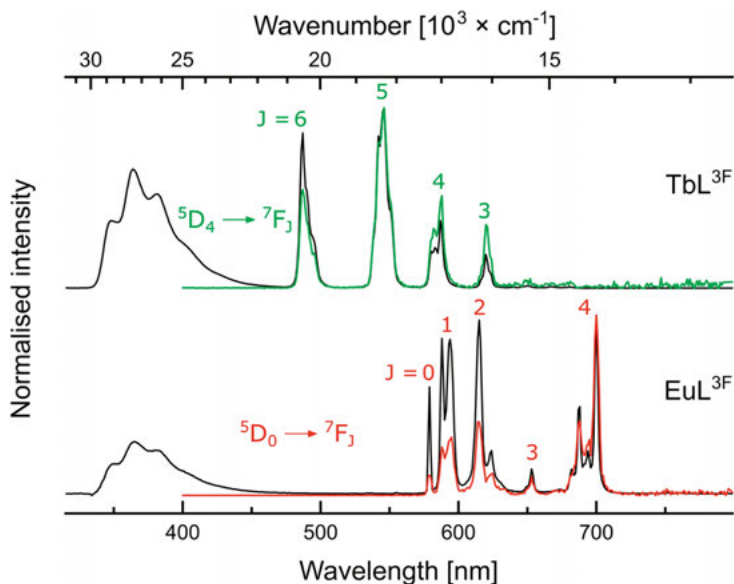


Figure 30 Superimposed steady-state (black) and time-resolved (green for Tb, red for Eu) emission spectra of **TbL^{3F}** (top) and **EuL^{3F}** (bottom).

$\Delta J = 2$ transition in Eu complexes are hypersensitive to the local environment,⁹⁶ therefore any significant intensity change of this transition suggests the change in the coordination sphere of the metal. A plausible explanation might be the coordination of another H₂O in the excited state to the metal while one of the coordinating arms detaches **LnL^{3F}**. This hypothesis is somewhat supported by the similarity of the spectral shape and the ratio of intensities to that of the $q = 2$ Eu(III) complexes of triazole-substituted heptadentate DO3A-based ligands.⁹⁷ To better understand the deviations in **LnL^{3F}** compared to other **LnL^F** further work is needed.

4.6 Conclusions

A series of monofluorinated carbostyrils **CS^F** were synthesised via photochemical cyclisation reaction. **CS^F** were incorporated into DO3A-based ligands and their Gd(III), Eu(III) and Tb(III) chelates were prepared. The Ln(III) complexes were characterised by ¹H NMR, cyclic voltammetry, UV-Vis absorption, and steady-state and time-resolved emission spectroscopies. PeT is feasible for several Lns (Eu, Yb, Sm and Dy) and a prominent quenching mechanism of Ln(III) emission. Fluorination of the antennae was expected to render the chromophores less reducing, therefore decreasing PeT. Structural similarities of **LnL^F** were confirmed by similar solution geometries (¹H NMR), similar emission spectral shape, and τ_{rad} and $\phi_{\text{Ln}}^{\text{Ln}}$ values with the exception of **LnL^{3F}**. Unexpectedly, monofluorination of the antenna resulted

no significant improvements in the photophysical properties. The photophysical properties of **LnL**^{3F} suggested the presence of several emitting species and altered coordination sphere in the excited state compared to other **LnL**^F. The reasons of anomalies seen in **LnL**^{3F} are unclear, therefore further work is needed.

5 Synthesis of fluorinated carbostyryl antennae for the sensitization of Eu(III), Tb(III) luminescence. (Paper IV)

5.1 Introduction

Ln(III) complexes have been widely utilised in cellular imaging.⁶¹ Ln(III) compounds are complementary to organic fluorophores in imaging. Ln(III) emission consists of narrow, line like bands which is characteristic to the metal and has long lived, often ms luminescent lifetimes (for Eu(III) and Tb(III)) which allow for time-delayed detection.³ To develop bright Ln(III) emitters has always attracted attention, indeed, optimising EnT and diminishing quenching are the key components. PeT is one of the effective Ln(III) luminescence quenching processes for reducible Lns (e.g. Eu, Yb, Sm and Dy).²¹ PeT can be modulated by shifting the redox potential of the Ln by changing the coordination sphere⁷¹ or by appropriate functionalisation of the sensitizer. EWG groups (e.g. CF₃) on the carbostyryl was found to reduce PeT in Eu(III) complexes, however be detrimental to Tb(III) luminescence.^{21,72}

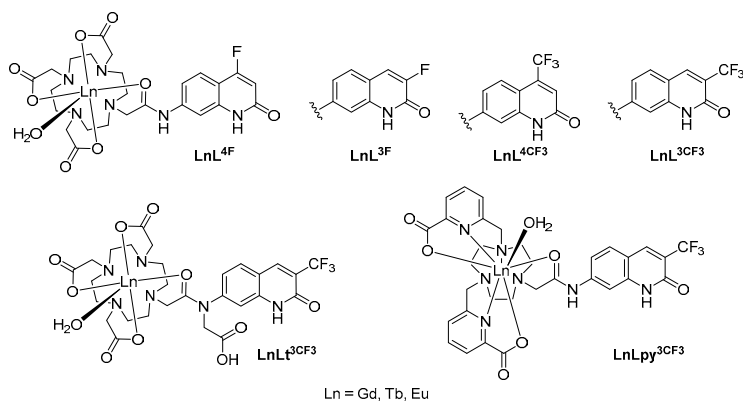


Figure 31 Synthesised Ln(III) complexes bearing fluorinated antennae

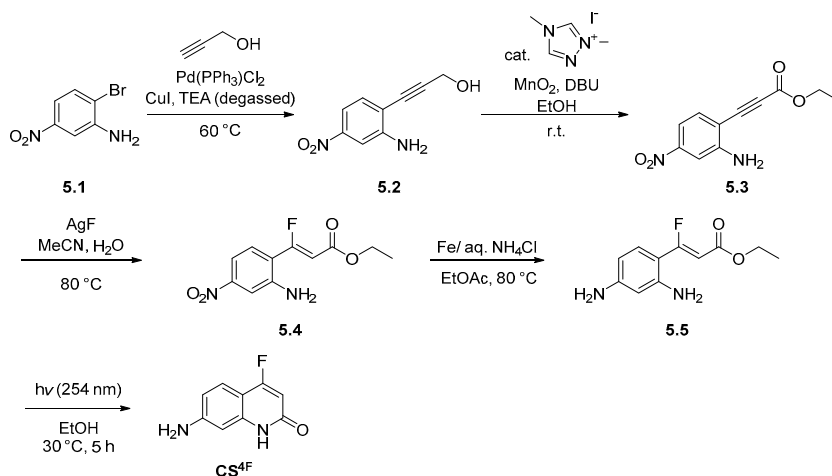
In Chapter 4 we discussed the synthesis and photophysical characterisation of monofluorinated carbostyryls and their DO3A-based Ln(III) complexes. Electronegative fluorine was expected to decrease the quenching by PeT by making the antenna less reducing. Results revealed that some of the fluorinated species had improved photophysical properties compared to the

non-substituted analogue.⁹⁸ As an effort to obtain bright Ln(III) emitters we synthesised new chromophores furnished with EWG groups (e.g. F and CF₃) and Ln(III) complexes. 4-fluoro-7-aminocarbostyryl **CS**^{4F} completed the series of monofluorinated carbostyryls, on the other hand 3-trifluoromethyl-7-aminocarbostyryl **CS**^{3CF3} allowed to compare the effect of the same substituent, but in a different position in the chromophore. The antennae were incorporated into DO3A-based secondary- and tertiary-amide, and pyridyl TACN-based ligand frames affording **L**^R, **Lt**^R and **Lpy**^R, respectively. Ln(III) complexes of the ligands **LnL**^R, **LnLt**^R and **LnLpy**^R (Ln = Gd, Eu, Tb, Dy and Sm) were synthesised for photophysical characterisation (**Figure 31**). The new chromophores let us compare the affect in the photophysical properties possibly caused by switching the position of a fluorine or CF₃-group between position 3 and 4 in the carbostyryl.

5.2 Synthesis of **CS**^R, ligands **L**^R, **Lt**^R and **Lpy**^R, their Ln(III) complexes and model compounds

5.2.1 Preparation of **CS**^{4F}

In Chapter 4.2.3 we discussed the synthetic attempts for the preparation of **CS**^{4F}. Sadly, none of the designed synthetic routes were feasible mainly due to the instability of either reactants or intermediates. To overcome incompatibility problems in the Sonogashira coupling we decided to break the initial transformation into two steps: i) formation of the substituted propargylic alcohol, ii) oxidation of the alcohol to ester (**Scheme 15**).



Scheme 15 Synthesis of **CS**^{4F}

In the first step, **5.1** was reacted with propargylic alcohol in the presence of $\text{Pd(PPh}_3)_2\text{Cl}_2$ and CuI in TEA.⁹¹ The reaction was carried out under an inert atmosphere using Schlenk line techniques. The reaction mixture was degassed prior to placing it in the oil bath. The reaction was run for 40 h at 60 °C. Aqueous work-up was performed, and the crude product was purified by column chromatography on silica. The substituted propargylic alcohol **5.2** was isolated in 66% yield on a relatively large scale (using 4 g starting material). Based on literature precedents two alternatives were tested for the oxidative esterification. First, **5.2** was heated at reflux in MeOH in the presence of I_2 and K_2CO_3 .⁹² HPLC-MS analysis showed no reaction, even though the reaction time was run for 72 h. Second, excess of MnO_2 and NaCN were mixed with alcohol **5.2** in EtOH.⁹³ HPLC-MS analysis indicated full consumption of the starting material into the desired ester **5.3**. This method required super-stoichiometric amounts of NaCN , which is a highly toxic and difficult-to-handle substance. N-heterocyclic carbenes (NHC) have been used for the oxidation of alcohols to esters. In 2009, Maki B. E. demonstrated the synthetic versatility of NHCs as catalysts in oxidation reactions.⁹⁴ Successful application of that reaction to our substrate gave access to compound **5.4**. The reaction was carried out in the presence of 20 mol% 1,4-dimethyl-1,2,4-triazolium iodide (NHC), 20 mol% DBU and 15 equiv. MnO_2 in EtOH. After stirring the reaction mixture for 20 h, the product was isolated by column chromatography in 46% yield.

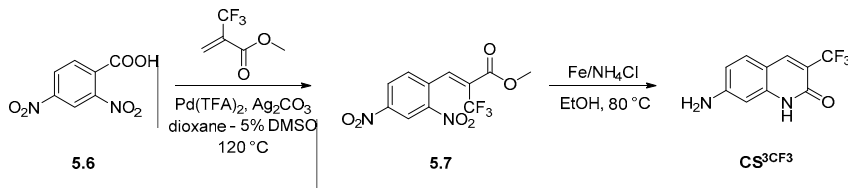
The insertion of fluoride was performed according to a literature procedure. Alkyne **5.3** was reacted with 2 equiv. AgF in a mixture of MeCN and H_2O at 80 °C.^{84b} Test reactions indicated the formation of the product reproducibly and scalably; this chemical step seemed to be robust. Scale-up reaction resulted in 48% yield for **5.4** after column chromatography. The position of the fluoride was confirmed with 1D and 2D NMR techniques and **5.4** was isolated as a single *Z* stereoisomer based on $^3J_{\text{HF}} = 34.8$ Hz. The excellent stereoselectivity is possibly due to the *ortho* amine group.

The rest of the synthesis was straightforward. Iron-mediated reduction was performed on compound **5.4** according to the optimised conditions. The cyclisation step was carried out in the presence of light ($h\nu = 254$ nm) following the conditions discussed in Chapter 4.2.2. **CS^{4F}** was isolated in 55% yield over two steps.

5.2.2 Preparation and functionalisation of **CS^{3CF3}**

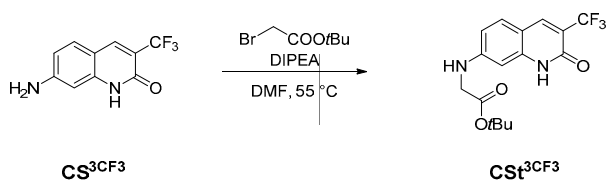
To broaden the scope of our study we aimed to prepare the derivative of the known compound **CS^{4CF3}**. Moving the CF_3 group from position 4 to 3 might have unexpected effects on photophysical properties in Ln(III) complexes. In order to realise the CF_3 group in position 3 we utilised the same strategy that was described for the synthesis of **CS^{3F}** in Chapter 4.2.2. Methyl-2-

trifluoromethyl acrylate readily reacted with 2,4-dinitrobenzoic acid **5.6** under decarboxylative conditions (**Scheme 16**). The Heck coupling was carried out in the presence of Pd(TFA)₂, Ag₂CO₃ in 1,4-dioxane mixed with 5% DMSO. The reaction mixture was stirred at 120 °C for 24 h. 2,4-dinitro olefin **5.7** was isolated in 27% yield. The alkene **5.7** was formed and isolated as a ~50:50 mixture of *E/Z* isomer based on ¹⁹F NMR analysis.^{85c} It was demonstrated in Chapter 2.2.2 that methyl-2-fluoroacrylate provided excellent stereoselectivity for the formation of the *Z* isomer due to a steric clash between the ester functional group and the aromatic ring. The presence of the bulkier CF₃ group resulted in increased steric hindrance prior to the β-hydride elimination step. Consequently, the poor stereoselectivity could be attributed to the lack of steric control in that transition state.^{85c} Dinitro reduction was carried out in the presence of iron and NH₄Cl. Optimisation of the reaction revealed that changing the reaction media from the previously used biphasic system to EtOH and lengthening the reaction time to 24 h turned the formation of CS^{3CF3} into a one-pot reduction-cyclisation process. This is somewhat unexpected in light of the two-step procedure described earlier, but unlike other substituted carbostyrils discussed in this thesis (e.g. CS^{6F} or CS^{4F}), CS^{3CF3} showed excellent solubility in common solvents, such as EtOAc, providing more flexibility during the work-up and purification. Filtration of the reaction mixture followed by aqueous work-up yielded the desired CS^{3CF3} in 65% yield.



Scheme 16 Two-step synthesis of CS^{3CF3}

We have previously seen that tertiary amide linkers can beneficially influence the photophysical properties of the Ln(III) complexes. Therefore, further functionalisation was carried out via mono-alkylation of the NH₂ group to access the tertiary-functionalised ligand Lt^{3CF3}.^{62,72} CS^{3CF3} was reacted with 2.4 equiv. *tert*-butyl bromoacetate in the presence of DIPEA in DMF at 55 °C (**Scheme 17**). The alkylation proceeded slowly, thus after 36 h another portion of *tert*-butyl bromoacetate was added and let the reaction stirred for another 36 h. CS^{3CF3} was isolated after column chromatography on silica in 51% yield.

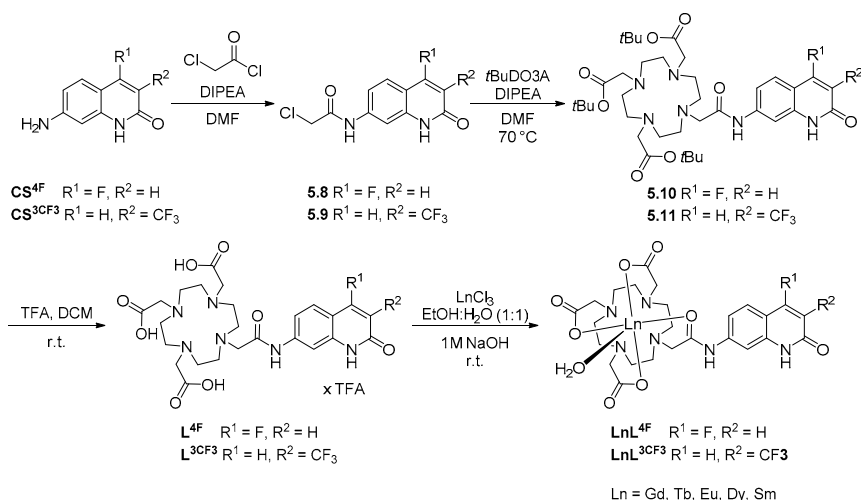


Scheme 17 Functionalisation of CS^{3CF_3}

5.2.3 Assembly of $\text{L}^{4\text{F}}$, L^{3CF_3} , Lt^{3CF_3} and $\text{Lpy}^{\text{3CF}_3}$, and preparation of their Ln(III) complexes

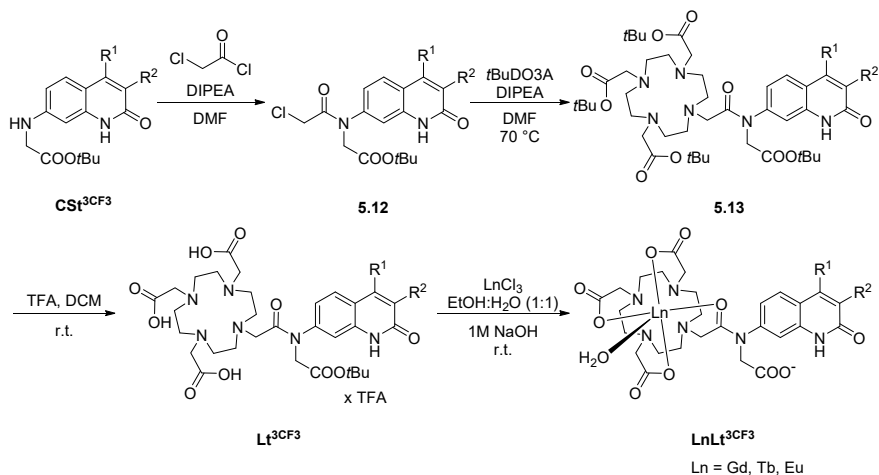
With the CF_3 -substituted carbostyryls in hand the preparation of ligands was accomplished using well-established methods.^{73,72,21} In order to be able to compare the new chromophores $\text{CS}^{4\text{F}}$ and CS^{3CF_3} to the mono-fluorinated series $\text{CS}^{6\text{F}}$, $\text{CS}^{5\text{F}}$ and $\text{CS}^{3\text{F}}$ the same ligand environment (DO3A) was targeted in the synthesis (**Scheme 18**). To allow further comparison and understanding of the photophysical properties, i) a tertiary-linked version of the DO3A ligand **Lt** was prepared (**Scheme 19**) and ii) a TACN based analogue **Lpy** was synthesised (**Scheme 20**). CS^{4CF_3} incorporated into DO3A, tertiary-DO3A and TACN has been already investigated, therefore for this purpose we chose CS^{3CF_3} as the sensitising antenna. We envisioned that the moving of the CF_3 group from position 4 to 3 would help us better understand structure-activity relations in Ln(III) complexes. Gd, Eu and Tb complexes of each new ligand were prepared.

$\text{CS}^{4\text{F}}$ and CS^{3CF_3} were reacted with α -chloroacetyl chloride in the presence of DIPEA in DMF. **5.8** and **5.9** were isolated through precipitation upon addition of water. *t*Bu-ester protected ligands **5.10** and **5.11** were prepared in DMF using DIPEA as the base at 70 °C. After stirring for 24 h the reaction mixtures were directly purified by column chromatography on basic alumina. Basic alumina provided better separation and purity compared to neutral alumina. Ligand $\text{L}^{4\text{F}}$ and L^{3CF_3} were prepared through hydrolyses of **5.10** and **5.11** in the presence of TFA and DCM. The ligands were isolated as their TFA salt after trituration in a mixture of MeOH and DEE. $\text{L}^{4\text{F}}$ and L^{3CF_3} were incorporated into **LnL** where Ln = Gd, Eu, Tb, Dy and Sm according to the general complexation procedure.



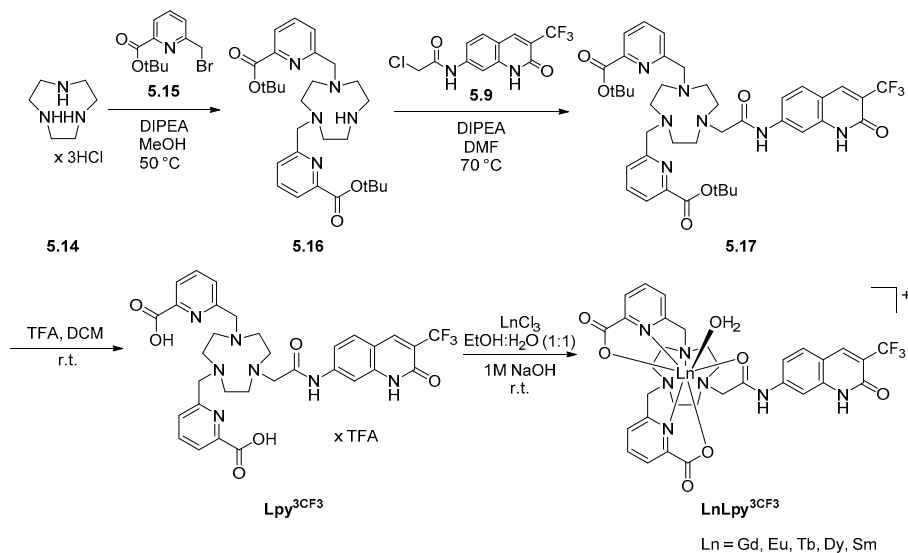
Scheme 18 Preparation of DO3A complexes with **CS^{4F}** and **CS^{3CF3}** antennae

The tertiary amide ligand **Lt** and its Ln(III) complexes were synthesised in a similar fashion as the secondary amide-containing **L** ligands (**Scheme 19**). Acetylation of the functionalised antenna **CSt^{3CF3}** yielded intermediate **5.12** after precipitation. Alkylation of *t*BuDO3A was achieved in the presence of DIPEA in DMF at elevated temperature (70 °C). Hydrolysis was performed in a mixture of TFA and DCM at r.t. for 24 h, and **Lt^{3CF3}** was isolated after trituration of the crude product with a mixture of MeOH and DEE as the TFA salt. Gd, Eu and Tb complexes of **Lt^{3CF3}** were synthesised analogously to **LnL^{3CF3}** in a mixture of EtOH and H₂O while adjusting the pH to 8 by the addition of 1M NaOH solution. Column chromatography was performed in each case to purify the complexes.



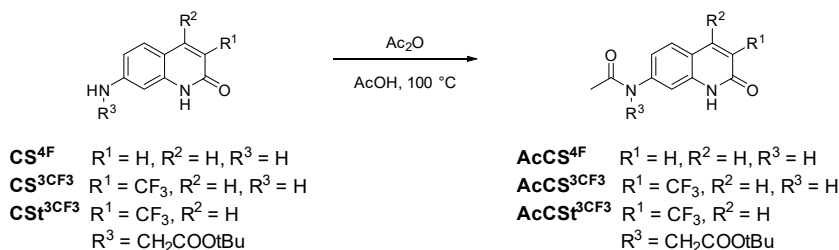
Scheme 19 Preparation of tertiary amide-linked DO3A based Ln complexes

The synthesis of **Lpy**^{3CF₃} was performed according to the modified procedure discussed in Chapter 2.2.2 (**Scheme 20**). Bromomethyl picolinate **5.15** was prepared following a literature precedent.⁹⁵ The presence of the *t*Bu-ester allowed us to carry out the hydrolysis under the desired acidic conditions. The amide-bond of the linker and the carbostyryl could be sensitive to basic conditions. To overcome unintended side reactions, and therefore, the need of purification by column chromatography acidic hydrolysis is preferred. TACN trihydrochloride **5.14** was alkylated with 1.5 equiv. of **5.15** in the presence of DIPEA in MeOH at 50 °C. Intermediate **5.16** was isolated by column chromatography on basic alumina; gradient elution (0→10% (MeOH:Acetone 1:1) in DCM) was utilised. Compound **5.16** was further reacted with chloroacetamide **5.9** under previously described conditions (DIPEA, DMF, 70 °C). Purification on basic alumina (0→5% (MeOH:Acetone 1:1) in DCM) yielded the *t*Bu-protected ester **5.17**. Hydrolysis in a mixture of TFA and DCM followed by the chelation under previously discussed conditions resulted **LnLpy**^{3CF₃} (Ln = Gd, Eu, Tb, Dy, Sm).



Scheme 20 Synthesis of TACN base Ln complexes **LnLpy**^{3CF₃}

5.2.4 Preparation of model compounds for cyclic voltammetry measurements



Scheme 21 Preparation of acetylated model compounds **AcCS^{4F}**, **AcCS^{3CF3}** and **AcCS^{t3CF3}**

Model compounds for cyclic voltammetry measurements were prepared via acetylation of the appropriate **CS** (**Scheme 21**) according to the developed procedure. The reactions were performed in a mixture of acetic anhydride and acetic acid at elevated temperature⁷⁴. The products were precipitated by the addition of water, the solids were separated by centrifugation, and washed with water and DEE to afford **AcCS^{4F}**, **AcCS^{3CF3}** and **AcCS^{t3CF3}** in analytically pure form.

5.3 Electrochemical characterisation of model compounds

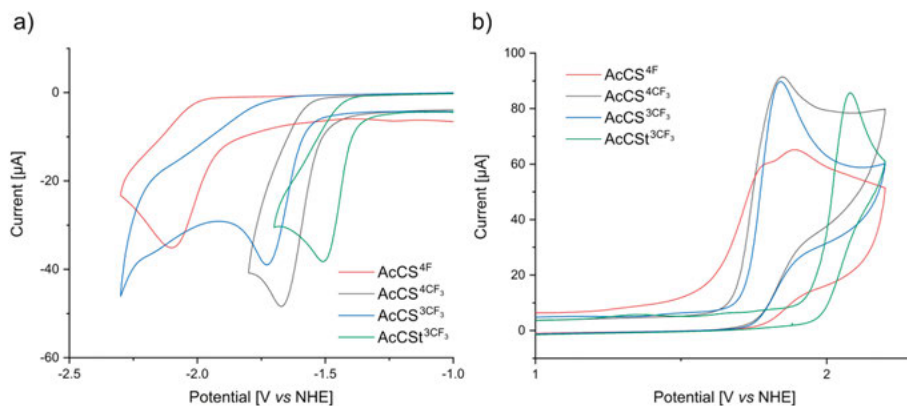


Figure 32 Superimposed cyclic voltammograms of 2 mM **AcCS^R** in 100 mM TBAPF₆ as a supporting electrolyte in MeCN under Ar using a glassy carbon working electrode, Ag/AgCl/KCl(sat.) reference electrode, and a Pt wire counter electrode. a) Cathodic events. b) anodic events.

The oxidation potentials of the model compounds (**AcCS^{4F}**, **AcCS^{3CF3}**, **AcCS^{4CF3}**, **AcCS^{3CF3}** and **AcCS^{4CF3}**) were determined by cyclic voltammetry

(**Figure 32**). Measurements were carried out in 100 mM TBAPF₆ solutions in MeCN under an Ar atmosphere using a glassy carbon working electrode, Ag/AgCl/KCl_(sat.) reference electrode, and a Pt wire counter electrode. Analyte concentration was kept at 2 mM. The antenna oxidation potentials were determined to be +1.89, +1.85, +1.84, and +2.08 V (vs NHE) for **AcCS**^{4F}, **AcCS**^{4CF₃}, **AcCS**^{3CF₃} and **AcCSt**^{3CF₃}, respectively. Moving the fluoride from position 3 to 4 shifted the oxidation potential by +160 mV making **AcCS**^{4F} more difficult to oxidise. The position of the trifluoromethyl group did not affect the oxidation potential that much (+1.85 V and +1.84 V vs NHE for **AcCS**^{4CF₃} and **AcCS**^{3CF₃}, respectively). However, introduction of the tertiary amide arm resulted in a +240 mV shift in the oxidation potential (+1.84 and +2.08 vs NHE for **AcCS**^{3CF₃} and **AcCSt**^{3CF₃}, respectively).

5.4 Photophysical characterisation of **CS**^R and **LnL**^R

After their successful synthesis the photophysical properties of antennae **CS**^{4F} and **CS**^{3CF₃} were compared to the analogous **CS**^{3F} and **CS**^{4CF₃}. **CS**^R were characterised by UV-Vis absorption and steady-state emission spectroscopies. Due to their low solubility in aqueous media the characterisation was carried out in MeCN at a concentration of 10 μM.

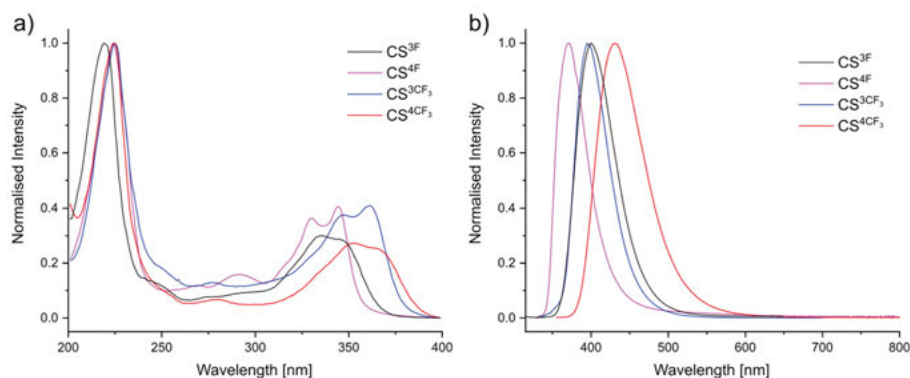


Figure 33 a) Superimposed normalised absorption spectra b) superimposed normalised emission spectra of **CS**^R (R = 3F, 4F, 3CF₃ and 4CF₃). λ_{ex} = 332, 330, 365 and 354 nm for **CS**^{3F}, **CS**^{4F}, **CS**^{3CF₃} and **CS**^{4CF₃}, respectively.

Results are summarised in **Table 11**. The characteristic absorption bands attributed to π - π^* transitions were found in the 335–365 nm range (**Figure 33a**). λ_{max} in **CS**^{4F} was red-shifted by 9 nm compared to **CS**^{3F}, however the absorption maximum of **CS**^{4CF₃} was slightly blue-shifted versus that of **CS**^{3CF₃} (λ_{max} = 352 and 365 nm, respectively). Excitation at λ_{max} resulted in fluorescent emission, and maxima were located at λ_{em} = 400, 372, 395 and 431 nm in **CS**^{3F}, **CS**^{4F}, **CS**^{3CF₃} and **CS**^{4CF₃}, respectively (**Figure 33b**). λ_{em} for **CS**^{4F} and **CS**^{3CF₃} were blue shifted by 28 nm and 36 nm compared to **CS**^{3F} and **CS**^{4CF₃}, respectively. Inverse relation was observed in λ_{max} and λ_{em} when comparing **CS**^{3F} to **CS**^{4F} and **CS**^{3CF₃} to **CS**^{4CF₃}: the compound with the most

blue-shifted λ_{max} had the most red-shifted λ_{em} (Table 11). Stokes shifts were $\sim 5000 \text{ cm}^{-1}$ for $\text{CS}^{3\text{F}}$ and CS^{4CF_3} , and $\sim 2000 \text{ cm}^{-1}$ for $\text{CS}^{4\text{F}}$ and CS^{3CF_3} . Φ_{L} was determined for the new chromophores $\text{CS}^{4\text{F}}$ and CS^{3CF_3} including CS^{4CF_3} relative to quinine sulfate ($\Phi = 0.59$) in H_2SO_4 . $\text{CS}^{3\text{F}}$ had the highest fluorescence quantum yield, $\Phi_{\text{L}} = 56\%$. Fluorine in the 4-position lowered the fluorescence quantum yield to $\Phi_{\text{L}} = 15\%$. Φ_{L} in the fluorinated series followed the order of $\text{CS}^{3\text{F}} > \text{CS}^{5\text{F}} \approx \text{CS} > \text{CS}^{4\text{F}} > \text{CS}^{6\text{F}}$, with $\Phi_{\text{L}} = 56, 25, 27, 15$ and 10% , respectively. Changing the position of CF_3 group from the 4- to the 3-position lowered Φ_{L} from 38% in CS^{4CF_3} to 25% in CS^{3CF_3} .

Table 11 Photophysical properties of CS^{R^a} and GdL^{R^b}

	λ_{max} [nm]	λ_{em} [nm] ^c	S_1 [cm^{-1}] ^d	T_1 [cm^{-1}] ^d	Φ_{L} [%] ^e
CS^{3F}	335	400	–	–	56
CS^{4F}	344	372	–	–	15
CS^{3CF₃}	365	395	–	–	25
CS^{4CF₃}	352	431	–	–	38
GdL^{4F}	326	364	29200	23200	7.3
GdL^{3CF₃}	340	387	27800	22700	4.9
GdLt^{3CF₃}	336	390	27500	22900	3.7
GdLpy^{3CF₃}	339	388	27700	22700	4.5

^a In acetonitrile at $10 \mu\text{M}$ concentration. ^b In aqueous PIPES buffer (10 mM), $\text{pH } 6.5$, at $10 \mu\text{M}$ complex concentrations. ^c $\lambda_{\text{ex}} = 332 \text{ nm}$ ($\text{CS}^{3\text{F}}$), 330 nm ($\text{CS}^{4\text{F}}$), 365 nm (CS^{3CF_3}), 354 nm (CS^{4CF_3}), 325.5 nm ($\text{GdL}^{4\text{F}}$), 327 nm ($\text{GdL}^{3\text{CF}_3}$), 333 nm ($\text{GdLt}^{3\text{CF}_3}$), 337 nm ($\text{GdLpy}^{3\text{CF}_3}$). ^d Calculated from the 0–0 transitions of the Gd-complexes recorded at 77 K . ^e Relative to quinine sulfate ($\Phi = 0.59$) in H_2SO_4 (0.05 M).⁶⁹

The absorption maximum in $\text{GdL}^{4\text{F}}$ was 1 nm longer than in $\text{GdL}^{3\text{F}}$ (326 vs 325 nm , respectively). Excitation at λ_{max} resulted in ligand fluorescence with $\lambda_{\text{em}} = 364 \text{ nm}$ for both complexes. CF_3 -substituted Gd(III) complexes showed similar properties, λ_{max} in $\text{GdL}^{3\text{CF}_3}$ was 2 nm shorter (342 vs 340 nm) than what was seen in $\text{GdL}^{4\text{CF}_3}$. λ_{em} was shortened by 3 nm in $\text{GdL}^{3\text{CF}_3}$ compared to $\text{GdL}^{4\text{CF}_3}$; 387 vs 390 nm , respectively. The introduction of tertiary amide linker shortened λ_{max} compared to the secondary amide $\text{GdL}^{3\text{CF}_3}$, however λ_{em} was somewhat red-shifted; 336 nm in $\text{GdLt}^{3\text{CF}_3}$ and 390 nm in $\text{GdLpy}^{3\text{CF}_3}$, respectively. Changing the coordination sphere to pyridyl-TACN did not change λ_{max} and λ_{em} (339 and 388 nm , respectively) in $\text{GdLpy}^{3\text{CF}_3}$ compared to the DO3A-based $\text{GdL}^{3\text{CF}_3}$ complex. As expected, a characteristic absorption band was observed in the $260\text{--}310 \text{ nm}$ range attributed to the pyridine $\pi\text{--}\pi^*$ transitions (Figure 34). Absorption and emission maxima in $\text{GdLt}^{3\text{CF}_3}$ and $\text{GdLpy}^{3\text{CF}_3}$ were found to be 3 nm shorter than in the analogous $\text{GdLt}^{4\text{CF}_3}$ and $\text{GdLpy}^{4\text{CF}_3}$. Nevertheless, neither the position of the CF_3 group

(3 vs 4), nor structural modifications (tertiary amide linker or different coordination environment) altered the antenna absorption and emission properties significantly in **GdL**.

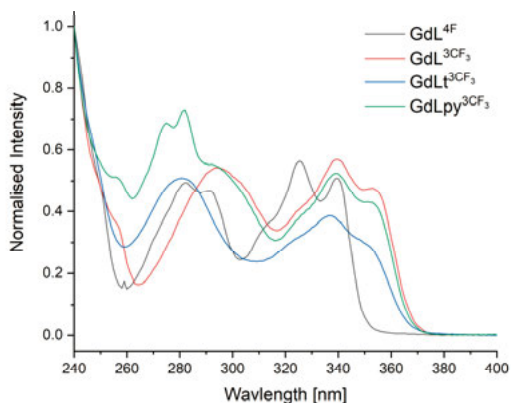


Figure 34 Superimposed normalised absorption spectra of **GdL^R**

The ligand excited state levels were estimated from the 0–0 phonon transitions of the phosphorescent bands in the steady-state emission spectra of Gd(III) complexes. Samples were measured at 77 K with 10% glycerol added to the nominally 10 μ M, PIPES buffered aqueous solutions. Determination of T_1 energy level is crucial in terms of EnT and BET in Tb(III) complexes. Excitation at λ_{max} resulted in well-resolved fluorescence and phosphorescence bands. Excitation spectra at 77 K were similar to the absorption spectra in every case (**Figure 35**). T_1 in **GdL^{3F}** was located only 1700 cm^{-1} above the Tb(III) $^5\text{D}_4$ excited state, therefore **TbL^{3F}** was expected to suffer from BET. Fluorination in the 4-position moved T_1 in **GdL^{4F}** to 23200 cm^{-1} creating a large enough gap (2800 cm^{-1}) between T_1 and Tb(III) excited state to prevent BET in **TbL^{4F}**. Similar effect was found for the trifluoromethylated antennae, only to a milder extent. T_1 in **GdL^{3CF3}** was 300 cm^{-1} higher than in **GdL^{4CF3}** (22700 vs 22400 cm^{-1} , respectively) suggesting that BET might have been shut down in **TbL^{3CF3}** due to the incremental change in T_1 (**Table 11**).

In DO3A-based ligand environment the presence of the tertiary amide linker turned out to be beneficial over the secondary amide one. The presence of the tertiary amide linker increased T_1 from 22400 cm^{-1} in **GdL^{4CF3}** to 23100 cm^{-1} in **GdLt^{4CF3}** preventing BET in **TbLt^{4CF3}**. The response to the integration of the tertiary amide linker is smaller in 3- CF_3 substituted antennae; T_1 in **GdLt^{3CF3}** was located at 22900 cm^{-1} (vs 22700 cm^{-1} in **GdL^{3CF3}**). The pyridyl TACN coordination environment had no influence on T_1 which was at 22700 cm^{-1} in **GdLpy^{3CF3}**. However, **GdLpy^{3CF3}** had 1000 cm^{-1} higher lying T_1 compared to **GdLpy^{4CF3}** (21700 cm^{-1}). Due to this lift in T_1 , the antenna T_1

was possibly better positioned for EnT and high enough to preclude BET in **TbLpy**^{3CF3}. Undoubtedly, T_1 in **GdL**^{4F}, **GdL**^{3CF3}, **GdLt**^{3CF3} and **GdLpy**^{3CF3} were well-positioned for EnT in Eu(III) and Tb(III) complexes as they were at least 2500 but no more than 5000 cm⁻¹ higher than the Ln(III) excited levels (Table 11).

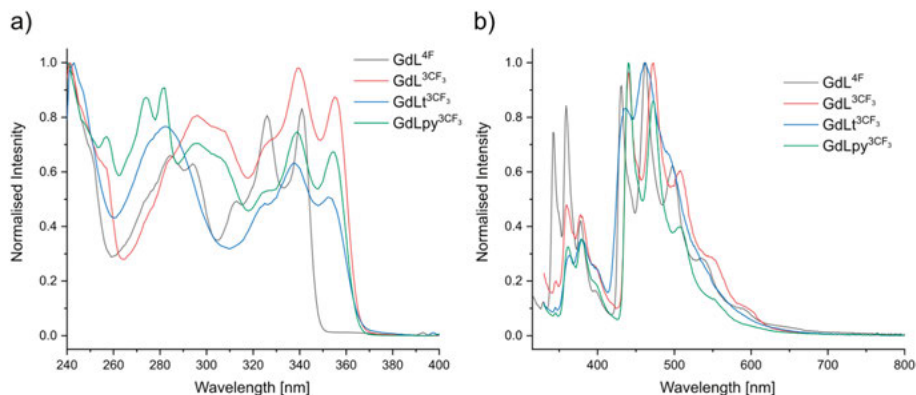


Figure 35 Superimposed a) excitation and b) steady-state emission spectra of **GdL**^R at 77 K. $\lambda_{em} = 431, 440, 436, 440$ nm and $\lambda_{max} = 325.5, 337.5, 333$ and 337 nm for **GdL**^{4F}, **GdL**^{3CF3}, **GdLt**^{3CF3} and **GdLpy**^{3CF3}, respectively.

The luminescence quantum yields of the complexes were determined in 10 mM aqueous PIPES buffer (pH = 6.5) using quinine sulfate ($\Phi = 0.59$) in H₂SO₄ (0.05 M)²⁸ as the reference. Results are summarised in Table 11, Table 12 and Table 13 for Gd, Tb and Eu complexes, respectively. The residual ligand fluorescence in **GdL** serves as the reference, as before. Φ_L was lower in **GdL**^{4F} ($\Phi_L = 7.3\%$) compared to **GdL**^{3F} ($\Phi_L = 12.8$). Somewhat larger Φ_L was found in **GdLt**^{3CF3} than in **GdLt**^{4CF3} ($\Phi_L = 3.7$ vs 3.2% , respectively). Φ_L were identical in **GdL** and **GdLpy** complexes regardless the position of the CF₃-group ($\Phi_L = 4.9$ for **GdL**^{3CF3} and **GdL**^{4CF3}; $\Phi_L = 4.5$ for **GdLpy**^{3CF3} and **GdLpy**^{4CF3}).

Excitation at λ_{max} resulted in robust Tb- and Eu-centred emissions in all cases (Figure 36). As expected, the Tb and Eu excitation spectra matched the absorption spectra in each case, confirming that emission is sensitized through the antennae. Ln emissions were located at $\lambda_{em} = 579, 593, 615, 653$ and 700 nm for Eu (**EuL**^{4F}, **EuL**^{3CF3} and **EuLt**^{3CF3}), and $\lambda_{em} = 487, 546, 587, 620, 650, 667$ and 681 nm for Tb (**TbL**^{4F}, **TbL**^{3CF3} and **TbLt**^{3CF3}), corresponding to the $^5D_0 \rightarrow ^7F_J$ ($J = 0-4$) and $^5D_4 \rightarrow ^7F_J$ ($J = 6-0$) transitions, respectively (Figure 36a, b and c). In all DO3A-based complexes the major transition was the $^5D_0 \rightarrow ^7F_4$ (at 700 nm) in Eu and $^5D_4 \rightarrow ^7F_5$ (at 546 nm) in Tb. Slightly different emission maxima were observed for the **LnLpy** complexes.

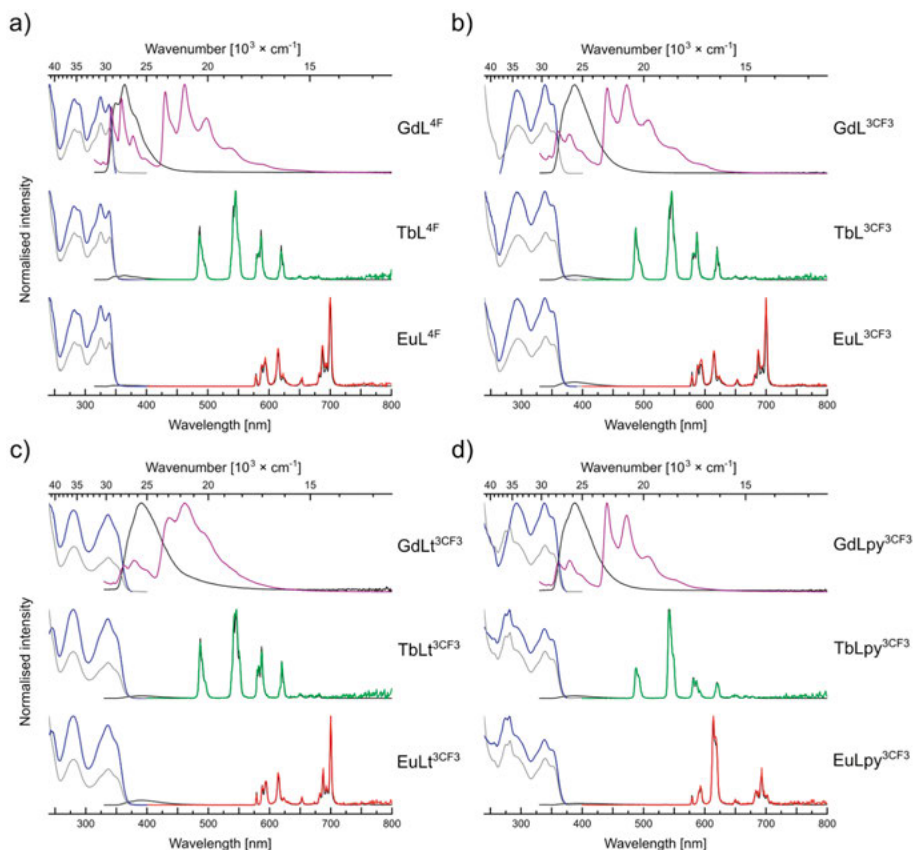


Figure 36 Normalised absorption (grey). Excitation [blue, $\lambda_{\text{em}} = 364, 368, 390, 389$ nm (Gd), $\lambda_{\text{em}} = 546, 546, 546, 541$ nm (Tb), $\lambda_{\text{em}} = 615, 615, 700, 614$ nm (Eu) for **LnL^{4F}**, **LnL^{3CF3}**, **LnLt^{3CF3}**, **LnLpy^{3CF3}**, respectively, 298K], steady-state emission [purple, $\lambda_{\text{ex}} = 325.5, 337.5, 333, 337$ nm, for **GdL^{4F}**, **GdL^{3CF3}**, **GdLt^{3CF3}**, **GdLpy^{3CF3}**, respectively, 77 K] steady-state emission (black, 298 K), and time-resolved emission (green (Tb), red (Eu), $\lambda_{\text{ex}} = 325.5, 337.5, 333, 337$ nm for **LnL^{4F}**, **LnL^{3CF3}**, **LnLt^{3CF3}**, **LnLpy^{3CF3}**, respectively, spectra of a) **LnL^{4F}**, b) **LnL^{3CF3}**, c) **LnLt^{3CF3}** and d) **LnLpy^{3CF3}** complexes.

Ln emissions were found at $\lambda_{\text{em}} = 579, 593, 614, 649$ and 693 nm for Eu, and $\lambda_{\text{em}} = 488, 542, 582, 620, 653, 668$ and 678 nm for Tb, corresponding to the $^5\text{D}_0 \rightarrow ^7\text{F}_J$ ($J = 0-4$) and $^5\text{D}_4 \rightarrow ^7\text{F}_J$ ($J = 6-0$) transitions, respectively (Figure 36d). As the emission profile is sensitive to the coordination geometry, the ratio of emission peaks in **LnLpy** were different compared to DO3A-based Ln complexes. The major transition in **EuLpy** corresponded to the $^5\text{D}_0 \rightarrow ^7\text{F}_2$ ($\lambda_{\text{em}} = 614$ nm) transition. However, in **TbLpy** the $^5\text{D}_4 \rightarrow ^7\text{F}_5$ ($\lambda_{\text{em}} = 546$ nm) transition remained the most intense, but the ratio of the intensity of the transitions was altered (**Figure 36d**). The spectral shape and the ratio of peaks were highly similar to those of analogous Eu and Tb complexes.

Table 12 Photophysical characterisation of **TbLR**^a

	Φ_L (%) ^b	Φ_{Ln} (%) ^b	τ_{H_2O} (ms) ^c	τ_{D_2O} (ms) ^c	q^d
TbL ^{3F}	8.1	5.6	0.34	0.38	1.4
TbL ^{4F}	4.4	43.4	1.73	2.98	0.9
TbL ^{3CF3}	4.1	31.1	1.44	2.25	1.0
TbL ^{4CF3}	4.5	3.0	0.14	0.15	–
TbLt ^{3CF3}	3.0	40.1	1.82	2.95	0.8
TbLt ^{4CF3}	3.1	15.9	0.7	1.34	–
TbLpy ^{3CF3}	4.2	41.0	1.06	1.57	1.2
TbLpy ^{4CF3}	4.2	3.2	0.09	0.16	–

^a [LnL] = 10 μ M in 10 mM PIPES buffered H₂O at pH 6.5. ^b Relative to quinine sulfate ($\Phi = 0.59$) in H₂SO₄ (0.05 M).⁶⁹ ^c Lifetime values were averaged from three independent measurements and are subjected to an error of $\pm 10\%$. ^d Calculated using $q = (5 \text{ ms}) \cdot (1/\tau_{H_2O} - 1/\tau_{D_2O} - 0.06 \text{ ms}^{-1})$.^{16,17}

Both the DO3A-based and TACN complexes were octadentate. The complexes carry a Ln-bound water molecule, as determined using the lifetime method described above. The luminescent lifetimes of Tb(III) and Eu(III) complexes were determined using time-resolved luminescent spectroscopy (**Table 12** for Tb and **Table 13** for Eu). Lifetimes measured in water (τ_{H_2O}) were basically identical in **EuL**^R when comparing 3-CF₃ series to the 4-CF₃ analogous and **EuL**^{3F} to **EuL**^{4F} (**Table 13**). τ_{D_2O} values varied slightly, but despite the differences $q = 1$ was found for **EuL**^R. τ_{H_2O} in **TbL**^R was varied; values of 1.06, 1.44, 1.82 and 1.73 were obtained in **TbLpy**^{3CF3}, **TbL**^{3CF3}, **TbLt**^{3CF3}, and **TbL**^{4F}, respectively. Lifetimes measured in D₂O were in the $\tau_{D_2O} = 1.6$ – 3.0 ms range. The lifetime method is not applicable in complexes undergoing BET. In all the listed 4-CF₃ substituted Tb complexes unrealistic q -values were obtained due to BET (**Table 12**). More reliable q -values were observed within experimental error (± 0.5) for **TbL**^{3F} and **TbL**^{4F}, and **TbL**^{3CF3}, **TbLt**^{3CF3} and **TbLpy**^{3CF3} which were both $q = 1$.

Φ_L in **TbL** complexes were $\sim 10\%$ lower than in **GdL** complexes with the exception of **TbL**^{4F} where Φ_L was lowered by 40% ($\Phi_L = 7.3\%$ in **GdL**^{4F} vs 4.4% in **TbL**^{4F}). This decrease might be attributed to S₁-mediated EnT to the Tb(III). The position of the CF₃-group had marginal effects in Φ_L , almost identical values within the experimental error were found for **TbL**^{3CF3} and **TbL**^{4CF3} (4.1 and 4.5%, respectively), for **TbLt**^{3CF3} and **TbLt**^{4CF3} (3.0 and 3.1%, respectively) and for **TbLpy**^{3CF3} and **TbLpy**^{4CF3} (4.2%). The largest difference was observed between **TbL**^{3F} and **TbL**^{4F} with $\Phi_L = 8.1$ and 4.4%, respectively.

Φ_{Ln} of **TbL** reached as high as 43% along the series of the new Tb(III) complexes. Metal-centred quantum yields around 40% for Tb(III) are the

highest reported amongst coumarin- and carbostyryl-sensitized Tb complexes. $\Phi_{\text{Tb}} = 43, 31, 40$ and 41% were determined in **TbL**^{4F}, **TbL**^{3CF₃}, **TbLt**^{3CF₃} and **TbLpy**^{3CF₃}, respectively. Regarding the position of the substituent (-F or -CF₃) on the carbostyryl, a reversed effect was observed in Φ_{Tb} . It is clear that the trifluoromethyl group in 3-position was favorable in **TbL**. Φ_{Tb} was found to be 10-, 2.5- and 12-fold higher in **TbL**^{3CF₃}, **TbLt**^{3CF₃} and **TbLpy**^{3CF₃}, respectively, than in their 4-CF₃ analogue likely due to their higher-energy T_1 , which prevents BET. Introduction of the tertiary amide linker further increased Φ_{Tb} to 40% in **TbLt**^{3CF₃}. This effect of the tertiary amide linker was seen before and could be attributed to the small changes in T_1 resulting in probably a better spectral overlap for EnT between the chromophore and Tb(III). Φ_{Tb} was 2.5-fold larger in **TbLt**^{3CF₃} compared to **TbLt**^{4CF₃}. The highest Φ_{Tb} within the CF₃ series was found in **TbLpy**^{3CF₃}, $\Phi_{\text{Tb}} = 41\%$. The pyridyl TACN ligand provided a Tb quantum yield that was as high as had been found in DO3A-based Tb(III) emitters. Fluorination in the 4-position yielded the highest Φ_{Tb} in the new series, $\Phi_{\text{Tb}} = 43\%$. The significantly higher T_1 energy level in **GdL**^{4F} (23200 cm^{-1} vs 22100 cm^{-1} in **GdL**^{3F}) eliminates the BET quenching pathway. The particularly high Φ_{Tb} in **TbL**^{4F} might be the result of a combination of a more efficient EnT and the absence of BET Compared to **TbL**^{3F}.

Table 13 Photophysical characterisation of **EuL**^a

	Φ_{L} (%) ^b	Φ_{Ln} (%) ^b	$\tau_{\text{H}_2\text{O}}$ (ms) ^c	$\tau_{\text{D}_2\text{O}}$ (ms) ^c	q^d	τ_{rad} (ms) ^e	$\Phi_{\text{Ln}}^{\text{Ln}}$ (%) ^f	η_{sens} (%) ^f
EuL ^{3F}	0.68	1.09	0.62	2.26	1.0	9.25	6.7	16
EuL ^{4F}	2.15	4.94	0.61	2.18	1.0	5.19	11.7	42
EuL ^{3CF₃}	1.63	7.42	0.61	2.16	0.9	5.15	11.7	64
EuL ^{4CF₃}	1.70	7.90	0.62	2.08	1.0	5.38	11.5	69
EuLt ^{3CF₃}	2.76	9.70	0.64	2.12	0.9	5.25	12.3	79
EuLt ^{4CF₃}	2.70	11.6	0.66	2.16	1.0	5.36	12.2	95
EuLpy ^{3CF₃}	0.61	6.30	0.51	1.34	1.0	2.81	18.1	35
EuLpy ^{4CF₃}	0.61	7.95	0.51	1.28	1.0	2.87	17.8	46

^a [LnL] = $10\text{ }\mu\text{M}$ in 10 mM PIPES buffered H₂O at pH 6.5. ^b Relative to quinine sulfate ($\Phi = 0.59$) in H₂SO₄ (0.05 M).⁶⁹ ^c Lifetime values were averaged from three independent measurements and are subjected to an error of $\pm 10\%$. ^d Calculated using $q = (1.2\text{ ms}) \cdot (1/\tau_{\text{H}_2\text{O}} - 1/\tau_{\text{D}_2\text{O}} - 0.25\text{ ms}^{-1} - m \cdot 0.075\text{ ms}^{-1})$ for Eu; m = number of nearby amide N-H oscillators.^{16,17} ^e Calculated using Eq. 2. ^f Calculated using Eq. 1.

Φ_{L} in **EuL**^R was substantially lower than in the analogous **GdL**^R. This is consistent with the combination of S_1 mediated EnT and the depopulation of the antenna S_1 by PeT. Moreover, PeT quenching often results in diminished Φ_{Eu} . Within the 3-CF₃ substituted series the extent of these processes might

be assumed to be almost the same as in the 4-CF₃ substituted series. For example, Φ_L in **GdL**^{3CF₃} and **GdL**^{4CF₃} is 4.9%, whereas in **EuL**^{3CF₃} and **EuL**^{4CF₃} it is 1.63 and 1.7%, respectively. Φ_L was lowered to 2.76 (**EuLt**^{3CF₃}) and 2.7% (**EuLt**^{4CF₃}) from 3.7 (**GdLt**^{3CF₃}) and 3.2% (**GdLt**^{4CF₃}). The residual antenna fluorescence dropped to 0.61% in **EuLpy**^{3CF₃} and **EuLpy**^{4CF₃} from 4.5% in **GdLpy**^{3CF₃} and **GdLpy**^{4CF₃}. Much larger changes were observed in case of **EuL**^{3F} and **EuL**^{4F}. The loss in Φ_L in **EuL**^{3F} (0.68%) and **EuL**^{4F} (2.15%) was 95 and 70%, respectively, compared to the parent **GdL**^{3F} (12.8%) and **GdL**^{4F} (7.3%). Φ_{Eu} were in the 5–11% range depending on the substituent of the carbostyryl or the coordination environment. In the 3-CF₃ series Φ_{Eu} were systematically lower than in the 4-CF₃ series: 7.42 in **EuL**^{3CF₃} and 7.9% in **EuL**^{4CF₃}; 9.7 in **EuLt**^{3CF₃} and 11.6% in **EuLt**^{4CF₃}; and 6.3 in **EuLpy**^{3CF₃} and 7.95% in **EuLpy**^{4CF₃}. Regardless the position of the CF₃-group or the ligand environment these emitters all showed exceptionally high Φ_{Eu} amongst other DO3A- and TACN-based Eu(III) emitters. Though, ~5-fold larger Φ_{Eu} was observed in **EuL**^{4F} than in **EuL**^{3F} – $\Phi_{Eu} = 4.94$ vs 1.09%, respectively.

The thermodynamic feasibility of PeT from antenna *S*₁ to the Eu(III) can be estimated using Eq. 5, where *E*_{ox} is the oxidation potential of the donor, *E*_{red} is the reduction potential of the acceptor (Eu(III)), *E*_s is the (singlet) excited state energy of the antenna and the last term was approximated to be ~0.15 eV. *E*_{ox} was determined to be +1.89, +1.85, +1.84, and +2.08 V (vs NHE) in **AcCS**^{4F}, **AcCS**^{4CF₃}, **AcCS**^{3CF₃} and **AcCSt**^{3CF₃}, respectively (see Chapter 5.3). *E*_{red} of Eu(III) was approximated with the cathodic potential of the overall uncharged 4-CF₃-substituted DO3A-based complex with a value of –0.89 V (vs NHE).⁷¹ *E*_s is the excited state energy of the antenna, determined from the first vibronic band of the appropriate **GdL** spectra at 77 K. Energies were found to be 3.62, 3.40, 3.44, and 3.40 eV for **GdL**^{4F}, **GdL**^{3CF₃}, **GdL**^{4CF₃} and **GdLt**^{3CF₃}, respectively. *E*_{ox} and *E*_s values were previously determined in **AcCSt**^{4CF₃} (*E*_{ox} = +2.20 V vs NHE, *E*_s = 3.39 eV, see Chapter 3.3). Data obtained previously for **GdL**^{4CF₃} (*E*_s = 3.40 eV) were used for the calculation. The driving force of PeT was estimated to be –0.99, –0.81, –0.86, –0.45 and –0.58 eV for **EuL**^{4F}, **EuL**^{4CF₃}, **EuL**^{3CF₃}, **EuLt**^{4CF₃} and **EuLt**^{3CF₃}, respectively.

To better understand EnT processes additional parameters were determined. τ_{rad} , Φ_{Ln}^n and η_{sens} were calculated for Eu(III) according to Eq. 1 and 2 using the corrected steady-state emission spectrum (**Table 13**). Fluorination slightly lengthened τ_{rad} (5.19, 5.25 and 5.28 ms in **EuL**^{4F}, **EuL**^{5F} and **EuL**^{6F}, respectively) with the exception of **EuL**^{3F} ($\tau_{rad} = 9.25$ ms) where almost 2-fold increase was observed compared to **EuL**^H ($\tau_{rad} = 5.18$ ms). The identical τ_{obs} within the series resulted in very similar Φ_{Ln}^n in the 11.5–11.9% range. Due to the unexpectedly long τ_{rad} in **EuL**^{3F} the intrinsic quantum yield was out of the abovementioned range, $\Phi_{Ln}^n = 6.7\%$. Both the similar radiative lifetimes and intrinsic quantum yields indicate a similar coordination sphere in the Eu(III) complexes; **EuL**^{3F} is the exception. η_{sens} in **EuL**^{4F} was ~2.5-fold larger than

in **EuL**^{3F} ($\eta_{sens} = 42$ and 16.1%, respectively). The sensitisation efficiency in **EuL**^{4F} is similar to what was seen in other fluorinated Eu(III) complexes (~43% for **EuL**^{5F} and **EuL**^{6F}), while still being higher than in **EuL**^H; $\eta_{sens} = 36\%$.

In the CF₃ substituted Eu(III) complexes τ_{obs} was the same within the experimental error (Table 13), as were the obtained Φ_{Ln}^{Ln} values. Previous results suggested that the tertiary-amide linker could improve Φ_{Eu} by increasing η_{sens} . The highest η_{sens} was found in **EuLt**^{4CF₃} (95%) which was ~15% higher than in **EuL**^{4CF₃} (69%). The same was observed in the current system. η_{sens} increased from 64% in secondary amide-linked **EuL**^{3CF₃} to 79% in tertiary amide-linked **EuLt**^{3CF₃}. As Φ_{Ln}^{Ln} were similar for the two sets of complexes, the increase in η_{sens} translated to a corresponding increase in Φ_{Eu} , to an excellent value of $\Phi_{Eu} = 11.6\%$ in water.

τ_{rad} in the pyridyl TACN complexes were 2.81 and 2.87 ms in **EuLpy**^{3CF₃} and **EuLpy**^{4CF₃}, respectively. The identical τ_{obs} (0.51 ms) resulted in insignificant differences between the intrinsic quantum yields of **EuLpy**^{3CF₃} (18.1%) and that of **EuLpy**^{4CF₃} (17.8%). η_{sens} in **EuLpy**^{3CF₃} was lower (35%) than in **EuLpy**^{4CF₃} (46%), which is the cause of the lower metal centred quantum yield in **EuLpy**^{3CF₃} (6.3%) than in **EuLpy**^{4CF₃} (7.95%).

In pyridyl-containing TACN-based Ln complexes additional electron transfer processes might operate in competition with the luminescence sensitisation (see Chapter 2). Having all the necessary data in hand, we can estimate the feasibility of an electron transfer from antenna S₁ to the pyridines (ΔG_{py}). $E_{red} = -1.36$ V vs NHE (for unsubstituted pyridine, see Chapter 2.3) was used. ΔG_{py} was estimated to be -0.35 and -0.38 eV in **GdLpy**^{3CF₃} and **GdLpy**^{4CF₃}, respectively. This means, that even if such electron transfer took place in **LnPy** it would be expected to be responsible for a very similar degree of quenching.

The change in antenna T_1 in **LnLpy**^{3CF₃} (22700 cm⁻¹ in **GdLpy**^{3CF₃} vs 21700 cm⁻¹ in **GdLpy**^{4CF₃}) made the 3-CF₃ substituted carbostyryl an excellent sensitizer of Tb(III) ($\Phi_{Tb} = 41\%$ in **TbLpy**^{3CF₃}), however might be responsible for the lower η_{sens} in **EuLpy**^{3CF₃} compared to **EuLpy**^{4CF₃}.

5.4 Conclusions

Here, we reported new 4-fluoro and 3-CF₃ substituted carbostyryls (**CS**^{4F} and **CS**^{3CF₃}, respectively) as potential sensitizers of Eu(III) and Tb(III) emission. The new chromophores were incorporated into secondary and tertiary amide-linked DO3A-based and secondary amide-linked pyridyl-containing TACN-based ligands (**L**, **Lt** and **Lpy**, respectively). The corresponding Ln(III) complexes (Ln = Gd, Eu and Tb) were prepared. Previous results allowed us to compare the antenna properties of **CS**^{4F} to **CS**^{3F} and **CS**^{3CF₃} to **CS**^{4CF₃}.

Similarities in coordination geometry imposed by the same ligand environment were confirmed by the similar spectral shape, q -value analysis, and similar τ_{rad} and $\Phi_{\text{Ln}}^{\text{Ln}}$ values. The new ligands turned to be excellent sensitisers for Tb(III) emission reaching Φ_{Tb} as high as 43% in **TbLpy**^{3CF3} in water. Antenna T_1 was blue-shifted enough in **GdL**^{4F} and **GdL**^{3CF3} compared to **GdL**^{3F} and **GdL**^{4CF3}, respectively, to preclude BET in **TbL**^{4F} and **TbL**^{3CF3}. The insertion of tertiary amide linker yielded ~30% increase in Φ_{Eu} and Φ_{Tb} in **LnLt**^{3CF3} compared to the secondary amide **LnL**^{3CF3}. Φ_{Eu} and η_{sens} were lower in the 3-CF₃ series compared to the 4-CF₃ series, possibly due to differences in η_{sens} .

Concluding remarks and outlook

The rational design of bright lanthanide (Ln) emitters has always been exceptionally challenging. The presence of various processes in the excited state (e.g. energy transfer, electron transfer, thermal back energy transfer, quenching) makes these systems extremely complicated. This thesis was focused to better understand energy transfer processes and quenching pathways through structural modifications of Ln(III) complexes. Subtle changes in the ligand might be detrimental for some quenching pathways, however it could decrease the overall brightness of certain emitters depending on the Ln.

A set of picolinate-containing TACN-based Ln(III) complexes was synthesised and photoinduced electron transfer (PeT) from the excited state antenna to the pyridines was studied. The reducibility of the picolinate pedants was controlled by the careful choice of *para*-substituent. Such intraligand PeT was thermodynamically feasible and dependent on the electron accepting ability of the pyridines. Hence, this alternative process was competing with energy transfer and ligand-to-metal PeT in the reducible Eu(III) complexes, moreover decreased the residual antenna fluorescence in non-redox active Gd(III) and Tb(III) complexes.

A selection of the picolinate-containing TACN-based Ln(III) complexes were equipped with a methylcaboxylate-substituted tertiary-amide linker. Structural similarities enabled us to compare the luminescent properties with complexes possessing secondary-amide linkers and cyclen-based systems lacking the reducible pyridines. The presence of tertiary amide linker resulted in enhanced metal quantum yield compared to the secondary amide compounds. Such high quantum yields were comparable and, in some cases even higher than, those obtained for cyclen-based systems lacking the quenching pyridine. As a result, suppressing PeT and BET quenching pathways yielded highly photostable and robust emitters.

Several new fluorinated carbostyryl were synthesised via a photochemical cyclisation reaction. The reaction was robust, reproducible and scalable. Such photochemical reaction is the mildest towards sensitive substituents, consequently there could be a huge potential in the development and applications of this transformation.

A small library of Ln(III) complexes equipped with fluorinated antennae, and DO3A- and TACN-based ligands was prepared. Photophysical

characterization revealed that monofluorination yielded no significant improvements in the luminescent quantum yields compared to other non-fluorinated analogues, although the highest Tb(III) quantum yield was observed in the 4-fluoro sensitized Tb(III) complex. Interestingly, fluorine in the 3-position of the carbostyryl resulted in unexpected excited state behavior compared to the other fluorinated parents. Findings suggested the presence of several emitting species and the change in the coordination sphere of the metal in the excited state. We hypothesised that deviations might be originated from the 3-fluoro antenna, therefore further work would be carried out investigating both the 3-fluoro carbostyryl and its Ln(III) complexes. Compounds would be studied by infrared spectroscopy, ^1H and ^{19}F NMR, UV-Vis absorption, and steady-state and time-resolved emission spectroscopy in various solvents.

The 3- CF_3 substituted antennae were robust sensitizers of Eu(III) and Tb(III) emission. Eu(III) quantum yields in the 3- CF_3 series were slightly lower compared to the 4- CF_3 series possibly due to less efficient sensitization. However, Tb(III) quantum yields were 5–12-fold larger in the 3- CF_3 substituted complexes compared to the 4- CF_3 functionalised analogues.

Carbostyryls are capable of sensitizing several Lns, thus these ligands might potentially be used in multiplex imaging. Preparation and characterization of additional Ln(III) complexes, such as Dy(III), Sm(III), and even the near-infrared emitter Yb(III) are of interest.

Fluorine is an attractive element and has been widely used in molecular and cellular imaging. ^{18}F is a radioactive isotope used in positron emission tomography (PET) for early detection of tumors. ^{18}F labeling requires sufficient late stage functionalisation strategies using either electrophilic or nucleophilic fluorinating reagents. Thus, the development of reactive intermediates for late stage fluorination may be crucial. ^{19}F magnetic resonance has attracted attention in cellular imaging (^{19}F -MRI) due to the absence of radioactivity. Fluorinated Ln compounds offer tunability: ^{19}F relaxation rate is controlled through the choice of Ln and appropriate molecular design.

Fluorinated luminescent Ln(III) complexes might be an interesting platform for multimodal imaging.

Popular science summary

Lanthanides are a group of metals. Their +3 charged (trivalent) ions have unique luminescent properties, that is, their compounds can emit light after excitation. Each lanthanide has a characteristic emission, like a fingerprint. The color of the emission can be, for example, red (for europium) or green (for terbium). Lanthanide complexes are often excited by energy transfer from a nearby organic compound that absorbs light efficiently, called an 'antenna'. Light emission from the lanthanide excited state can be diminished (quenched) by certain environmental factors. The most studied of these factors are the O–H, N–H and C–H bonds in and around the molecule. The best example is water, the solvent in which many of the lanthanide complexes are used, and which effectively quenches Ln luminescence. In order to shield lanthanides from their environment they are often encapsulated in a macrocycle which is usually connected to the antenna; the whole construction is called the 'ligand'. Another quenching pathway is photoinduced electron transfer (PeT), in which the antenna, instead of giving up its energy, gives up an electron to the lanthanide ion. This is most common for reducible lanthanide ions, e.g. europium (Eu). PeT often results in the decrease of lanthanide luminescence. Gadolinium (Gd) and terbium (Tb) are, on the other hand, lanthanides with trivalent ions which are hard to reduce.

In the first part of this thesis we investigated electron transfer processes originating from the excited antenna. We were interested in whether an electron can be given to other parts of the complex than the metal, and if we may be able to control this process. The type of ligand that we used for these studies contains a popular metal-binding motif called a picolinate, which is a derivative of the electron-poor, i.e. reducible, pyridine compound. In order to test that scenario we prepared versions of the basic ligand with more or less reducible picolines by modifying the pyridine to make it more or less electron poor. We found out that indeed several electron transfer processes could take place in these complexes, including to the picolines. Electron transfer to the reducible units decreased the overall brightness of the emitters. More importantly, these processes could be controlled through ligand modification, for example, using easier- and harder-to-reduce units or changing the linker. Therefore, an optimised ligand carrying reducible parts can provide as bright emitters as those of lacking the reducible groups. These

results underline the importance of ligand design when substituents might be involved in electron transfer processes.

In the second part of the thesis we prepared a library of fluorinated carbostyrils as potential sensitizers of Ln emission. Fluorine is the element with the highest electronegativity, and our hypothesis was that adding fluorine to the antenna would make it less reducing towards the lanthanide ions. We also expected that the position to which the fluorine is attached would decide how large this effect would be. Much to our surprise we found that a single fluorine in the antenna did not necessarily improve the luminescent properties significantly. Furthermore, unexpected effects were seen when adding the fluorine to the 3-position of the antenna. These results show that the design of antennae that do not take part in PeT is not straightforward, and that it can be difficult to predict all the excited-state processes a lanthanide complex will participate in.

Other antennae were functionalized with trifluoromethyl (CF_3) groups and subtle changes in the position of the CF_3 group led to improved Ln emission properties. The CF_3 -group is also strongly electron-withdrawing, and was tested as an alternative to the fluorination. This strategy proved much more successful, resulting in excellent Eu and Tb emitters.

Fluorinated compounds have been utilized for biomedical applications. For instance, fluorine-18 (^{18}F) – a fluorine radioisotope – has been used in positron emission tomography (PET) for early detection of tumors. Fluorine-19 (^{19}F) is an attractive element in cellular imaging (^{19}F -MRI) in the combination with lanthanides. These examples show the importance of fluorinated Ln substances and that the development of further compounds might be of interest in biomedical applications.

Populärvetenskaplig Sammanfattning

Lantanoider är en grupp av metaller. Deras +3-laddade (trivalenta) joner har unika luminiscenta egenskaper, det vill säga, föreningar där de ingår kan utstråla ljus vid excitering. Varje lantanoid har en karaktäristisk ljusemission, likt ett fingeravtryck. Färgen på emissionen kan exempelvis vara röd (för europium) eller grön (för terbium). Lantanoidkomplex exciteras ofta via energiöverföring från en närliggande organisk förening som absorberar ljus effektivt, en så kallad "antenn". Ljusemission från lantanoidens exciterade tillstånd kan försvagas (dämpas) av olika miljöfaktorer. De mest studerade miljöfaktorerna är O–H-, N–H- och C–H-bindningar i och runt molekylerna. Det bästa exemplet är vatten, vilket är ett lösningsmedel som används för många lantanoidkomplex som effektivt dämpar Ln-luminiscens. För att skydda lantanoiderna från deras omgivning innesluts de ofta i en makrocyclisk organisk molekyl, som vanligen är kopplad till antennen; hela konstruktionen kallas en "ligand". En annat sätt som ljusemissionen kan dämpas är genom ljusinducerad elektronöverföring (PeT), där antennen istället för att avge energi ger ifrån sig en elektron till lantanoidjonen. Detta är vanligast för reducerbara lantanoidjoner, såsom europium (Eu). PeT leder ofta till en försvagad luminiscens från lantanoiden. Gadolinium (Gd) och terbium (Tb) är däremot lantanoider med svårreducerade trivalenta joner.

I första delen av den här avhandlingen undersöktes elektronöverföringsprocesser som börjar från den exciterade antennen. Målet var att avgöra huruvida en elektron kan överföras till andra delar av komplexet än metalljonen och om det är möjligt att styra denna process. Den typ av ligand som vi använde för dessa studier innehåller ett ofta använt metallbindande motiv som kallas pikolinat, vilket är ett derivat av den elektronfattiga, dvs reducerbara, föreningen pyridin. För att testa detta så tillverkades varianter av grundliganden med mer eller mindre reducerbara pikolinater genom modifiering av pyridingruppen för att göra den mer eller mindre elektronfattig. Vi observerade att flera elektronöverföringsprocesser kunde ske i dessa komplex, inklusive överföringar till pikolinater. Elektronöverföring till de reducerbara delarna av liganden leder till minskad emission från ljusutsändaren. Dessa processer kan kontrolleras genom modifiering av liganden, exempelvis genom användandet av enheter som är lättare eller svårare att reducera, eller genom att byta ut föreningen som kopplar samman ligandens delar. En optimerad ligand som innehåller av reducerbara delar kan ge upphov till lika stark ljusemission som en ligand som

saknar reducerbara delar. Dessa resultat understryker betydelsen av liganddesign i ligander där substituenterna kan vara en del av elektronöverföringsprocessen.

I den andra delen av avhandlingen sammanställdes ett bibliotek av fluorinerade karbostyriler som potentiella sensibilisatorer för Ln-emission. Fluor är det mest elektronegativa grundämnet, och vår hypotes var att genom att inkorporera fluor i antennen skulle den bli mindre reducerbar gentemot lantanoidjonerna. Vi förväntade oss också att fluoratomens placering skulle påverka hur betydande effekten skulle bli. Till vår förvåning fann vi att en ensam fluoratom i liganden inte nödvändigtvis förbättrade de luminiscenta egenskaperna nämnvärt. Dessutom, oförutsedda sidoeffekter uppstod när fluoratomen fästes vid 3-positionen på antennen. Resultaten visar att utformningen av antennerna som inte tar del i PeT-processen inte är självklar, och att det är svårt att förut säga alla processer ett lantanoidkomplex kan genomgå vid excitering.

Andra antenner funktionaliserades med trifluormetyl-grupper (CF_3) och små förändringar i den gruppens placering ledde till förbättrade Ln-emissionsegenskaper. CF_3 -gruppen är också ytterst elektrondragande, och undersöktes därför som ett alternativ till fluorinering. Detta tillvägagångssätt visade sig vara betydligt mer lyckat och resulterade i Eu- och Tb-föreningar med utmärkt ljusemission.

Fluorinerade föreningar har använts till biomedicinska tillämpningar. Exempelvis, fluor-18 (^{18}F) – en fluorisotop – har använts inom positronemissionstomografi (PET) för tidig upptäckt av tumörer. Kombinationen av fluor-19 (^{19}F) tillsammans med lantanoider har lovande tillämpningar inom cellavbildning (^{19}F -MRI). Dessa exempel visar att fluorinerade Ln-föreningar har viktiga användningsområden, och att vidare utveckling av denna typ av ämnen kan leda till intressanta biomedicinska framsteg och tillämpningar.

Acknowledgments

My work at Uppsala University would not have been possible without the help of a great number of people.

I am truly grateful to my supervisor **Eszter Borbas**, for giving me the opportunity to be part of her research group. Working with you allowed me to grow scientifically and as a person, too. I am thankful for the freedom you gave me, the lessons you taught me, and the constant belief and supportive attitude. I thank for the hard times you put me in, because without those I would not have been able to achieve that many things. Thank you for being extremely patient and open-minded, these things make you exceptional.

I thank to my co-supervisor **Henrik Ottosson**, for always being behind me. I enjoyed sharing science with you, because you could often express a different point of view. Thank you for the small talks and coffee breaks.

I am thankful to **Sascha Ott**, for letting me be part of SMC. Your management skills are absolutely high-end. There was so much to learn from you about how to be a great leader. You taught me many things about how to deal with issues on a higher institutional level, from communication, through measures, to acts. Thank you for checking up on me from time to time, the belief you had in me and the constant support.

I thank **Andreas Orthaber** for taking great initiatives at the department and the collaborations we had. It was nice having a chat with you every time, regardless if it was about science or something else. Your good sense of humour always cheered me up :)

I am grateful to **Anders Thapper** for all the work you have done in the background for all of us. Special thanks for helping me out last minute with the Swedish translation of the popular science summary.

I would like to thank **Stefano Crespi** for being extremely nice and responsible, you are very much appreciated at the department.

Monika Tomar, I feel lucky that I met you. I thank for ALL the fun we had in and out of the lab: LUNCH!, fika, dinners, a little bit of gossiping :D, trips and skiing! Also, you showed me an example of a very disciplined scientist/person and I am grateful for that, I learnt from you. You were always so selfless and helped me out many times. I hope that I could give you something

in return even if we would never be even. I owe you! I wish you the best of luck with your PhD and future. You will anyways nail it :)

Rohan Bhimpuria, your arrival gave quiet a push to the group. You are so dedicated and disciplined. Sometimes when I was going through a harder or unsuccessful period you often motivated me not to give up. I am glad that I have met you and wish the best.

I am thankful to the former members of the group: **Salauat** for helping me a lot with measurements and instruments; **Emilie** for being a professional co-worker and friend at the same time, we had such a good time together in Uppsala; last but not least, **Parvathy** and **Kiran** for being great colleagues.

I am thankful to all the students I have met and worked with during my PhD studies. **Eirini**, **Mathilde**, **Rosa**, **Fiona**, **Ali** and **Jules** you all taught me how to become a better mentor and person. I would like to wish all the best for all of you and I hope that you will find your way in the future.

I am extremely grateful to **Anna Beiler** and **Leon Leid**. Guys, we had so much fun together, I enjoyed every minute of chatting, sharing a drink, having dinner parties, going dancing, having hiking and skiing trips, climbing... and the list is endless. I feel lucky to have you Guys :) Thanks for the fun times in Tarragona and Leon, most importantly for the 'type 2 fun' bike rides!

Köszönöm **Kovács Daninak** a sok segítséget, a folyamatos támogatást és a hosszúra nyúló barátságot. Igaz már több mint 4 éve nem találkoztunk és arra sem emlékszem, hogy nézel ki :D de a facetime beszélgetések mindig is sokat jelentettek és örülök, hogy tartjuk a kapcsolatot. Azon leszek, hogy ez ne változzon! Réka, alig várom, hogy személyesen is találkozzunk!

I am thankful to **Anna Arkhypchuk** for being an amazing colleague and a friend. Thanks for all the help and support you gave with whatever I needed :), for being so proactive at the department, it is truly appreciated. I enjoyed all the lunches, fikas and talks we had together.

I would like to thank **Starla** for everything, I MEAN, your energies are insane. It always fascinated me. I am glad that we got along and had fun with climbing, cycling and dancing sometimes. You have been my English teacher since the beginning and I appreciate that a lot. Special thanks for proofreading my licentiate and doctoral thesis!

Nicholas, thanks for being a great colleague and friend. Times change and sometime I miss those years we spent together in Uppsala. It was so much fun :) I am glad that we are still in touch and I hope that will not change!

I thank to **Ludo** and **Robin** for spending time together in and out of the lab. Climbing trips, dinners and parties were fun!

Alex és Fanni, köszönöm, hogy vagytok nekem. Nagyon sok támogatást és segítséget kaptam tőletek az elmúlt években és ezért nagyon hálás vagyok. Bízom benne, hogy egyszer majd mindazt viszonzni tudom.

I am grateful to **Anna Di Marco** and **Alve** for your friendship. Anna, thank you for the fun times in Uppsala and for being my Italian guide. I feel like you are one of those who understands me :). Alve, thanks for the good talks, dinners/beers we had together, I hope we will continue with that in the future!

Marleen, I am truly happy that I have met you. I am grateful for having dinners together, nice talks and obviously, being my cycling buddy for a while :) You made my time happy in Uppsala.

Jacob, thanks for the great talks in the lab and surely the fun rides together. I hope you will find yourself in the future. Just do not give up on funny socks and do not forget to have a Flapjack :D

I would like to thank to all the members and alumni of SMC, **Toma, Rajesh, Asif, Roman, Thuan, Nina, Wanja, Amol, Jingguo, Corentin, Nathalie, Sindhujaa, Matias, Jorn, Péter, Emil, Carlos, and Ashleigh, Leandro, Brian, Jordan, Kelly, Timofey** and **Juri** for being great colleagues and creating a friendly atmosphere.

I am grateful to other colleagues and alumni in House 7, **Sigrid, Martin, Belinda, Astrid, Claudia, Beri, Vitor, Kim, Conrad, Max, Paul** and **Moritz** for creating such a great environment.

I thank to **Kate** for all the time we spent together. You meant a lot to me.

I am thankful to **Sven** for the day-to-day help!

I would like to thank to some people from BMC, **Erdélyi Máté, Kinga, Scott, Fabio, Stefan** and **Mariya** for having fun together outside the lab. I thank to Máté and Scott for the endless wee hours on the bike.

Végül, de nem utolsó sorban, pedig szeretném megköszönni **családomnak** a mérhetetlen szeretetet és támogatást amit kaptam. Apa, Anya, Bence, Csilla, Sári és Szonja, köszönöm, hogy mellettem álltatok és hittetek bennem. Nélkületek ez nem jöhetett volna létre. Köszönöm Nagymamámnak a sok finomságot.

Hálás vagyok a támogatásért és családi összejövetelekért a többieknek is, **Mariann, Pali, Péter, Ernő, Zsuzsa és Tamás**.

Doktori értekezésemet mélységes tisztelettel és végtelen szeretettel ajánlom a nemrég tragikus hirtelenséggel élete delén elhunyt **Dr. Szabados Pál Szabolcs** ügyésznek, a Nagynéném férjének, akinek a magán- és szakmai élete, harmonikus személyisége gyermekkorom óta etikailag példaértékű. Megtanított arra, hogyan váljak felelős, becsületes, szorgalmas emberré, s

tanulmányaim folyamán is végigkísért megkülönböztetett jóságos figyelme, törődése. Sajnos, már nem élheti meg, hogy megvédjem doktori értekezésemet, de mindig derűs, keresztény hittől és életszeretettől sugárzó tekintete tiszta forrásként egész életpályám folyamán velem marad.

References

- 1 Cotton, S. In *Lanthanide and Actinide Chemistry* John Wiley & Sons, Ltd, **2006**, 1–7.
- 2 Eliseeva, S. V.; Bünzli, J.-C. G. *Chem. Soc. Rev.*, **2010**, *39*, 189–227.
- 3 Bünzli, J.-C. G. *Chem. Rev.* **2010**, *110*, 2729–2755.
- 4 a) Evans, W. J.; Zucchi, G.; Ziller, J. W. *J. Am. Chem. Soc.* **2003**, *125*, 10–11. b) MacDonald, M. R.; Bates, J. E.; Fieser, M. E.; Ziller, J. W.; Furche, F.; Evans, W. J. *J. Am. Chem. Soc.* **2012**, *134*, 8420–8423. c) Fieser, M. E.; MacDonald, M. R.; Krull, B. T.; Bates, J. E.; Ziller, J. W.; Furche, F.; Evans, W. J. *J. Am. Chem. Soc.* **2015**, *137*, 369–382.
- 5 Cotton, S. In *Lanthanide and Actinide Chemistry* John Wiley & Sons, Ltd, **2006**, 61–87. b) Heffern, M. C.; Matosziuk, L. M.; Meade, T. J. *Chem. Rev.* **2014**, *114*, 4496–4539.
- 6 Parker, D. *Coord. Chem. Rev.* **2000**, *205*, 109–130.
- 7 Kleinerman, M. *Chem. Phys.* **1969**, *51*, 2370.
- 8 Lakowicz, J. R. *Principles of Fluorescence Spectroscopy*, 3 ed. Springer-Verlag, US, **2006**.
- 9 Ward, M. D. *Coord. Chem. Rev.* **2010**, *254*, 2634–2642.
- 10 Horrocks, W. D.; Bolender, J. P.; Smith, W. D.; Supkowski, R. M. *J. Am. Chem. Soc.* **1997**, *119*, 5972–5973.
- 11 a) Werts, M. H. V.; Jukes, R. T. F.; Verhoeven, J. W. *Phys. Chem. Chem. Phys.* **2002**, *4*, 1542–1548. b) Andres, J.; Chauvin, A.-S. *Phys. Chem. Chem. Phys.* **2013**, *15*, 15981.
- 12 Cotton, S. In *Lanthanide and Actinide Chemistry* John Wiley & Sons, Ltd, **2006**, 9–22.
- 13 a) Parker, D.; Dickins, R. S.; Puschmann, H.; Crossland, C.; Howard, J. A. K. *Chem. Rev.* **2002**, *102*, 1977–2010. b) Butler, S. J.; Delbianco, M.; Lamarque, L.; McMahon, B. K.; Neil, E. R.; Pal, R.; Parker, D.; Walton, J. W.; Zwier, J. M. *Dalton Trans.* **2015**, *44*, 4791.
- 14 Bünzli, J.-C. G.; Eliseeva, S. V. Basics of Lanthanide Photophysics. In *Lanthanide Luminescence: Photophysical, Analytical and Biological Aspects*; Springer-Verlag Berlin Heidelberg, **2010**; pp 1–45.
- 15 Beeby, A.; Parker, D.; Williams, J. A. G. *J. Chem. Soc., Perkin Trans. 2* **1996**, 1565.

- 16 a) Beeby, A.; Clarkson, I. M.; Dickins, R. S.; Faulkner, S.; Parker, D.; Royle, L.; De Sousa, A. S.; Williams, J. A. G.; Woods M. J. *Chem. Soc., Perkin Trans. 2*, **1999**, 493–503. b) Dickins, R. S.; Parker, D.; de Sousa, A. S.; Williams, J. A. G. *Chem. Commun. (Cambridge)* **1996**, 697–698.
- 17 Horrocks, W. D.; Sudnick, D. R. *Acc. Chem. Res.* **1981**, *14*, 384–392.
- 18 Hueting, R.; Tropiano, M.; Faulkner, S. *RSC Adv.* **2014**, *4*, 44162.
- 19 Parker, D.; Williams, J. A. G. *J. Chem. Soc., Perkin Trans. 2*, **1996**, 1581.
- 20 Morss, L. R. *Chem. Rev.* **1976**, *76*, 827.
- 21 Kovacs, D.; Lu, X.; Meszaros, L. S.; Ott, M.; Andres, J.; Borbas, K. E. *J. Am. Chem. Soc.* **2017**, *139*, 5756–5767.
- 22 Weller, A. *Pure Appl. Chem.* **1968**, *16*, 115–123.
- 23 Weller, A. *Phys. Chemie* **1982**, *133*, 93–98.
- 24 Bart, S. C. *Inorg. Chem.* **2023**, *62*, 3713–3714.
- 25 Daly, S. R.; Kim, D. Y.; Girolami G. S. *Inorg. Chem.* **2012**, *51*, 7050–7065.
- 26 Balogh, E.; Tripier, R.; Ruloffa, R.; Toth, E. *Dalton Trans.* **2005**, 1058–1065.
- 27 a) Placide, V.; Pitrat, D.; Grichine, A.; Duperray, A.; Andraud, C.; Maury, O. *Tetrahedron Letters* **2014**, *55*, 1357–1361. b) Butler, S. J.; Lamarque, L.; Pal, R.; Parker, D. *Chem. Sci.* **2014**, *5*, 1750–1756.
- 28 Thomsen, M. S.; Parsons, A.; Sørensen, T. J. *Dalton Trans.* **2022**, *51*, 15725–15733.
- 29 Nielsen, L. G.; Sørensen, T. J. *Inorg. Chem.* **2020**, *59*, 94–105.
- 30 Kotková, Z.; Pereira, G. A.; Djanashvili, K.; Kotek, J.; Rudovský, J.; Hermann, P.; Elst, L. V.; Muller, R. N.; Geraldès, C. F. G. C.; Lukeš, J.; Peters, J. A. *Eur. J. Inorg. Chem.* **2009**, *1*, 119–136.
- 31 Gateau, C.; Mazzanti, M.; Pécaut, J.; Dunand, F. A.; Helm, L. *Dalton Trans.* **2003**, 2428–2433.
- 32 a) Neil, E. R.; Funk, A. M.; Yufit, D. S.; Parker, D. *Dalton Trans.* **2014**, *43*, 5490–5504. b) Walton, J. W.; Carr, R.; Evans, N. H.; Funk, A. M.; Kenwright, A. M.; Parker, D.; Yufit, D. S.; Botta, M.; Pinto, S. D.; Wong, K.-L. *Inorg. Chem.* **2012**, *51*, 8042–8056. c) Salaam, J.; Tabti, L.; Bahamyirou, S.; Lecointre, A.; Alba, O. H.; Jeannin, O.; Camerel, F.; Cianferani, S.; Bentouhami, E.; Nonat, A. M.; Charbonniere, L. J. *Inorg. Chem.* **2018**, *57*, 6095–6106.
- 33 Howard, J. A. K.; Kenwright, A. M.; Moloney, J. M.; Parker, D.; Port, M.; Navet, M.; Rousseaub, O.; Woods, M. *Chem. Commun.* **1998**, 1381–1382.
- 34 Parker, D.; Dickins, R. S.; Puschmann, H.; Crossland, C.; Howard, J. A. K. *Chem. Rev.* **2002**, *102*, 1977–2010.
- 35 Nonat, A.; Giraud, M.; Gateau, C.; Fries, P. H.; Helm, A.; Mazzanti M. *Dalton Transactions* **2009**, *38*, 8033–8046.

- 36 Weissman, S. I. *J. Chem. Phys.* **1942**, *10*, 214–217.
- 37 Amoroso, A. J.; Pope, S. J. A. *Chem. Soc. Rev.* **2015**, *44*, 4723–4742.
- 38 McMahon, B.; Mauer, P.; McCoy, C. P.; Lee, T. C.; Gunnlaugsson, T. *J. Am. Chem. Soc.* **2009**, *131*, 17542–17543.
- 39 Quici, S.; Cavazzini, M.; Marzanni, G.; Accorsi, G.; Armaroli, N.; Ventura, B.; Barigelletti, F. *Inorg. Chem.* **2005**, *44*, 529–537.
- 40 Beeby, A.; Botchway, S. W.; Clarkson, I. M.; Faulkner, S.; Parker, A. W.; Parker, D.; Williams, J. A. G. *J. Photochem. Photobiol. B* **2000**, *57*, 83.
- 41 Bobba, G.; Frias, J. C.; Parker, D. *Chem. Commun.* **2002**, 890–891.
- 42 Zhanel, G. G.; Fontaine, S.; Adam, H.; Schurek, K.; Mayer, M.; Noreddin, A. M.; Gin, A. S.; Rubinstein, E.; Hoban, D. J. *Treat. Respir. Med.* **2006**, *5*, 437–465.
- 43 Hong, W. P.; Shin, I.; Lim, H. N. *Molecules* **2020**, *25*, 5450.
- 44 Murugan, A. S.; Vidhyalakshmi, N.; Rameshb, U.; Annaraj. J. *J. Mater. Chem. B* **2017**, *5*, 3195–3200.
- 45 Hua, Z.; Dengb, Q.; Yanga, S.; Guo, D. *Colloids Surf. A* **2020**, *599*, 124861.
- 46 Lee, S. B.; Lee, N.-J.; Jung, Y. R.; Kim, D.; Hong, K. B.; Choi, S. *Chem. Lett.* **2018**, *47*, 433–435.
- 47 Ganesan, P.; Chandiran, A.; Gao, P.; Rajalingam, R.; Gratzel, M.; Nazeeruddin, M. K. *J. Phys. Chem. C* **2014**, *118*, 16896–16903.
- 48 Córdese, N. A.; Ziegler, Jr., C. B.; Hrncjez, B. J.; Heck, R. F. *J. Org. Chem.* **1978**, *43*, 2952–2958.
- 49 Bernini, R.; Cacchi, S.; Fabrizi, G.; Sferrazza, A. *Heterocycles* **2006**, *69*, 99 - 105.
- 50 Borhade, S. R.; Waghmode, S. B. *Can. J. Chem.* **2011**, *89*, 1355–1363.
- 51 Manley, P. J.; Bilodeau, M. T. *Org. Lett.* **2004**, *6*, 2433–2435.
- 52 Lončarić, M.; Gašo-Sokač, D.; Jokić, S.; Molnar, M. *Biomolecules* **2020**, *10*, 151.
- 53 Wahsner, J.; Gale, E. M.; Rodríguez-Rodríguez, A.; Caravan, P. *Chem. Rev.* **2019**, *119*, 957–1057.
- 54 Kostelnik, T. I.; Orvig, C. *Chem. Rev.* **2019**, *119*, 902–956.
- 55 Heffern, M. C.; Matosziuk, L.M.; Meade, T.J. *Chem. Rev.* **2014**, *114*, 4496–4539.
- 56 Banerjee, S. *Chem. Rev.* **2015**, *115*, 2934–2974.
- 57 de Jong, M.; Breeman, W. A. P.; Bernard, B. F.; Bakker, W. H.; Visser, T. J.; Kooij, P. P. M.; van Gameren, A.; Krenning, E. P. *J. Nucl. Med.* **2001**, *42*, 1841–1846.
- 58 Müller, C.; Zhernosekov, K.; Köster, U.; Johnston, K.; Dorrer, H.; Hohn, A.; van der Walt, N. T.; Türlér, A.; Schibli, R. *J. Nucl. Med.* **2012**, *53*, 1951–1959.
- 59 Ung, P.; Clerc, M.; Huang, H.; Qiu, K.; Chao, H.; Seitz, M.; Boyd, B.; Graham, B.; Gasser, G. *Inorg. Chem.* **2017**, *56*, 7960–7974.

- 60 Law, G.-L.; Pal, R.; Palsson, L. O.; Parker, D.; Wong, K.-L. *Chem. Commun.* **2009**, 7321-7323.
- 61 Gahlaut, N.; Miller, L. W. *Cytometry Part A* **2010**, 1113-1125.
- 62 Kovacs, D.; Kiraev, S. R.; Phipps, D.; Orthaber, A.; Borbas, K. E. *Inorg. Chem.* **2020**, 59, 106-117.
- 63 Andres, J.; Borbas, K. E. *Inorg. Chem.* **2015**, 54, 8174-8176.
- 64 Poh, J.-S.; Makai, S.; von Keutz, T.; Tran, D. N.; Battilocchio, C.; Pasau, P.; Ley, S. V., *Angew. Chem. Int. Ed.* **2017**, 56, 1864-1868.
- 65 Teixeira, M. C.; Felix, F. S.; Thomasi, S. S.; Magriotis, Z. M.; Da Silva, J. M.; Okumura, L. L.; Saczk, A. A. *Microchemical Journal* **2019**, 148, 66-72.
- 66 Kiraev, S. R.; Mathieu, E.; Siemens, F.; Kovacs, D.; Demeyere, E.; Borbas, K. E. *Molecules*, **2020**, 25, 5282.
- 67 Nonat, A.; Gateau, C.; Fries, P. H.; Mazzanti, M. *Chem. Eur. J.* **2006**, 12, 7133-7150.
- 68 Mason, K.; Harnden, A. C.; Patrick, C. W.; Poh, A. W. J.; Batsanov, A. S.; Suturina, E. A.; Vonci, M.; McInnes, E. J. L.; Chilton, N. F.; Parker, D. *Chem. Commun.* **2018**, 54, 8486-8489. b) Vonci, M.; Mason, K.; Suturina, E. A.; Frawley, A. T.; Worswick, S. G.; Kuprov, I.; Parker, D.; McInnes, E. J. L.; Chilton, N. F. *J. Am. Chem. Soc.* **2017**, 139, 14166-14172.
- 69 Suzuki, K.; Kobayashi, A.; Kaneko, S.; Takehira, K.; Yoshihara, T.; Ishida, H.; Shiina, Y.; Oishi, S.; Tobita, S. *Phys. Chem. Chem. Phys.*, **2009**, 11, 9850-9860
- 70 a) Monteiro, J. H. S. K.; Machado, D.; De Hollanda, L. M.; Lancelotti, M.; Sigoli, F. A.; De Bettencourt-Dias, A. *Chem. Commun.*, **2017**, 53, 11818. b) Latva, M.; Takalo, H.; Mukkala, V.-M.; Matachescu, C.; Rodriguez-Ubis, J. C.; Kankare, J. *J. Lumin.* **1997**, 75, 149-169.
- 71 Kovacs, D.; Mathieu, E.; Kiraev, S. R.; Wells, J. A. L.; Demeyere, E.; Sipos, A.; Borbas, K. E. *J. Am. Chem. Soc.*, **2020**, 142, 13190-13200.
- 72 Kovacs, D.; Phipps, D.; Orthaber, A.; Borbas, K. E. *Dalton Trans.*, **2018**, 47, 10702.
- 73 Kovacs, D.; Kocsi, D.; Wells, J. A. L.; Kiraev, S. R.; Borbas, K. E. *Dalton Trans.*, **2021**, 50, 4244.
- 74 a) Priya, N.; Gupta, A.; Chand, K.; Singh, P.; Kathuria, A.; Raj, H. G.; Parmar, V. S.; Sharma, S. K. *Bioorg. Med. Chem.* **2010**, 18, 4085-4094. b) Kathuria, A.; Priya, N.; Chand, K.; Singh, P.; Gupta, A.; Jalal, S.; Gupta, S.; Raj, H. G.; Sharma, S. K. *Bioorg. Med. Chem.* **2012**, 20, 1624-1638.
- 75 Beeby, A.; Faulkner, S.; Williams, J. A. G. *J. Chem. Soc., Dalton Trans.* **2002**, 1918-1922.
- 76 Parker, D.; Senanayake, P. K.; Williams, J. A. G. *J. Chem. Soc., Perkin Trans. 2* **1998**, 2129-2139.

- 77 Thayer, A. N. *Chem. Eng. News* **2006**, *84*, 15–24.
- 78 Chalmers, K. H.; Kenwright, A. M.; Parker, D.; Blamire, A. M. *Magnetic Resonance in Medicine* **2011**, 66931–936.
- 79 Alauddin, M. A. *Am. J. Nucl. Med. Mol. Imaging* **2012**, *2*, 55–76.
- 80 Strohmeier, G. A.; Fabian, W. M. F.; Uray, G. *Helv. Chim. Acta* **2004**, *87*, 215–226.
- 81 a) Heck, R. F. “Palladium-Catalyzed Vinylation of Organic Halides,” In: *Organic Reactions* 1982, *27*, 345–390. b) Rousee, K.; Bouillon, J.-P.; Couve-Bonnaire, S.; Pannecoucke, X. *Org. Lett.* **2016**, *18*, 540 – 543.
- 82 a) Wang, M. Z.; Xu, H.; Feng, Q.; Wang, L.-Z.; Wang, S.-H.; Li, Z.-M. *J. Agric. Food Chem.* **2009**, *57*, 7912–7918. b) Lv, F.; Li, Z.; Hu, W.; Wu, X. *Bioorg. Med. Chem.* **2015**, *23*, 7661–7670.
- 83 Whritenour, D. C.; Brenek, S. J.; Tom, N. J. *Org. Proc. Res. Dev.* **2001**, *5*, 539–541. b) Merlic, C. A.; Motamed, S.; Quinn, B. *J. Org. Chem.* **1995**, *60*, 3365 – 3369.
- 84 a) Guo, R.; Qi, X.; Xiang, H.; Geaneotes, P.; Wang, R.; Liu, P.; Wang, Y.-M. *Angew. Chem. Int. Ed.* **2020**, *59*, 16651–16660. b) Li, Y.; Liu, X.; Ma, D.; Liu, B.; Jiang, H. *Adv. Synth. Catal.* **2012**, *354*, 2683.
- 85 a) Myers, A. G.; Tanaka, D.; Mannion, M. R. *J. Am. Chem. Soc.* **2002**, *124*, 11250–11251. b) Hossian, A.; Bhunia, S. K.; Jana, R. *J. Org. Chem.* **2016**, *81*, 2521–2533. c) Bouazzaoui, O.; Rousée, K.; Mulengi, J. K.; Pannecoucke, J.; Bouillon, J.-P.; Couve-Bonnaire, S. *Eur. J. Org. Chem.* **2018**, 3705 – 3715.
- 86 a) Gagey, N.; Neveu, P.; Benbrahim, C.; Goetz, B.; Aujard, I.; Baudin, J.-B.; Jullien, L. *J. Am. Chem. Soc.* **2007**, *129*, 9986–9998. b) Metternich, J. B.; Gilmour, R. *J. Am. Chem. Soc.* **2015**, *137*, 11254–11257.
- 87 Götzinger, A. S.; Michaelis, C. S.; Müller, T. J. *J. Dyes and Pigments* **2017**, *143*, 308–316.
- 88 Nair, R. N.; Lee, P. J.; Rheingold, A. L.; Grotjahn, D. B. *Chem. Eur. J.* **2010**, *16*, 7992–7995.
- 89 a) Bertram, H.-J.; Böhm, S.; Born, L. *Synthesis* **1991**, *11*, 937–938. b) Billaud, E. M. F.; Maisonia-Besset, A.; Rbah-Vidal, L.; Vidal, A.; Besse, S.; Bequignat, J.-B.; Decombat, C.; Degoul, F.; Audin, L.; Deloye, J.-B.; Dolle, F.; Kuhnast, B.; Madelmont, J.-C.; Tarrit, S.; Galmier, M.-J.; Borel, M.; Auzeloux, P.; Miot-Noirault, E.; Chezal, J.-M. *Eur. J. Med. Chem.* **2015**, *92*, 818–838.
- 90 a) Uchida, H.; Ogawa, S.; Makabe, M.; Maeda, Y. US20100016285, 2010. b) Calabri, F. R.; Colotta, V.; Catarzi, D.; Varano, F.; Lenzi, O.; Filacchioni, G.; Costagli, C.; Galli, A. *Eur. J. Med. Chem.* **2005**, *40*, 897–907.
- 91 Wagner, A.; Koniev, O. WO2015001117, 2015.
- 92 Moria, N.; Togo, H. *Tetrahedron* **2005**, *61*, 5915–5925.

- 93 Foot, J. S.; Kanno, H.; Giblin, G. M. P.; Taylor, R. J. K. *Synthesis* **2003**, 7, 1055-1064.
- 94 Maki, B. E.; Chan, A.; Phillips, E. M.; Scheidt, K. A. *Tetrahedron* **2009**, 65, 3102-3109.
- 95 Li, K.; Kuo, H.-T.; Wang, X.; Merkens, H.; Colpo, N.; Radchenko, V.; Schaffer, P.; Lin, K.-S.; Bénardc, F.; Orvig, C. *Dalton Trans.* **2020**, 49, 7605–7619.
- 96 Pal, R.; Parker, D. *Org. Biomol. Chem.* **2008**, 6, 1020-1033.
- 97 Jauregui, M.; Perry, W. S.; Allain, C.; Vidler, L. R.; Willis, M. C.; Kenwright, A. M.; Snaith, J. S.; Stasiuk,, G. J.; Lowe, M. P.; Faulkner, S. *Dalton Trans.* **2009**, 6283-6285.
- 98 Kocsi, D.; Orthaber, A.; Borbas, K. E. *Chem. Commun.* **2022**, 58, 6853-6856.

Acta Universitatis Upsaliensis

Digital Comprehensive Summaries of Uppsala Dissertations from the Faculty of Science and Technology 2325

Editor: The Dean of the Faculty of Science and Technology

A doctoral dissertation from the Faculty of Science and Technology, Uppsala University, is usually a summary of a number of papers. A few copies of the complete dissertation are kept at major Swedish research libraries, while the summary alone is distributed internationally through the series Digital Comprehensive Summaries of Uppsala Dissertations from the Faculty of Science and Technology. (Prior to January, 2005, the series was published under the title "Comprehensive Summaries of Uppsala Dissertations from the Faculty of Science and Technology".)



Distribution: publications.uu.se
urn:nbn:se:uu:diva-514326

ACTA UNIVERSITATIS
UPSALIENSIS
2023